LUND UNIVERSITY

Precision mapping of gene expression and proteins in the brain using gene editing and barcoded viral vectors

Avallone, Martino

2023

[Link to publication](#)

Precision mapping of gene expression and proteins in the brain using gene editing and barcoded viral vectors

MARTINO AVALLONE
EXPERIMENTAL MEDICAL SCIENCE | FACULTY OF MEDICINE | LUND UNIVERSITY

MARTINO AVALLONE completed his bachelor's degree in Biology from Rome University in 2015. Inspired by the laboratory experience at the University of Strasburg, he continued his studies at the University of Trieste, where he obtained his master's degree in Neuroscience. In 2019, Martino undertook a PhD under the supervision of Tomas Björklund in the Molecular Neuromodulation laboratory. He focused his research on studying the function of the Arc protein in the mammalian brain and investigating gene expression alterations that happen during the progression of Parkinson's disease.

FACULTY OF
MEDICINE

Precision mapping of gene expression and proteins in the brain using gene editing and barcoded viral vectors

Martino Avallone

LUND
UNIVERSITY

DOCTORAL DISSERTATION

By due permission of the Faculty of Medicine at Lund University, this thesis will be publicly defended on 29th of September at 9.00 in Belfregesalen, BMC D15 klinikgatan 32, Lund, Sweden

Faculty opponent

Professor Veerle Baekelandt

Neurobiology & Gene Therapy
KU Leuven Brain Institute
Leuven, Belgium

Organization:	LUND UNIVERSITY		
Document name: DOCTORAL DISSERTATION		**Date of issue:** 29/09/2023	
Author: MARTINO AVALLONE		**Sponsoring organization:**	

Title and subtitle: Precision mapping of gene expression and proteins in the brain using gene editing and barcoded viral vectors

Abstract:

The human brain is a masterpiece of intricate design and impeccable functionality. It serves as the ultimate command center for our thoughts, sensations, and actions, which define our very existence. This organ operates flawlessly, with billions of neurons working in perfect harmony to process information, create memories, and regulate our emotions. The brain's neural network is composed of trillions of connections, consisting of interconnected cells that communicate through electrical impulses and chemical signals at remarkable speeds. These connections, also known as synapses, serve as the means of communication that allow for information to travel uninterrupted throughout the brain. This intricate network enables us to think, learn, reason, and react to our surroundings. However, neurological disorders have the potential to disrupt this delicate balance, leading to a range of manifestations. These can include gradual memory erosion in Alzheimer's disease to the slow progression of motor and cognitive impairment in Parkinson's disease. Each condition presents a unique puzzle for scientists and researchers to decipher. The intricate interactions of genes, proteins, and neural circuits create a complex landscape that holds the key to understanding these disorders' origins and potential treatments.

In this thesis, we worked on understanding a new type of neuronal communication based on the retrotransposon protein of Arc. The investigation was conducted using a gene editing technique based on the CRISPR/Cas9 system, next-generation sequencing technologies, and refined immunohistochemistry protocol. Using a mouse animal model, our findings reinforced the hypothesis that Arc has the capacity for inter-neuronal transport, as previously proposed in vitro studies. An additional objective of the thesis has been the investigation of molecular changes occurring within the Substantia Nigra throughout the progression of Parkinson's disease. At the core of this disorder's pathophysiology lies the alpha-synuclein protein. With this objective in mind, we developed a single-cell methodology to effectively investigate modifications in gene expression provoked by an overload of alpha-synuclein in animal models of rodents. From this data set, the overarching goal is to train a machine learning able to predict the disease course and to establish possible therapeutic interventions.

Key words: CRISPR/Cas9, Gene editing, barcodes, AAV, PLA, gene therapy, Parkinson's disease, single nuclei RNAseq, alpha-synuclein

Classification system and/or index terms (if any)

Supplementary bibliographical information

Language: English

ISSN and key title: 1652-8220	**ISBN:** 978-91-8021-451-3
Recipient's notes:	**Number of pages:** 105
Price:	Security classification

Signature   Date 2023-08-18

Precision mapping of gene expression and proteins in the brain using gene editing and barcoded viral vectors

Martino Avallone

LUND
UNIVERSITY

from

MOLECULAR NEUROMODULATION

Department of Experimental Medical Science, Faculty of Medicine

Lund University, Lund, Sweden

Thesis cover conceptualized by Martino Avallone and drawn by the artistic hand of Matilde Negrini. The cover is a cartographic representation of a mouse brain section focusing on the region of the Substantia Nigra. Just as brave explorers once used to navigate dangerous seas, modern researchers now embark on the complex and mysterious world of life science.

A set square with nucleotides as digits, a compass with an embedded figure of an Adeno-associated virus, and a powerful lens alluding to a microscope.

Daje forte...

Sempre

To Itaca

Table of Contents

Introduction

Aims

Results

Discussion

Methods

References

Acknowledgements

List of Papers

I. **Martino Avallone**, Joaquín Pardo, Tadiwos F. Mergiya, Jana Rájová, Atte Räsänen, Marcus Davidsson, Malin Åkerblom, Luis Quintino, Darshan Kumar, Clive R. Bramham and Tomas Björklund. Visualizing Arc protein dynamics and localization in the mammalian brain using AAV- mediated in situ gene labeling (2023) *Frontiers in Molecular Neuroscience*

II. Joaquin Pardo*, **Martino Avallone***, Janitha Mudannayake, Sara Palo, Jana Rájová, Atte Räsänen, Anna Hammarberg, Jenny Johansson, Ulrich Pfisterer, Alessandro Fiorenzano and Tomas Björklund. Development of a novel rat model for Parkinson's disease using retrograde transport of barcoded AAV vectors (2023) *Manuscript in preparation.*

III. **Martino Avallone**, Joaquin Pardo, Sara Palo, Jana Rájová, Anna Hammarberg, Jenny Johansson, Alessandro Fiorenzano and Tomas Björklund (2023) *Manuscript in preparation.*

IV. Jana Rájová, Marcus Davidsson, **Martino Avallone**, Morgan Hartnor, Patrick Aldrin-Kirk, Tiago Cardoso, Sara Nolbrant, Annelie Mollbrink, Petter Storm, Andreas Heuer, Malin Parmar and Tomas Björklund (2023) *Molecular Therapy: Methods & Clinical Development.*

Abstract

The human brain is a masterpiece of intricate design and impeccable functionality. It serves as the ultimate command center for our thoughts, sensations, and actions, which define our very existence. This organ operates flawlessly, with billions of neurons working in perfect harmony to process information, create memories, and regulate our emotions. The brain's neural network is composed of trillions of connections, consisting of interconnected cells that communicate through electrical impulses and chemical signals at remarkable speeds. These connections, also known as synapses, serve as the means of communication that allow for information to travel uninterrupted throughout the brain. This intricate network enables us to think, learn, reason, and react to our surroundings. However, neurological disorders have the potential to disrupt this delicate balance, leading to a range of manifestations. These can include gradual memory erosion in Alzheimer's disease to the slow progression of motor and cognitive impairment in Parkinson's disease. Each condition presents a unique puzzle for scientists and researchers to decipher. The intricate interactions of genes, proteins, and neural circuits create a complex landscape that holds the key to understanding these disorders' origins and potential treatments.

In this thesis, I worked on understanding a new type of neuronal communication based on the retrotransposon protein of Arc. The investigation was conducted using a gene-editing technique based on the CRISPR/Cas9 system, next-generation sequencing technologies, and refined immunohistochemistry protocol. Using a mouse animal model, our findings reinforced the hypothesis that Arc has the capacity for inter-neuronal transport, as previously proposed *in vitro* studies. An additional objective of the thesis has been the investigation of molecular changes occurring within the Substantia Nigra throughout the progression of Parkinson's disease. At the core of this disorder's pathophysiology lies the alpha-synuclein protein. With this objective in mind, we developed a single-cell methodology to effectively investigate modifications in gene expression provoked by an overload of alpha-synuclein in animal models of rodents. From this data set, the overarching goal is to train a machine learning able to predict the disease course and to establish possible therapeutic interventions.

ABSTRACT

Populärvetenskaplig sammanfattning

Den mänskliga hjärnan är ett mästerverk med intrikat design och felfri funktion. Den agerar som kommandocentral för våra tankar, känslor och handlingar vilka i sin tur definierar vår existens. Detta organ fungerar helt felfritt med miljarder nervceller som samverkar i en perfekt harmoni med att bearbeta information, skapa minnen och styra våra känslor. Hjärnans neurala nätverk består av triljoner kopplingar skapade av sammankopplade nervceller som kommunicerar med hjälp av elektriska impulser och kemiska signaler med en ofattbar hastighet. Dessa kopplingar, också kallade synapser, medger att information kan färdas obehindrat genom hjärnan och bygger upp ett nätverk som möjliggör att vi kan tänka, lära oss nya färdigheter, resonera och reagera på vår omgivning. Neurodegenerativa sjukdomar kan dock störa denna delikata balans vilket leder till många olika av symptom. Dessa symptom inkluderar allt från gradvis nedbrytning av vårt minne vid Alzheimers sjukdom till ett långsamt försämrande av vår motoriska och kognitiva förmåga vid Parkinsons sjukdom. Var sjukdom har sina unika gåtor för oss forskare att lösa. Den intrikata interaktionen mellan gener, proteiner och neurala kretsar skapas ett komplext landskap där nyckeln till förståelsen av dessa sjukdomars ursprung och potentiella behandlingar kan finnas gömd.

I denna avhandling har jag arbetat med att utöka vår förståelse kring en ny typ av neural kommunikation som baseras på retrotransposomen Arc. Dessa försök baseras på genediteringstekniken CRISPR/Cas9, nya sekvenseringstekniker och ett förfinat immunohistokemiskt protokoll. Våra resultat, baserade på en musmodell, stödjer hypotesen att Arc kan transporteras mellan nervceller såsom tidigare påvisats i cellkulturer. Ett andra mål med denna avhandling var att studera de molekylära förändringar som sker i mellanhjärnan vid Parkinsons sjukdom. Proteinet alfasynuklein är en central aktör i alla skeden av sjukdomen. Med detta i åtanke så har vi utvecklat en helt ny metodologi där vi kan studera förändringar i genuttryck på encellsnivå efter överuttryck av alfasynuklein i mellanhjärnan på två djurmodeller. Med hjälp av dessa data så är målet att träna en maskininlärningsmodell för att förutspå sjukdomsprocessen och etablera en grund för att ta fram nya behandlingar.

Riassunto

Il cervello umano è un capolavoro di intricato design e impeccabile funzionalità. Serve come centro di comando supremo per i nostri pensieri, sensazioni e azioni, che definiscono la nostra stessa esistenza. Questo organo opera senza difetti, con miliardi di neuroni che lavorano in perfetta armonia per elaborare informazioni, creare ricordi e regolare le nostre emozioni. La rete neurale del cervello è composta da trilioni di connessioni, costituite da cellule interconnesse che comunicano attraverso impulsi elettrici e segnali chimici a velocità notevoli. Queste connessioni, note anche come sinapsi, fungono da mezzi di comunicazione che consentono alle informazioni di viaggiare ininterrottamente in tutto il cervello. Questa intricata rete ci permette di pensare, apprendere, ragionare e reagire al nostro ambiente. Tuttavia, i disturbi neurologici hanno il potenziale per interrompere questo delicato equilibrio, portando a una serie di manifestazioni. Queste possono includere l'erosione graduale della memoria nella malattia di Alzheimer fino alla lenta progressione dell'impairment motorio e cognitivo nella malattia di Parkinson. Ogni condizione presenta un puzzle unico per gli scienziati e i ricercatori da decifrare. Le intricate interazioni tra geni, proteine e circuiti neurali creano un panorama complesso che detiene la chiave per comprendere le origini di questi disturbi e i possibili trattamenti.

In questa tesi, abbiamo lavorato per comprendere un nuovo tipo di comunicazione neuronale basata sulla proteina retrotrasposone di Arc. L'indagine è stata condotta utilizzando una tecnica di modifica genetica basata sul sistema CRISPR/Cas9, tecnologie di sequenziamento di nuova generazione e un protocollo raffinato di immunocitochimica. Utilizzando un modello animale di topo, le nostre scoperte hanno rafforzato l'ipotesi che Arc abbia la capacità di trasporto interneuronale, come precedentemente proposto in studi in vitro. Un ulteriore obiettivo della tesi è stata l'indagine dei cambiamenti molecolari che avvengono all'interno della Substantia Nigra durante la progressione della malattia di Parkinson. Al centro della patofisiologia di questo disturbo si trova la proteina alfa-sinucleina. Con questo obiettivo in mente, abbiamo sviluppato una metodologia a singola cellula per indagare efficacemente le modifiche nell'espressione genica provocate da un sovraccarico di alfa-sinucleina in modelli animali di roditori. Da questo insieme di dati, l'obiettivo principale è addestrare un'apprendimento automatico in grado di prevedere il corso della malattia e stabilire possibili interventi terapeutici.

Abbreviations

6-OHDA	6-hydroxydopamine
αSyn	alpha-synuclein
AD	Alzheimer's disease
AMPAr	α-amino-3-hydroxy-5-methyl-4-isoxazole propionic acid
ANN	artificial neuronal network
Arc	activity-regulated cytoskeleton protein
AAP	associated accessory protein
AAV	adeno-associated virus
BC	barcode
Cap	capsid
Cas9	CRISPR-associated protein 9
CNS	central nervous system
CRISPR	clustered regularly interspaced short palindromic repeats
DAT	dopamine transporter
DBS	deep brain stimulation
DG	dentate gyrus
DLB	dementia with LBs
DSB	double-strand break
DT	donor template
EM	electron microscopy
EVs	extracellular vesicles
FACS	fluorescent activated cells sorting
FANS	fluorescent-activated nuclei sorting
fEPSPs	filed evoked postsynaptic potential
FvM	fetal ventral midbrain
GABA	gamma-aminobutyric acid
GCIs	glia cytoplasmic inclusions
GFAP	glial fibrillary acidic protein
GPe	globus pallidus external
GPi	globus pallidus internal
GDNF	glia-derived neurotrophic factor
H2B-GFP	Histone H2B Green fluorescent protein
HDR	homology-directed repair
hESC	human embryonic stem cells
HFS	high-frequency stimuli
HITI	homology independent targeted integration
HSPG	heparan sulfate proteoglycans
IEGs	immediate early genes
IHC	immunohistochemistry
L-DOPA	l-3,4-dihydroxyphenylalanine

LBs	Lewy bodies
LFS	low-frequency stimuli
LNs	Lewy neurites
LTD	long-term depression
LTP	long-term potentiation
LV	lentivirus
MFB	medial forebrain bundle
MMEJ	microhomology-mediated end joining
MSA	multiple system atrophy
NAC	non-amyloid component
NHEJ	non-homology mediated end joining repair
NHP	non-human primate
NTD	N-terminal domain
ORF	open reading frame
PD	Parkinson's disease
PFFs	preformed fibrils
scAAV	self-complementary AAV
scRNAseq	single-cell RNA sequencing
SNpc	substantia nigra pars compacta
SPN	spiny projection neurons
STN	subthalamic nuclei
TH	tyrosine hydroxylase
PAM	protospacer adjacent motif
PLA	proximity ligation assay
PMT	post-translational modification
POI	population of interest
pSer129	phosphorylated Serine 129
RCA	rolling circle amplification
Rep	replication
ROI	region of interes
ROS	reactive oxygen species
RT	reverse transcriptase
ST	spatial transcriptomics
SYN1	synapsin 1
TALEN	transcription activator-like effector nuclease
TSO	template switching oligonucleotide
UMAP	unifold manifold approximation projections
UMI	unique molecular identifier
UTR	untranslated terminal region
VLMCs	vascular leptomeningeal cells
VLP	virus-like particles
WT	wild type

Introduction

Neural networks evolution

Since the emergence of life on Earth, unicellular organisms like bacteria and protists have developed rudimentary sensory systems to experience their environment and respond to external stimuli. The primitive neuronal networks, consisting of sensory receptors and ion channels, helped transmit crucial signals for necessary survival functions. Driven by competition for nutrients and resources, organisms evolved into pluricellular entities, where the specialization of cell groups enabled coordinated movements, energy transformation, and more complex behaviors and interactions with their surroundings (Jékely, 2011; Arendt et al., 2015; Arendt, 2021).

The transition from sparse nerve nets to ganglia marked an evolutionary milestone in the development of nervous systems. Within organisms, these neuronal networks specialize in processing information and coordinating responses to diverse stimuli resulting in more centralized nervous systems leading to complex behavioral responses (Figure 1) (Sarnat and Netsky, 2002; Balavoine and Adoutte, 2003).

Across epochs, organisms continued to evolve, compelled by the competition to occupy and defend ecological niches. This led to increasingly complex neuronal networks involving more nerve cells, expanding their connections and ultimately forming the brain (Burkhardt and Sprecher, 2017).

Within this organ, nerve cells differentiated into diverse populations, forming distinct anatomical structures specialized in various types of signaling. In mammals, particularly primates, the enlargement of the neocortex significantly contributed to cognitive advancements such as memory, problem-solving, and social interactions. With billions of intricate connections among communicating neurons, the human brain regulates higher-order cognitive abilities, including abstract thought, complex language systems, and self-awareness (Nicholls et al., 2012).

This elaborated neuronal network has enabled *Homo sapiens* to colonize most areas of the world, domesticate other species, establish sophisticated societies, and drive progress through scientific discoveries (Harari, 2015).

INTRODUCTION

To understand how the brain works, humans have built artificial neuronal networks (ANNs) to mimic brain-like information processing (Crick, 1989). The continuous advancement in this field, with the development of deep learning and generative artificial intelligence, has provided scientists with powerful tools which could unravel the mysteries of thinking matter. This field is advancing remarkably, with breakthroughs and applications coming along every single day (Rajpurkar et al., 2022).
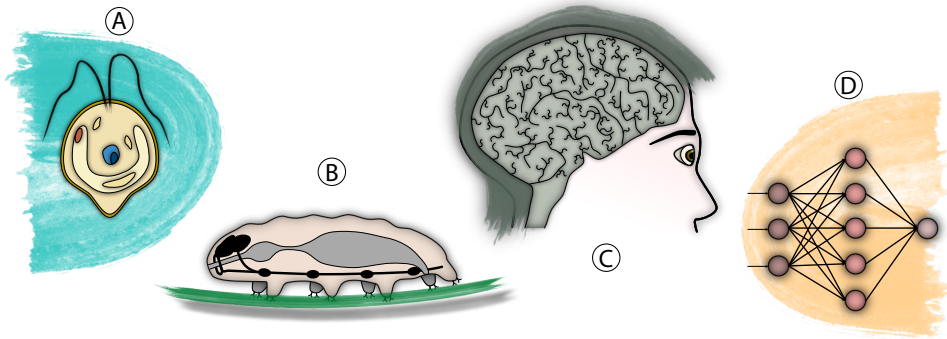
Figure 1 | Neural network evolution sketch. [A] Chlamydomonas, a small unicellular alga with locomotor cilia. **[B]** Tardigrade, the brain is comprised of several lobes, and a ventral nerve cord connects all the ganglions along the segment. **[C]** Adult human brain showing the surface of the cortex folded into gyri (ridges) and sulci (grooves). **[D]** Artificial neural network (ANN) with nodes forming from left to right: the input layer, hidden layer, and output layer.

Cell-cell communication in the brain

Neurons facilitate communication through electrical and chemical signals in the central nervous system (CNS). The basis of electrical signaling lies in the action potential, a brief and rapid change in the neuron's membrane potential. The resting membrane potential of neurons is maintained at a negative charge relative to the outside. When a stimulus is strong enough to depolarize the neuron, voltage-gated ion channels open, allowing an influx of positively charged ions like sodium ($Na+$), causing a rapid change in charge from negative to positive. This charge propagates along the neuron's axon, reaching the synaptic terminal (Sullivan, 2017).

Upon reaching the presynaptic terminal, the electrical signal triggers the release of neurotransmitters, which diffuse across the synaptic cleft, where they bind to specific receptors on the postsynaptic neuron. This binding can either excite or inhibit the postsynaptic neuron, influencing the continuation or inhibition of the signal. Several

types of neurotransmitters in the brain are involved in different neural communications. Excitatory neurotransmitters like glutamate and acetylcholine promote neuronal activity and facilitate signal transmission. In contrast, inhibitory neurotransmitters like gamma-aminobutyric acid (GABA) and glycine reduce neuronal excitability (Niyonambaza et al., 2019).

Additionally, modulatory neurotransmitters influence neural circuits' overall activity and responsiveness depending on their binding receptor. An example is dopamine (DA) which plays a crucial role in reward, motivation, and motor control. Disruptions in the delicate balance of neurotransmitters can lead to neurological and psychiatric disorders. For instance, reduced level of DA in the brain has been linked to Parkinson's disease (PD). This will further discuss in this thesis (Triarhou., 2013; Teleanu et al., 2022).

In recent years, alternative methods of intercellular communication within the CNS have been suggested. Nanotube-like structures establish connections between two cells, forming a continuous pathway in their cellular layer that enables the exchange of cellular cargo. Through these connections, the two cells can share cytoplasmic fluid, allowing them to interact with internal organelles, such as ion channels and mitochondria (Tardivel et al., 2016; Kalargyrou et al., 2021; Khattar et al., 2022). Exosomes, a prominent class of extracellular vesicles (EVs), are tiny lipid-bilayer enclosed structures that transport nucleic acids, proteins, and lipids between cells. They play a crucial role in modulating synaptic plasticity, neurotransmitter release, and neurite growth. Interestingly, these small vesicles have been observed to participate in neuron-glia signaling during inflammatory processes (Men et al., 2019; Pascual et al., 2020; Vilcaes et al., 2021; Xia et al., 2022). The last one to be added to this list is the viral-like particles (VLPs) mechanism proposed upon observations of the activity-regulated cytoskeleton-associated protein (Arc) in genetic material transfer (Ashley et al., 2018; Pastuzyn et al., 2018; Hantak et al., 2021; Eriksen and Bramham, 2022).

The retrotransposon element of Arc

Gene and protein structure

The Arc protein is encoded by the Arc/arg3.1 gene, which belongs to the immediate early genes (IEGs) family, rapidly responding to neuronal stimulation or activity.

Phylogenetic studies have reported that its sequence has been introduced in higher-order species and is highly conserved across many species living above sea level. In the mouse genome, Arc is localized on chromosome 15, spanning a length of 3488 base pairs (bp), and comprises three exons with only exon 1 containing the coding region (Pastuzyn et al., 2018).

INTRODUCTION

Upon cellular activation, phosphorylated cascades stimulate the activation of specific transcription factors, which subsequently bind upstream of the Arc open reading frame (ORF). Within the Arc promoter regions, two robust activity-responsive elements have been identified: an enhancer element located 1.4 kilobases (kb) upstream and another positioned 6.5 kb upstream, in addition to an activity-sensing element situated 7 kb upstream (Kawashima et al., 2009; Pintchovski et al., 2009).

The mRNA transcript of Arc spans a length of 3055 bp and encompasses several regulatory elements that meticulously govern its distribution and expression. Notably, the 5′UTR harbors binding sites for regulatory elements that ensure precise Arc translation. Conversely, within the 3′UTR, the presence of exon junction complexes confers upon Arc a tightly regulated expression through the mechanism of nonsense-mediated decay. Additionally, a pivotal regulatory element located at the 3′UTR facilitates the translocation of Arc mRNA into neuronal dendrites (Kobayashi et al., 2005; Bramham et al., 2010).

Arc/Arg3.1 encodes for a 396 amino acidic protein which comprises two terminal domains separated by an unstructured linker sequence, the N-terminal domain (NTD) and the C-terminal domain (CTD), which are oppositely charged and interacting (Figure 2). Crystallographic studies have revealed that the N-terminal domain (NTD) of Arc consists of two α-helices forming an anti-parallel coiled coil. This domain has been associated with its interactions with mRNA molecules and Arc oligomerization (Hallin et al., 2018; Eriksen et al., 2021; Eriksen and Bramham, 2022). On the other hand, the C-terminal domain (CTD) comprises two unstructured globular N-lobe and a C-lobe domain, exhibiting conformational similarity with the capsid-forming Gag proteins of HIV and RSV retroviruses and underlying the CTD role in the capsid assembling processes (Zhang et al., 2015).

Biology

During synaptic plasticity in the mammalian brain, Arc is critical in interacting with other proteins localized in the spines or the nucleus. During long-term potentiation (LTP) in activated synapses, Arc is involved in filament actin polymerization, remodelling, and stabilization, hence its name (Lyford et al., 1995; Messaoudi et al., 2007). While for long-term depression (LTD), Arc interacts with clathrin-based endocytic proteins to regulate the trafficking of AMPA-type glutamate receptors (AMPARs), leading to synaptic scaling (Chowdhury et al., 2006; Shepherd et al., 2006; DaSilva et al., 2016). Arc protein-protein interaction is at the core of long-lasting modification after synaptic activity.
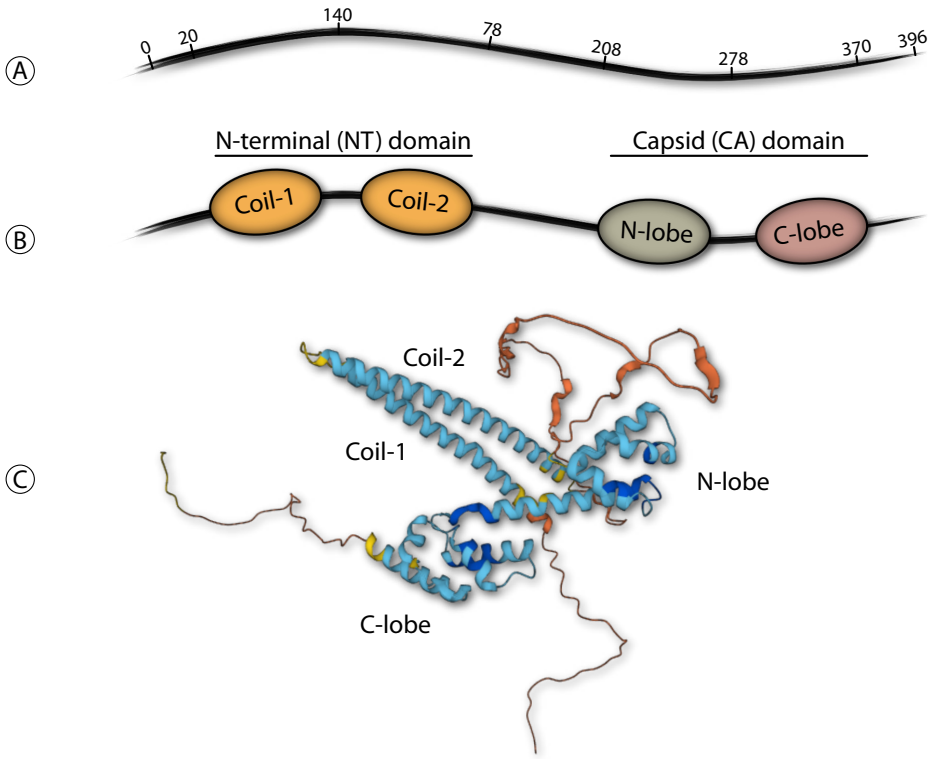
Figure 2 | Arc domains and 3D structure. [A] Arc protein is composed of 396 amino acids, forming its primary structure. **[B]** Schematic representation of Arc domains with structured and unstructured domains **[C]** 3D structural prediction of Arc based on its amino acid sequence using alpha fold.

Observations at the post-synaptic site have identified several Arc binding partners such as TARPγ2 (Stargazin), NMDAR subunit 2A, as well as coffin, drebrin A, and WAVE1 (Lyford et al., 1995; Messaoudi et al., 2007; Zhang et al., 2015; Nair et al., 2017). Notably, in the visual cortex, Arc is required to transduce experience into long-lasting changes (McCurry et al., 2010). Its considerable regulatory activity at the synaptic level highlights Arc's pivotal role in the molecular mechanisms underlying learning and memory.

The Arc protein has the intriguing ability to spontaneously self-assemble into VLPs that serve as carriers for mRNA encapsulation. Subsequently, these VLPs are released from neurons into the extracellular space, specifically targeting recipient cells. Once delivered, the Arc mRNA undergoes activity-dependent translation in the targeted cells. This unique feature has been hypothesized to be associated with a vestige of an ancient retroviral infection involving essential components reminiscent of a GAG protein (Ashley et al., 2018; Pastuzyn et al., 2018).

Parkinson's Disease

General discussion

As we have seen, neuronal communication is very complex, involving many players. Disruptions of this delicate balance can lead to neurological and psychiatric disorders. For instance, an example is the neurotransmitter DA, where low levels are associated with hallmark symptoms of PD (Teleanu et al., 2022).

PD was named after the English physician James Parkinson, who first described it in 1817 in a publication titled "An Essay on the Shaking Palsy" (Parkinson, 2002). It is a progressive neurodegenerative disorder that primarily affects the CNS. Current data indicates that the prevalence of PD has doubled over the past 25 years. As of 2019, the estimated number of individuals living with PD exceeded 8.5 million worldwide, an 81% increase since 2000 (WHO, 2022). These numbers are projected to rise in the early future, given that aging is considered a significant risk factor and life expectancy is increasing due to improved lifestyle practices.

At the core of PD lies the gradual degeneration of DAergic neurons residing in the substantia nigra pars compacta (SNpc), leading to a decline in DA levels within the basal ganglia circuitry (Crittenden and Graybiel, 2011). Notably, motor symptoms, such as tremors, rigidity, bradykinesia, and postural gait abnormalities, become evident when individuals with PD have around 30% of cell loss and approximately 60% of DAergic projections compromised (Fearnley and Lees, 1991; Greffard et al., 2006). Conversely, non-motor symptoms may emerge years before the onset of motor manifestations, encompassing hyposmia (olfactory dysfunction), constipation, sleep disturbances, and memory impairment. Moreover, progressive cognitive decline significantly diminishes patients' quality of life, giving rise to depression and anxiety (Khoo et al., 2013).

The pathophysiology seen in patients with PD has been associated with abnormal aggregation of alpha-synuclein (αSyn) protein, leading to the formation of intracellular inclusions known as Lewy bodies (LBs) and Lewy neurites (LNs) (Polymeropoulos et al., 1997; Spillantini et al., 1997; Wood et al., 1999). Despite extensive research, the precise mechanism by which αSyn aggregation triggers neurodegeneration still needs to be more adequately defined and understood. Further investigations are warranted to unravel the intricate molecular processes underlying this phenomenon and gain deeper insights into the mechanisms driving PD pathology. Hopefully, this will be the case for **Paper III**.

Braak and his colleagues put forward a theory about how the disease progresses. They introduced the concept of Braak staging, which considers the distribution of Lewy bodies (LBs) pathology, both in terms of space and time (Braak et al., 2003) The hypothesis encompasses six stages, where the first stages cover non-motor symptoms, and the following 3 or 4 stages are marked with motor impairments.

In stages I and II, the pathology appears in the periphery of the nervous system, affecting regions responsible for olfactory loss and autonomic dysfunctions. In stages III and IV, LBs spread to other critical areas, leading to motor impairments. Ultimately, in stages V and VI, the spread reaches cortical layers of the brain, intensifying motor symptoms and inducing cognitive decline. The progression of the steps depicts a spreading pattern of LBs pathology along anatomically interconnected areas in the brain.

The sequential stages illustrate the propagation of LBs pathology within interconnected brain regions. This pattern of spread holds critical implications for understanding the pathogenesis of PD.
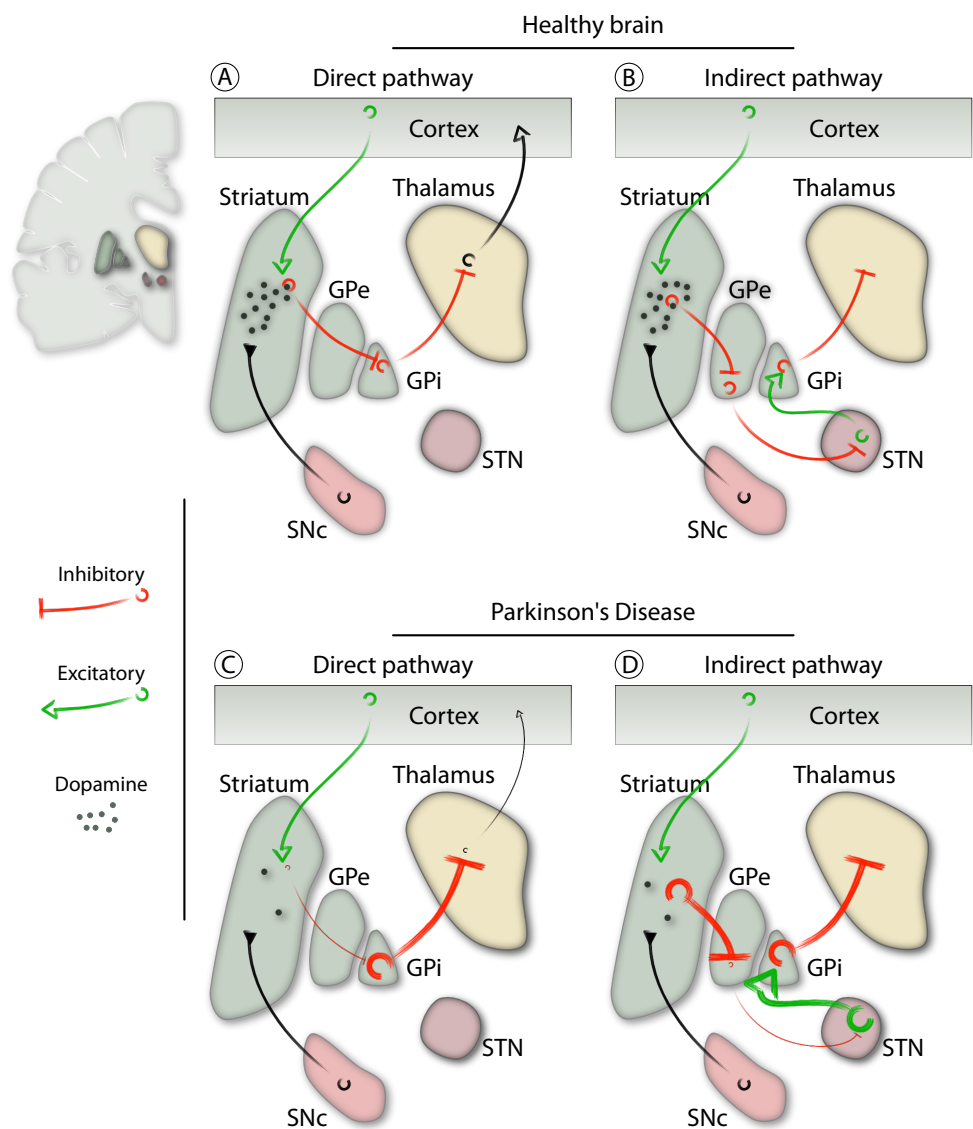
Basal Ganglia

The basal ganglia are a group of interconnected nuclei located below the cortex. They are responsible for various functions, including motor control, learning, and emotion. The anatomical structures within the motor circuitry consist of several nuclei. The caudate and putamen forming the striatum, the substantia nigra pars compacta and reticulata (SNpc and SNpr), the external and internal globus pallidus (GPe and GPi), and the subthalamic nuclei (STN).

Due to the research focus of this thesis, the following section will describe how they work as a relay station, receiving inputs from different parts of the brain related to motor control and integrating this information to tune the motor output finely. A well-functioning motor circuitry is vital to select voluntary movements and suppress unwanted ones by activating the direct and indirect pathways loop.

To facilitate comprehension, we will present the traditional model of the basal ganglia. However, contemporary research indicates that this model represents a simplified perspective of a more intricate organization, making it challenging to predict specific outputs based on inputs (Bolam et al., 2000). Despite its constraints, this foundational model has significantly influenced our understanding of DA's role in motor output and how alterations in DA levels give rise to motor symptoms in PD (Albin et al., 1989; DeLong, 1990).

The direct pathway is primarily responsible for promoting and facilitating voluntary movements. It is activated with the cerebral cortex, sending glutamatergic input to the dorsal part of the striatum. Here, spiny projection neurons (SPNs) expressing the D1 receptor, substance P, and dynorphin (dSPNs) are activated. This specific population is further stimulated by DA signaling from the SNpc. The activated dSPNs send their inhibitory projections to the GPi, where γ-Aminobutyric acid (GABA) is released. The inhibitory GABAergic projections from the GPi to the thalamus are now inhibited. When this happens, the thalamus becomes disinhibited and sends signals to the motor cortex through glutamatergic outputs, facilitating movement (Figure 3).

Figure 3 | Schematic of the classical model of the basal ganglia motor circuitry. [A] The direct pathway in a healthy brain. Dopamine release in the striatum acts on D1 receptors of dSPNs. The inhibition of the GPi inhibitory projections results in a disinhibition of the thalamus, resulting in increased excitatory signal to the cortex and movement execution. **[B]** The indirect pathway from a healthy brain. The tonic inhibition of the GPi to the thalamus results in reduced movement. **[C]** and **[D]** The direct and indirect pathways in a PD brain. Due to lower levels of dopamine in the striatum, the GPi and STN are less inhibited. As a result, the thalamus is strongly inhibited, leading to challenges in initiating movements.

On the other hand, the indirect pathway is essential in inhibiting and suppressing unwanted movements. The indirect pathway also originates in the cerebral cortex, which sends excitatory signals to the striatum. However, this time, DA released from the SNpc projections will act as inhibitory molecule on SPNs expressing the D2 receptor, Adenosine A2A, and encephalin (iSPNs). iSPNs send their GABAergic projections to the GPe neurons inhibiting their activity. Their deactivated inhibitory projections result in the STN excitatory projections turning on GPi activity. GABAergic projections from GPi will inhibit thalamus excitatory glutamatergic projections, resulting in reduced movement (Gerfen et al., 1990).

In PD patients, the degeneration of DAergic cells in the substantia nigra pars compacta SNpc leads to a decline in DA signaling within the striatum. This decrease in DA availability disrupts the intricate balance between the direct and indirect pathways, contributing to motor impairments. Specifically, the reduced activation of striatal dSPNs in the direct pathway and the diminished inhibition of iSPNs in the indirect pathway lead to challenges initiating movement and manifest as involuntary shaking tremors during rest.

Synucleinopathies

The accumulation of LBs and LNs in the brain is not exclusive to PD. This characteristic pathological feature is shared with other neurodegenerative disorders, such as Dementia with Lewy Bodies (DLB) and Multiple System Atrophy (MSA), which exhibit protein aggregates in the neuronal and glial cell population, respectively (Spillantini, 1999).

DLB stands out as the second most common form of dementia, with an estimated incidence of 1 person every 2000 per year, accounting for around 5% of all clinically diagnosed dementia cases (Hogan et al., 2016). However, its prevalence may be underestimated due to frequent misdiagnoses as other more common types of dementia, such as Alzheimer's disease (AD) (Litvan et al., 1998). DLB was initially considered atypical PD or AD, but it wasn't until recently recognized as a distinct disorder with unique clinical features. The first documented case of DLB was described as "diffuse Lewy body disease" in 1984, marking the beginning of the investigation into this neuropathological disorder (Kosaka et al., 1984).

While PD and DLB share the hallmark of LBs, DLB's pathology appears to originate in the cerebral cortices, spreading towards the basal forebrain, causing neuronal dysfunction and loss of cortical acetylcholine. This disease mechanism is separate from what is observed in PD (Perry et al., 1985; Marui et al., 2002).

Non-motor symptoms characterized by cognitive decline with memory impairment, deficits in attention and executive function, visual hallucinations, apathy, depression, and REM sleep disturbances are the first to arise. As the disease advances, parkinsonian motor symptoms may also manifest. However, they typically differ from those seen in PD, showing postural instability, gait disorders, or symmetric kinetic rigid syndrome rather than tremors (Del Ser et al., 2000). Distinguishing between PD with dementia is clinically challenging, and the onset of dementia symptoms in relation to motor symptoms is used to aid in the differential diagnosis. Moreover, confirmation of the correct diagnosis still comes after examination of the *postmortem* tissue (McKeith et al., 2017).

The MSA term was initially coined to characterize the degeneration of neurons observed in different medical conditions, including striatonigral degeneration, Shy-Drager syndrome1, and olivopontocerebellar atrophy (Graham and Oppenheimer, 1969). MSA is a progressive neurodegenerative disease that sets itself apart from the rest of synucleinopathies. Unlike the others, it exhibits a rapid progression and is ultimately fatal, with median survival ranging from 6-10 years after the onset of initial symptoms (Schrag et al., 2008; Fanciulli and Wenning, 2015). It is relatively rare, with an estimated incidence of between 3.4 and 4.9 cases per 100,000 persons annually (Lee et al., 2019). Neuropathologically, MSA is characterized by the presence of glial cytoplasmic inclusions (GCIs) in oligodendrocytes, with the first pathological feature being myelin dysfunction, followed by demyelination and neurodegeneration (Tu et al., 1998). Clinical symptoms are similar to those of PD. However, unresponsiveness to L-DOPA for Parkinsonian symptoms makes MSA a challenging disease to treat (Wenning et al., 1994).

Structure and biology of α-synuclein

Research interest in alpha-synuclein grew significantly when an autosomal dominant mutation (A53T) in its encoding gene, SNCA, was discovered in patients with early-onset PD (Polymeropoulos et al., 1997). Since then, many laboratories have worked to identify the physiological role of alpha-synuclein, but there is still much to be understood about it (Bendor et al., 2013).

In 1988 Maroteaux and colleagues were the first to describe the alpha-synuclein protein. Comprising 140 amino acids (14.4kDa), alpha-synuclein is highly conserved and belongs to the synuclein family, which includes alpha, beta, and gamma synucleins. Among them, alpha-synuclein is the sole disease-related protein (Maroteaux et al., 1988; George, 2002).

The primary sequence of alpha-synuclein can be divided into three distinct domains. The N-terminal region (residues 1-60) contains six imperfect KTKEGV repeat motifs, giving it amphipathic properties that facilitate membrane binding. This interaction leads to conformational changes, resulting in an alpha-helical secondary structure. From residues 61 to 95, the non-amyloid Beta component (NAC) domain displays the characteristic amyloid cross-beta sheet structure and is hydrophobic, thought to drive protein aggregation (Dickson, 1999; Periquet et al., 2007; Soper et al., 2008). The C-terminal region (residues 96-140) consists of an acidic stretch that is highly charged and serves various functions, including metal iron- and protein-binding. This domain is also where most post-translational modifications take place (Figure 4).

Although alpha-synuclein is a ubiquitous protein, it is predominantly expressed in the CNS and operates as a neuronal protein. It is localized at the pre-synapse and in the nucleus, where multiple functions have been proposed. We do have a clearer picture at the synapse, though, where it has been observed to interact with synaptic transporters DA transporter (DAT), SERT, and VMAT, as well as modulating Tyrosine hydroxylase (TH) activity. Moreover, alpha-synuclein ensures correct neuronal homeostasis by tethering the synaptic vesicle pool. In other studies, it has been reported that alpha-synuclein interacts with the SNARE complex assembly to help in the synaptic vesicle release (Perez et al., 2002; Scott and Roy, 2012; Burré, 2015)
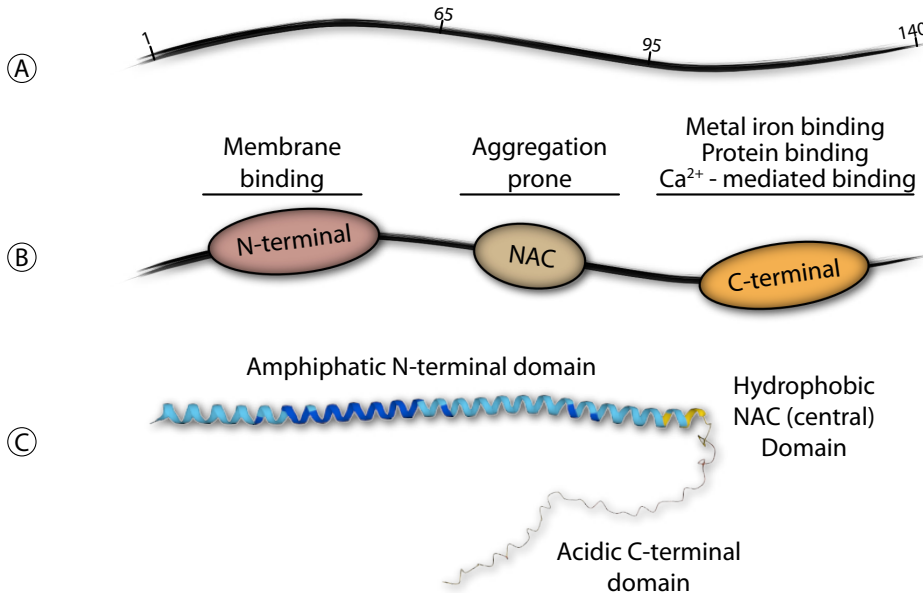
Figure 4 | α-syn domains and 3D structure. [A] α-syn protein is composed of 140 amino acids, forming its primary structure. **[B]** Schematic representation of α-syn protein domains and their properties. **[C]** 3D structural prediction of α-syn based on its amino acid sequence using alpha fold.

INTRODUCTION

Aggregation and pathology of α-synuclein protein

αSyn was initially believed to be an intrinsically disordered protein, natively unfolded, lacking a defined secondary structure. However, due to its natural conformation and the highly dense cellular environment, this protein is likely to interact with other molecules (Bertoncini et al., 2005). Evidence suggests that the native state of alpha-synuclein might instead be a tetramer, adding a new dimension to our understanding of its function (Lashuel et al., 2013).

Aggregates of αSyn play a central role in the pathogenesis of synucleinopathies. Normally, charges in the N- and C-terminal regions stabilize the protein structure, preventing aggregation. However, post-translational modifications such as truncation, phosphorylation, and nitrification disrupt this delicate equilibrium, exposing the NAC domain. Consequently, this central hydrophobic region facilitates the formation of oligomers and aggregates. Electron microscopy (EM) images revealed the structure of these oligomers to be spheres, chains, and rings, which are highly prone to interact with cellular membranes, leading to calcium ions influx (Lashuel et al., 2002; Rochet et al., 2004; Lashuel et al., 2013).

These ring-like structures disrupt membrane potential and are primarily localized in axons and dendrites, interfering with the synaptic vesicle release (Nemani et al., 2010; Scott et al., 2010; Lundblad et al., 2012b). Oligomers can recruit more αSyn proteins, initiating the formation of insoluble, proteinase K resistant, fibrillary structures, ultimately leading to the formation of LBs and LNs inclusions (Dickson et al., 1989; Giasson et al., 1999; Conway et al., 2000). Notably, the rate-limiting step in fibril formation is the initial seed formation, and once formed, αSyn fibrils grow exponentially (Lashuel et al., 2013).

The vast polymorphism of oligomers and fibrillary structures has complicated the quest to identify a unified structure causing cytotoxicity. For instance, recent findings have proved how different patient-derived αSyn fibrils could lead to distinct synucleinopathies (Peelaerts et al., 2015; Van der Perren et al., 2020).

Through genetic analysis, researchers have gained valuable insights into the toxicity and aggregation of αSyn. Studies have shown that elevated levels of αSyn are directly linked to the onset of familial PD, where the SNCA gene is duplicated or triplicated (Singleton et al., 2003; Chartier-Harlin et al., 2004; Oliveira et al., 2015; Konno et al., 2016). Additionally, six-point mutations in the SNCA gene have been linked to familial PD, including A30P, E46K, G51D, A53E, and A53T, predominantly located in the N-terminal region of the protein, affecting its native state and membrane binding capacity (Krüger et al., 1998; Zarranz et al., 2004; Appel-Cresswell et al., 2013; Lesage et al., 2013; Pasanen et al., 2014).

PD animal models

While the experimental use of animals presents clear limitations and ethical considerations, it also offers several advantages as valuable tools for scientific investigation. Animals help understand disease causes, develop new treatments, and test the safety of drugs, tasks that would be ethically and practically unfeasible on humans. Depending on the research question and initial hypothesis, animal models should be chosen appropriately since different species can address other inquiries.

A wide range of models has been developed and characterized in studying PD over the years. Genetic and environmental risk factors have been assessed in small invertebrates like *Drosophila Melanogaster* and *C. Elegans* (Guo, 2010; Maulik et al., 2017). Small fish and rodents have been extensively employed for behavioral assessments and functional studies (Matsui and Takahashi, 2018). Although non-human primates (NHP) offer the best PD-related phenotypes, ethical considerations, and their high maintenance cost limits their use to a few facilities worldwide. Multiple models enable the comparison of findings across species, enhancing scientific rigor and facilitating a deeper understanding of the biological principles underpinning the human disease (Yartsev, 2017). Ultimately, researchers should always adhere to the ethical guidelines of the country and refer to the 3Rs good-practice principle (Replacement, Reduction, and Refinement). The overall aim of researchers should be to translate results into valuable clinical applications using the least number of animals and avoiding unnecessary suffering. Because of the focus of the thesis, here I will discuss the most adopted rodent models for PD research.

6-hydroxidopamine lesion model

The 6-hydroxydopamine (6-OHDA) toxin-based model was first introduced in 1968 and has since been extensively utilized to test neuroprotective compounds for Parkinson's disease (PD) (Ungerstedt, 1968). When administered through intracranial injections, 6-OHDA is selectively taken up by the DAergic system via the DAT. The molecule generates reactive oxygen species (ROS) inside neurons, leading to mitochondrial dysfunction and subsequent cell death.

Disease modeling has predominantly employed unilateral injections, mainly targeting the SNpc, the medial forebrain bundle (MFB), and the striatum (Cenci and Björklund, 2020). This approach has facilitated the study of behavioral changes resulting from imbalances in the DAergic system between the two hemispheres and has precisely linked these changes to histological analysis.

This experimental paradigm demonstrates significant reproducibility, induces robust neurodegeneration, and shows evident motor deficits in behavioral assessments. However, it should be noted that this model causes a widespread depletion of DA neurons but does not fully replicate the aspect of synucleinopathies, which involves progressive neurodegeneration and accumulation of αSyn inclusions.

αSyn-based models

The α-synuclein-based model in PD originates from the discovery of its gene-related mutations linked to familial parkinsonism and observations of abundant α-synuclein protein in LBs (Polymeropoulos et al., 1997). Transgenic animal models were initially established, enabling a broad look at the disease development (van der Putten et al., 2000). Advancements in biomedical research introduced viral vectors (adeno-associated virus (AAV) and lentivirus (LV) to deliver wild-type or recombinant αSyn to specific brain regions or neuron types (Cenci and Björklund, 2020). Recently, researchers have adopted intracerebral injections of α-synuclein fibrils, both alone and in combination with viral vectors, to reproduce better the synucleinopathy' hallmarks, such as the seeding process, the cell-to-cell spread, and the disease progression. These models offer valuable insights into the molecular mechanisms of α-synuclein aggregation and its role in PD pathogenesis.

AAV-αSyn-based model

The first AAV-αSyn-based model employed the AAV2 serotype expressing wild type (WT) and recombinant A53T human αSyn in the SNpc of rats. Tissue analysis revealed PD-like-neurodegeneration in the nigrostriatal circuitries, linked with evident motor impairments typically seen in the 6-OHDA model (Kirik et al., 2002). This investigation laid the groundwork for developing the PD AAV-αSyn animal model, serving as a pivotal starting point for numerous other research laboratories to further advance the model. Subsequent efforts have focused on enhancing the model's efficacy by optimizing the AAV serotype, construct design, and injection routes (Decressac et al., 2012b; Bourdenx et al., 2015; Van der Perren et al., 2015b).

An appealing aspect of this model lies in its progressive neurodegenerative trajectory, driven by the time-dependent expression of the virus construct. In the initial months, αSyn accumulates within DA neurons, giving rise to axonal pathology and reduced DA levels. As αSyn overexpression continues, inclusions form, ultimately leading to cell death. Notably, the emergence of motor symptoms becomes evident during behavioral tests when only 50% of the DA cell population in the SNpc are left (Decressac et al., 2012a; Lundblad et al., 2012a; Van der Perren et al., 2015a).

However, this model presents one main drawback. Different laboratories raise the concern about significant variability in the neurodegenerative response. They observed inconsistent DA cell loss and several degrees of behavioral deficit depending on the viral vector production process (Volpicelli-Daley et al., 2016; Cenci and Björklund, 2020).

The combined AAV-αSyn preformed fibrils-based model

The ability of preformed αSyn fibrils (PFF) to function as a seeding scaffold and to spread between neurons has brought researchers to investigate their pathology using in vivo models.

The pathogenic mechanism of injected PFF hinges on recruiting soluble αSyn monomer into cellular inclusions. These highly phosphorylated structures, insoluble and ubiquitinated, exhibit numerous similarities with the LBs and LNs found in the tissue of PD patients (Peelaerts et al., 2015; Luk et al., 2016).

In response to the slow neurodegenerative progression observed in this model, researchers opted to combine PFF injections with AAVs overexpressing αSyn. Notably, when the αSyn protein originated from the same species, a more rapid aggregation process was observed (Luk et al., 2016). Due to the tendency of inoculated PFF to remain localized around the injection site, while AAVs demonstrate good diffusion in brain tissue, scientists previously administered the two components at different time points. However, this approach proved to be experimentally inconvenient, leading to a higher inflammatory response linked to surgical procedures. Recent studies have demonstrated that a single mixed injection could recapitulate PD pathological hallmarks and induce motor deficits during behavioral assessments within just four weeks post-surgery (Thakur et al., 2017; Hoban et al., 2020; Negrini et al., 2022).

INTRODUCTION

Current treatments and new therapeutic strategies in PD

Despite the extensive research on this devastating disease, a cure has not yet been discovered. However, numerous treatments are currently available, helping patients' quality of life by improving their symptoms. Therapeutic approaches revolve around the restoration of DAergic signaling using a diverse range of clinical strategies. Additionally, clinical trials, holding promising results, are being conducted worldwide, involving next-generation biomedical tools such as stem-cell and gene therapy.

Pharmacological treatments

One of the most widely adopted pharmacological treatments for PD is dihydroxyphenylalanine (L-DOPA), also known as Levodopa, the DA precursor. It was introduced in the 1970s and has since been extensively used to alleviate motor symptoms and improve patients' quality of life (Ehringer and Hornykiewicz, 1960; Abbott, 2010).

Once L-DOPA crosses the blood-brain barrier, surviving DA neurons convert it to DA through the enzymatic reaction of aromatic L-amino acid decarboxylase (AADC). Increased DA levels restore neurotransmission in the basal ganglia circuitry, leading to rapid relief of motor symptoms. The treatment is combined with carbidopa, which reduces peripheral metabolism and increases its bioavailability (Contin and Martinelli, 2010).

Patients may develop motor fluctuations and dyskinesias as the disease progresses, believed to result from pulsatile DA receptor stimulation due to intermittent L-DOPA dosing. To address these issues, various strategies have been employed. One such approach is Duodopa, which provides a more stable and sustained drug delivery (Nyholm et al., 2012; Ciurleo et al., 2018). Other approaches include DA agonists, monoamine-oxidase type B (MAO-B) (Rabey et al., 2000; Rascol et al., 2005), (Crosby et al., 2003), catechol-o-methyltransferase (COMT) (Nutt et al., 1994), and anticholinergics (Katzenschlager et al., 2003).

Deep brain stimulation

Deep brain stimulation (DBS) is currently the primary surgical procedure for treating PD patients. It involves implanting electrodes in the STN or GPi, to deliver electrical impulses (Dougherty, 2018). DBS offers particular advantages to patients who have experienced complications with pharmacologically based therapies. Benefits rely on the principle of the technique to be adjustable, allowing for personalized treatment and long-term symptom management. DBS modulates abnormal neuronal activity, providing significant symptom relief in PD patients. DBS offers particular advantages to patients who have encountered complications with pharmacologically based ther-

apies. The technique's adjustable nature facilitates personalized treatment and long-term symptom management (Groiss et al., 2009).

Cell base therapy

This approach is particularly interesting in PD since it can replace the DAergic cells responsible for the disease. Extensive research has been conducted in this area, with the first human clinical trial dating back to 1985, where autologous grafts from adrenal medullar tissue were transplanted to the striatum of two severely Parkinsonian patients (Katzenschlager et al., 2003). Unfortunately, this initial attempt did not yield significant clinical benefits. This strategy was later replaced by tissue transplantation from aborted fetuses and demonstrated promising results with clinically relevant improvements (Lindvall et al., 1989).

In the early 1990s, more PD patients were transplanted with fetal ventral mesencephalic (fVM) tissue in the striatum. Although results were variable, some patients reduced or completely stopped L-DOPA treatment reporting long-term symptomatic relief (Lindvall et al., 1990; Lindvall et al., 1994; Freeman et al., 1995; Brundin et al., 2000). After a quarter of a century, postmortem histopathological analysis of transplanted patients revealed how surviving grafts were well innervated in the host tissue (Barker et al., 2013; Kefalopoulou et al., 2014; Li et al., 2016).

However, one crucial concern was using tissue from aborted fetuses, which posed logistical and ethical challenges. The field continued to progress, searching for valuable alternatives, and significant advancements were made with refined and established protocols for generating and differentiating stem cells into DAergic neurons (Kirkeby et al., 2017; Nolbrant et al., 2017; Nolbrant et al., 2020). Several ongoing clinical trials in Japan, Europe, and the USA employ human induced pluripotent or embryonic stem cells. While the technical procedures have been successfully conducted, data reporting patients' clinical improvements are yet to be published.

Gene-based therapy

Gene-based therapies involve the introduction of functional genes or genetic material into targeted cells to correct or replace faulty genes. In this context, retroviral vectors are commonly used as delivery vehicles. Various vectors have been extensively examined to ensure the efficient delivery of therapeutic genes to specific brain regions. AAVs, in particular, have garnered significant attention due to their inherent biological attributes. These include their low immunogenicity and the ability to engineer their capsid for tailored cell tropism. However, I will discuss this in more detail in the following section and focus here more on their current and future clinical applications.

To date, 15 clinical trials have employed AAVs in treating PD patients. The initial approach aimed to restore the basal ganglia's physiological activity by delivering rate-limiting enzymes. The pioneering attempt in 2003 involved unilateral injection of AAV2-expressing GAD into the subthalamic nucleus in 12 patients (Luo et al., 2002; Emborg et al., 2007). Another strategy utilized AAV2 expressing the AADC enzyme to convert L-DOPA into DA in the putamen (Bankiewicz et al., 2000). Parallel research revealed the potential of neurotrophic factors to support the DAergic system (Rosenblad et al., 1999).

Researchers have identified and tested several neurotrophic factors for Parkinsonian patients, such as Glial cell line-derived neurotrophic factor (GDNF), neurturin (NRTN) , platelet-derived growth factor BB (PDGF-BB), and the cerebral DA neurotrophic factor (CDNF). Out of these, GDNF has shown the most promising results and has been the focus of seven clinical trials. The initial two attempts using AAV2-Neurturin were focused on the putamen and yielded satisfactory safety outcomes. However, the efficacy outcomes were generally disappointing, with significant variability observed in patients' symptoms (Bartus et al., 2014; Björklund and Davidsson, 2021).

GDNF has been the focus of numerous studies and has shown promise in treating neurological conditions. Two clinical trials using AAV2 targeting the putamen are still underway, but preliminary results have been conflicting. The inconsistent findings make it challenging to draw a definitive conclusion about GDNF's neuroprotective properties. Several factors, including delivery site and method, dosage, patient age, and disease stage, may have contributed to the lack of success in some cases (Bartus et al., 2014).

Adeno-associated virus

General discussion

In 1965, Bob Atchison discovered a tiny species of viruses (22nm) and named AAVs after finding them in the same preparation of Adenovirus (Atchison et al., 1965). AAVs belong to the family of Parvovirus, and since they require a helper virus, such as adenovirus or herpesvirus, to replicate efficiently in host cells, they were classified in the genus of Dependovirus. Wild-type AAVs possess a small single-stranded genome encoding for replication (rep), capsid (cap), assembly-activating protein (AAP) and membraneassociated accessory protein (MAAP) ORFs, flanked by inverted terminal repeats (ITRs) of 145 base pairs (bp). Upon cell transduction, AAVs can go through a lytic or lysogenic cycle.

Without a helper virus co-infection, the AAVs genome will take the lysogenic fate integrating into loci AAVS1 loci chromosome19 (q13.4) (Kotin et al., 1990). The lytic cycle occurs after AAVs co-infect the cell with Adenovirus or Herpes Simplex Virus (HSV). The DNA will replicate, and the capsid will form thanks to the external adenoviral genes.

The 4.7 kb genome is relatively small compared to other viral species but is sufficient to carry essential genetic information to allow gene replication, capsid synthesis, and viral particle packaging. Most general knowledge of AAVs comes from studies conducted on the AAV2 serotype. The Rep sequence encodes for four distinct nonstructural proteins (Rep40, Rep52, Rep68, Rep78) involved in the different steps of DNA replication. On the other hand, the Cap sequence encodes for three structural proteins, VP1, VP2, and VP3. A total of 60 subunits are assembled into a stable icosahedral non-enveloped capsid in a ratio of 1:1:10 respectively.

Variations in the aminoacidic sequences of the capsid proteins generate different AAV serotypes. Depending on the serotype, the protrusions and pores on the capsid will interact differently with molecules expressed on the cells' surface. Over a hundred AAV serotypes have been identified, each with distinct tissue tropisms. In comparing the different serotypes, researchers identified 12 highly variable surface regions, with most variations concentrated around the threefold proximal peaks (Xie et al., 2002; Gao et al., 2003).

The principal protein surface targeted by the AAV2 is the heparan sulfate proteoglycan (HSPG) (Summerford and Samulski, 1998). This serotype has also reported enhanced transduction efficacy upon the recognition of the fibroblast growth factor receptor 1 (FGFR1) and $\alpha V\beta 5$ integrin co-expressed on the cell surface (Qing et al., 1999; Summerford et al., 1999). In AAV serotypes 4 and 5, sialic acid is reported to mediate cell entry (Kaludov et al., 2001; Walters et al., 2001). Enhanced transduction for the AAV5 serotype was seen in the presence of platelet derived growing factor co-receptor. Serotypes AAV3 and AAV8 are Laminin dependent for cell endocytosis, while the N-linked galactose receptor is for AAV9 (Akache et al., 2006; Shen et al., 2011). These receptors are broadly expressed within the human body, making the AAVs family capable of targeting all tissue types. Moreover, the generally low immunogenicity and cytotoxicity observed show the vast potential of AAVs as a molecular tool not only to elucidate the intricate mechanisms behind diseases but also to become a possible treatment (Chirmule et al., 1999; Hernandez et al., 1999).

Gene transfer vectors

In 1984, Hermonat and Muzyczka made a significant breakthrough by recombining the AAV genome to express foreign genes in mammalian cells, laying the foundation for viral vector-based research (Hermonat and Muzyczka, 1984). To create recombinant AAVs, researchers replace the viral Rep and Cap genes with a transgene flanked

by ITRs. This modification eliminates viral genes, resulting in a replication-defective virus that prevents uncontrolled replication in the host cell. Additionally, without the Rep gene, the virus cannot integrate into the host genome and remains an episomal element within the cell.

As the ITRs are vital for capsid formation, the total available space for fitting the transgene into the AAV is limited between 4.5 to 4.7 kb. This limited loading capacity is considered the primary drawback of AAVs, leading researchers to explore more efficient and shorter expression cassettes. Various strategies have been employed, including the use of small promoters, enhancer elements, and polyA sequences, all of which have proven to be equally effective (Powell et al., 2015; Li and Samulski, 2020). Typically, AAVs package single-stranded DNA that must be synthesized into a double-stranded form before gene expression can occur. This process is a rate-limiting step that delays the expression. Scientists have developed self-complementary AAVs (scAAVs) to overcome this limitation, resulting in a higher and more rapid transgene expression. (McCarty et al., 2001). However, this approach comes with the trade-off of reducing the AAV's DNA capacity significantly.

One important goal for viral vector technologies is to limit the expression of the transgenes to the targeted cell population. While AAVs exhibit some natural tissue tropism based on their capsid heterogeneity, they can still result in undesirable off-target expression. Various methods can be implemented to achieve precise gene expression using viral vectors. One such method is the use of selective promoters, DNA sequences that activate transcription only in a specific cell type or tissue. For instance, in CNS applications, researchers have reported that the use of scAAVs that express a reporter gene under either the Synapsin-1 (Syn-1) or Glial fibrillary acidic protein (GFAP) promoters can efficiently facilitate gene expression in either the neuronal or glial cell populations (Kügler et al., 2003; Lawlor et al., 2009; Dashkoff et al., 2016). In experimental settings, off-target gene expression can be further minimized by utilizing transgenic Cre animals alongside AAVs-Cre-dependent cassettes. Transgenic animals express the bacterial Cre recombinase in specific cell populations using cell-type-specific promoters. The AAV-Cre-dependent cassette can be created with a double-floxed inverse ORF or a stop codon positioned between two loxP sequences (Haery et al., 2019).

AAV capsid engineering is another angle where researchers have put much effort into achieving precise gene delivery. Two primary approaches have been used: directed evolution and rational design. Directed evolution involves subjecting AAV libraries to selective pressures, leading to variants with improved traits, such as enhanced transduction efficiency or reduced immunogenicity (Maheshri et al., 2006; Asuri et al., 2012). In contrast, rational design relies on understanding capsid structure and function to engineer specific modifications that can optimize the viral vector's performance (Kanaan et al., 2017; Davidsson et al., 2019).

Molecular barcodes - AAV libraries

Researchers use molecular barcodes to label and examine individual molecules within complex mixtures. These barcodes are made up of short, unique sequences of DNA or RNA, typically around 20 base pairs in length. This versatile technique is widely used in various research fields, including single-cell genomics, high-throughput sequencing, and viral vector libraries. The barcode length can be customized to suit the specific needs of each application. As more nucleotides are added to the sequence, the number of potential combinations grows exponentially, providing greater flexibility and accuracy in molecular identification and tracking.

In single-cell genomics, where individual cells are isolated and analyzed separately, molecular barcodes display the heterogeneity and characteristics of individual cells (Delley and Abate, 2021). In high-throughput sequencing, molecular barcodes enable the sequencing of multiple samples simultaneously, resulting in time and resource savings (Reuter et al., 2015).

Viral vector technology uses molecular barcodes to track viral populations by assigning unique identifiers to each viral particle through genome integration. This approach has been used extensively adopt to develop new viral capsids (Adachi et al., 2014; Davidsson et al., 2019), study intricate connections (Kebschull et al., 2016), and investigate the molecular alteration between viruses and cells' hosts (Figure 5, see **Paper II** and **III**).

Figure 5 | Schematic representation of a barcoded viral vector. AAVs containing barcoded alpha-synuclein (αSyn). The molecular barcode is a highly variable nucleotide sequence that gives a unique identity to all the viral particles present in the suspension. A: Adenine, T: Thymine, G: Guanine, C: Cytosine. Letters B, D, H, and G can be any of the following nucleotides. B: Guanine, Thymine, Cytosine - D: Guanine, Thymine, Adenine - H: Adenine, Cytosine, Thymine - V: Guanine, Cytosine, Adenine.

Gene editing in the CNS

General discussion

Gene editing technologies allow for the accurate manipulation of genetic material. This can correct genetic defects, introduce new genes, or modify the expression of existing ones. (Naldini, 2015; Dunbar et al., 2018). During the early 2000s, scientists identified DNA-binding platforms that allowed for precise gene editing, such as zinc-finger nucleases (ZFNs) and transcription activator-like effector nucleases (TALENs). However, these technologies were complex and generally took much time to design (Christian et al., 2010; Urnov et al., 2010).

In 2012, Doudna and Charpentier led pioneering work that revolutionized the gene editing field. They identified Clustered Regularly Interspaced Short Palindromic Repeats (CRISPR)/CRISPR-associated protein 9 (Cas9) as a versatile and efficient tool. CRISPR-Cas9 works through a small RNA molecule named single-guide RNA (sgRNA), which guides the Cas9 enzyme to a specific DNA target sequence. Once Cas9 reaches its target, it creates a double-stranded break (DSB) in the DNA (Jinek et al., 2012). The DSB occurs in 2-6 base pairs upstream of a protospacer adjacent motif (PAM), determined by the Cas9 protein. This limits the system's ability to target any sequence. However, many new Cas proteins have been characterized and engineered, which require different PAMs (Westra et al., 2016; Wright et al., 2016).

CRISPR-Cas9 could be programmed by simply changing the sequence of the sgRNA to target different DNA locations. This made gene editing much more accessible and cost-effective. The simplicity and versatility of this system quickly captured the attention of scientists worldwide, and many laboratories started to implement it in their research lines (Hsu et al., 2014; Sander and Joung, 2014; Komor et al., 2017).

In the context of genome editing, the induction of a DSB leads to two distinct outcomes. These outcomes encompass non-homologous end-joining (NHEJ) and homology-directed repair (HDR) pathways. NHEJ is an error-prone mechanism with the insertion or deletion (indel) of nucleotides at the cut site, disrupting gene function. Conversely, HDR involves the precise insertion of a donor DNA template, often employed to rectify specific mutations within the targeted genomic region (Doudna and Charpentier, 2014).

The use of HDR-mediated gene editing shows promise for therapeutic purposes. However, it is often less effective than NHEJ and is typically limited to the G2 and S stages of the cell cycle (Mao et al., 2008; Heyer et al., 2010; Xue and Greene, 2021). Applying HDR-based editing to non-dividing cells like neurons can be challenging,

as many recombination factors are strictly downregulated (Orthwein et al., 2015). A study published in 2017 showed encouraging outcomes in the mammalian brain using HDR technology (Nishiyama et al., 2017). However, several research groups could not replicate the same results (Nishizono et al., 2020; Avallone et al., 2023). On the other hand, Suzuki and colleagues reported a successful NHEJ-based strategy named homologous independent targeted integration (HITI). In their experiments, they correctly inserted in non-dividing cells a reporter sequence at the 3′ of the tubulin gene (Suzuki et al., 2016). New applications have been developed based on the HITI mechanism, which improves and strengthens our understanding of this tool for gene editing in post-mitotic cells (Gao et al., 2019; Willems et al., 2020).

AAV-HITI system

Due to the relatively large size of the Cas9 (4 kb for the streptococcus pyogenes), the HITI system split the nuclease and the sgRNA with the donor template (DT) into two separate AAVs. Therefore, the gene editing technique needs the two AAVs to infect the same cell.

The system's design has the DT sequence flanked by the gRNA targeted sequence. When the gRNA/Cas9 complex is correctly formed and assembled, it will cause DSBs on the target site present in the host genome and the sequences flanking the DT. The system utilizes spCas9 to make a cut in the targeted sequence, which occurs three bp upstream to the NGG-PAM. This results in the targeted sequence being separated into a 17-bp and a 6-bp fragment (referred to as "long" and "short"). As the same cut is operated on the DT sequence, a long and a short fragment are also left flanking the DT. During the NHEJ repair, the DT can be integrated into the cell genome.

If the DT integration reconstructs the targeted sequence (long-short), the gRNA/Cas9 complex will identify the sequence and cut it again. However, if the DT integration does not reconstruct the target sequence (long-long or short-short), the gRNA/Cas9 complex will not cut further. As a result, the DT will be correctly knocked in (Figure 6). Due to the system's design, the regions flanking the knocked-in DT will always be long-long and short-short fragments. These sequences are palindromic, and other mutations might occur upon microhomology-mediated end-joining (MMEJ) repair (McVey and Lee, 2008).

Researchers have developed a machine learning tool to predict the highest mutation rate, which could happen during NHEJ repair (Allen et al., 2018; Chen et al., 2019). Implementing these technologies during the design of HITI experiments could save time and resources, as well as more predictable results.
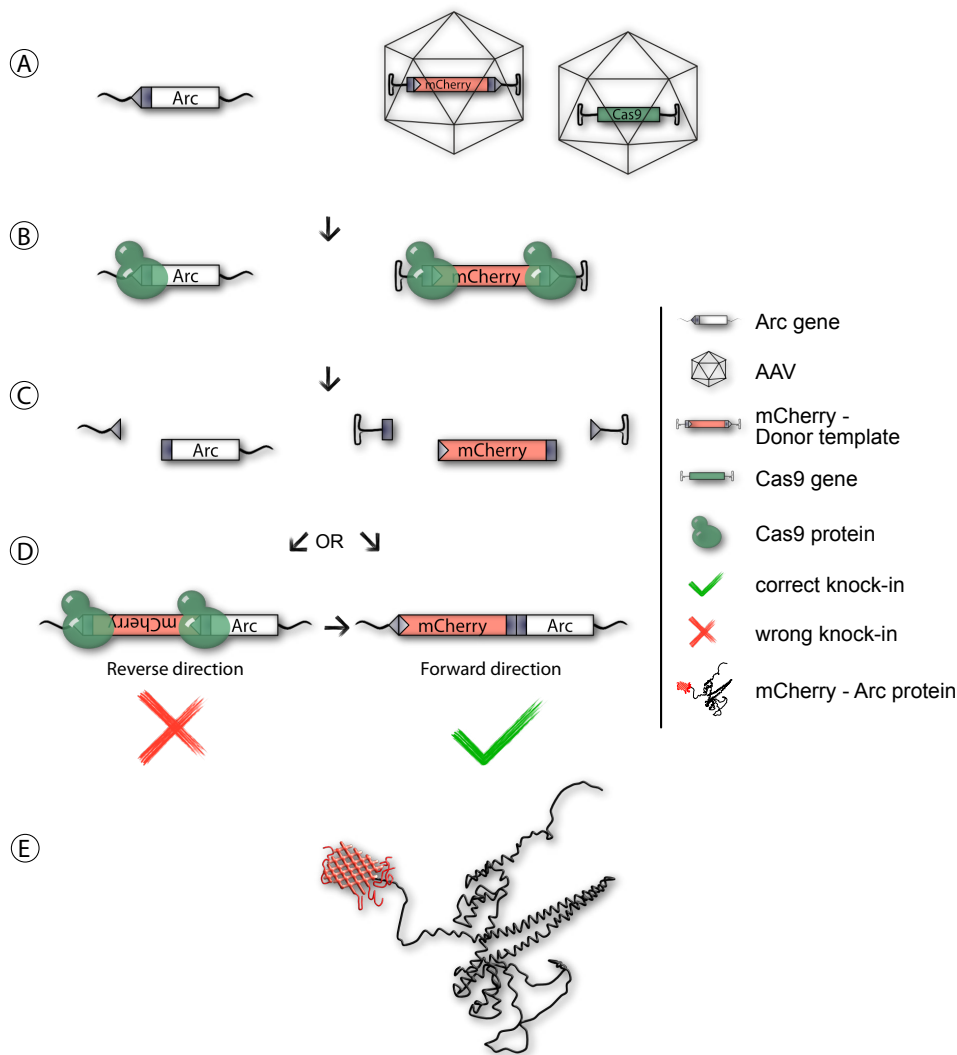
Figure 6 | Schematic representation of the HITI-gene editing mechanism targeting the Arc gene.
[A] Arc genomic locus. AAVs containing the donor template (DT) mCherry and the Cas9. **[B]** The Cas9
protein is shown in green and works together with the gRNA to bind to specific sequences in both the
Arc gene and the flanking regions of the DT, **[C]** operating a double-strand break (DBS). **[D]** The NHEJ
repair mechanism starts to fix the Arc gene. During NHEJ, the DT can be inserted in either a reverse or
forward direction. If inserted in the reverse direction, the targeted sequence is reconstructed, allowing
Cas9 to make another cut. If inserted in the forward direction, the DT is permanently integrated. **[E]** 3D
structural protein representation of the mCherry fluorescent protein fused on the N-terminal domain
of the Arc protein.

Single-cell RNA sequencing

Single-cell RNA sequencing (scRNA-seq) is a powerful technique to study the gene expression profiles of individual cells within a complex tissue or population. Traditional bulk RNA sequencing offers a general transcriptomic readout of all cells in a sample. However, scRNA-seq provides a deeper understanding of the variety and differences in gene expression at the individual cell level. This can be used to understand how cells differ from each other, how they change over time, and how they respond to different stimuli.

Since the establishment of the technology to the most recent and updated protocol, all single-cell methodologies involved precise cell isolation procedures while ensuring RNA integrity. In a general discussion, the amount of mRNA in a cell is limited and can quickly degrade. The initial step involves creating and increasing the amount of cDNA through synthesis and amplification. During reverse transcription, oligo-dT, random hexamers, or gene-specific primers that contain an adaptor sequence are utilized. When reverse transcriptase (RT) enzymes reach the end of mRNA, their intrinsic biology adds cytocines. A template-switching oligo (TSO) is used to facilitate second-strand DNA synthesis. The second adapter sequence from the TSO is then utilized for cDNA amplification. This is then followed by library generation, sequencing, and bioinformatics analysis.

Tang and colleagues were the first to report a successful investigation on unbiased transcriptomics analysis from single cells (Tang et al., 2009). In the field of single-cell transcriptomics, is key the development of techniques that allow for the profiling of a large number of cells in parallel. Inspired by Guo and colleagues' work, Linnarson's laboratory developed single-cell tagged reverse transcription (STRT) for unbiased transcriptomics readout of multiple cells simultaneously (Islam et al., 2011). Later on, from the same concept, the authors implemented unique molecular identifiers (UMIs) to quantitatively measure gene expression from 3000 transcriptomes from cortical and hippocampal neurons (Islam et al., 2014; Zeisel et al., 2015). Significant progress in detecting and measuring all types of transcript variants was made through the development of SMART-seq (Ramsköld et al., 2012) and its upgraded version, SMART-Seq2 (Picelli et al., 2014). These techniques utilize specialized RT for TSO reaction and cDNA amplification, improving read coverage throughout the transcripts.

During the technology's initial phases, cells were separated manually using tubes or plates to maintain single-cell precision. The methodology was improved by microfluidic systems like fluorescent activated cell sorter (FACS) and liquid handling robotics, which helped analyze more cells.

INTRODUCTION

A significant advancement was made through the use of Drop- and InDrop-Seq protocols. These technologies utilize a droplet-based approach to capture single cells and barcode their RNA transcripts for subsequent sequencing (Klein et al., 2015; Macosko et al., 2015). Combining this method with microfluidics has resulted in the development of the 10X Chromium system. This technology has recently gained popularity for its ability to provide consistent and predictable results. Research groups have implemented in their experiments to investigate tissue composition and cellular diversity.

The process begins with individual cells isolated and suspended in a special buffer. Using a microfluidic device, thousands of cells are separated and combined with Gel Beads that have unique barcodes. Within each tiny partition, the cells are broken down, releasing their RNA content and starting reverse transcription. This creates cDNA that includes the barcode sequence from the Gel Bead, connecting it to the original cell. Next, the partitions are broken, and the barcoded cDNA is combined and amplified for library preparation.

A different approach to multiplexing cells is found in instrument-free protocols. These protocols utilize combinatorial barcoding indexing in which cells are divided among wells in a multiwell plate. Each well has a unique barcode sequence. During cDNA synthesis, all transcripts are labeled with the first barcode. The cells are then mixed together and redistributed into wells with different barcodes on another plate. A second barcode is added to the cDNA through ligation. This process can be repeated several times, making it highly unlikely that any two cells' cDNA will share the same barcode combination. This method is known as SPLiT-Seq and was developed by Rosenberg et al. in 2018 (Rosenberg et al., 2018). It has since become a kit sold commercially by Parse Bioscience.

Studying single cells becomes difficult when preparing cell suspensions from specific tissues, particularly in disease settings. Recent studies reported that investigating single nuclei RNA sequencing could be a feasible alternative to exploring the entire cell transcriptome (Lake et al., 2016; Lake et al., 2017). Preparing nuclei has advantages such as cleaner suspensions leading to more accurate results. FACS methodologies have integrated nuclear preparations, resulting in Fluorescent-Activated Nuclear Sorting (FANS). By using targeted antibodies or intrinsic fluorescent markers, the nuclei subset of interest can be selectively enriched, increasing the sample size and the starting material.

Other methods exist to isolate and enrich the population of interest, such as laser-capture microdissection (LCM). Although LCM helps preserve spatial information, it is a low-throughput and not a very clean technique. Material from surrounding cells may be collected during the protocol execution (Shapiro et al., 2013)

Technology miscellaneous

Proximity ligation assay

The Proximity Ligation Assay (PLA) concept was introduced by Ulf Landegren's laboratory in 2002 (Fredriksson et al., 2002). The technology was further refined by combining it with rolling circle amplification (RCA) to directly visualize protein-protein interactions within cells and tissues (Banér et al., 1998; Söderberg et al., 2006). PLA involves using pairs of oligonucleotide-labeled antibodies, known as PLA probes. These probes recognize two distinct epitopes on the target proteins. When the PLA probes bind to their respective targets within a 30-40 nm range, they can be ligated, creating a circular DNA template. When the DNA template is amplified through RCA, it produces a single-stranded product consisting of several thousand-fold the length of the original DNA template. This product is covalently linked to the antibody-antigen complex. Fluorescent-labeled probes will bind to the RCA, producing a solid focal fluorescent signal. This signal indicates a protein-protein interaction with higher accuracy than traditional immunohistochemical approaches.

Since its development, the PLA approach has undergone significant refinements, becoming commercialized by many biotech companies. One particular variation is characterized by using the "UnFold" approach, which involves having all the necessary components for signal formation already fused within the probes. Researchers have demonstrated that this strategy yields notably lower background noise levels than traditional PLA and further increases its sensitivity and specificity (Figure 7) (Klaesson et al., 2018).
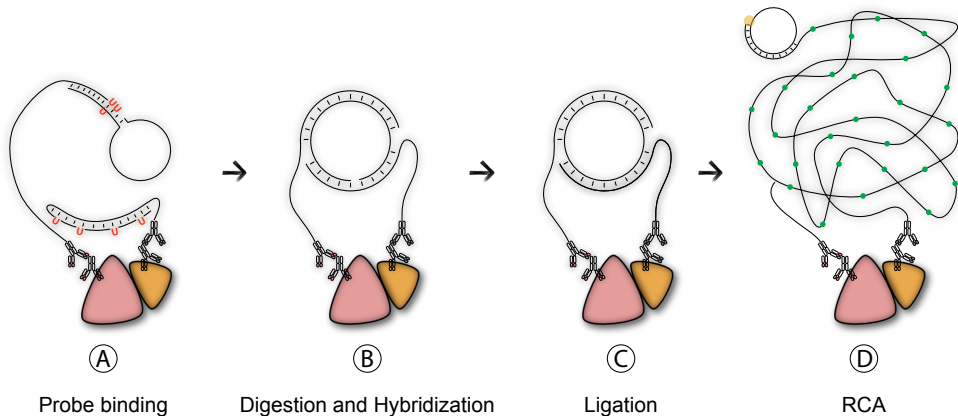
Figure 7 | Schematic drawing of the PLA biochemical reactions. [A] Epitope recognition by antibodies paired with oligonucleotides. **[B]** Digestion of the uracil residues releasing allows for the hybridization of the oligoprobes sitting on the antibodies. **[C]** Ligation sealed the double-strand structure. **[D]** A polymerase begins an RCA, which incorporates fluorescent nucleotides resulting in a strong signal.

Additional adaptations of the protocol have expanded the versatility of the original assay, allowing for the detection not only of interactions between endogenous proteins but also for post-translational modifications and even protein-nucleic acid interactions (Ghanipour et al., 2016; George et al., 2021).

Spatial transcriptomic

In the early 21st century, the introduction of high-throughput sequencing allowed for the examination of gene expression on a large scale. However, conventional transcriptomics techniques cannot retain spatial information, which limits the understanding of gene expression within the tissue architecture. To address this issue, scientists have developed spatial transcriptomics (ST) to obtain gene expression profiles that are spatially resolved (Ståhl et al., 2016).

In the initial ST experiment and **Paper IV**, the chip contained 1007 spots, with each label featuring around 200 million oligonucleotides attached. These oligonucleotides contain several important elements and are at the core of the technology. These oligonucleotides are essential to the technology and consist of various critical elements. Firstly, a specialized barcode provides unique spatial information for each position on the glass surface. Secondly, a UMI enables counting mRNA copies. Thirdly, the oligo-dT sequence captures the polyadenylated mRNA from the permeabilized tissue sample. Lastly, a T7 promoter, and a cleavage site for the USERTM enzyme, facilitate linear amplification and a release of reverse-transcribed transcripts.

ST has seen many technological advancements since its discovery. Various platforms like Slide-seq, Visium, and STARmap have emerged, each with unique strengths in resolution, throughput, and ease of use (Wang et al., 2018; Rodriques et al., 2019). Thanks to these platforms, spatial transcriptomics has been applied to various biological systems and research questions. For instance, RNA expression profiles of different human adult sarcoma, as well as for drug discovery (Ståhl et al., 2016; Ghorbani et al., 2022; Qi et al., 2022).

Aims of the thesis

I. To show the cell-cell transfer of the Arc retrotransposon in the mammalian brain, using a gene editing CRISPR/Cas9-based technology and advanced immunohistochemistry techniques.

II. To investigate the impact of αSyn overexpression in DAergic neurons utilizing CRE-dependent AAVs with molecular barcodes in the MNM008 capsid, enabling single-nuclei sequencing in TH CRE rats.

III. To elucidate the molecular changes at the single-cell resolution during PD development in the SN of a mouse model, with a focus on the impact of viral particle load and pre-formed fibrils.

IV. To evaluate spatial transcriptomics as a technology for cell-type classification and quantification compared to the single-cell sequencing methodology focusing on a human embryonic stem cell-based transplant.

Summary of key results

Paper I

In 2018, two studies were published reporting the observation of Arc forming VLPs and transferring genetic material to other cell types (Ashley et al., 2018; Pastuzyn et al., 2018). However, this phenomenon had not yet been demonstrated in the mammalian brain. To visualize this cellular trafficking, we considered knocking in a fluorescent tag to the Arc protein and using it as a reporter. In the attempt to do this, we extensively characterized the CRISPR/Cas9 Homology Independent Targeted Integration system (Suzuki et al., 2016).

We observed increased mCherry expression when Arc expression was induced with HFS-induced LTP in dentate granule cells. Consistent with previously published data, we found that the mCherry-Arc fused protein interacted with Stargazin at the post-synapse. Additionally, we show interneuronal transfer as PLAs formed with the presynaptic protein Bassoon.

Targeting Arc 5´ UTR using HITI yields an out-of-frame insertion

Initially, our focus was on targeting the 5' UTR while preserving the integrity of the 3' region, which is critical for capsid formation and neuronal uptake. We designed AAVs to deliver the HITI system to introduce either GFP or mCherry at the 2[-] site (Figure 8A). After three weeks following viral injection, animals were euthanized, and their tissues were processed for histological or molecular analyses. We successfully transduced neurons using GFP and mCherry AAVs with the sg2[-] sgRNA (Figure 8B, C). PCR analysis of the extracted DNA from the injected tissues confirmed the presence of the reporter sequences (Figure 8D).

However, Sanger sequencing demonstrated that despite efficient expression of mCherry and GFP, frameshift mutations occurred in the 3' region of the insertion, resulting in an out-of-frame translation of the Arc ORF. Consequently, the fluorescent protein failed to fuse with the Arc protein. This was further investigated and confirmed with NGS analysis of the mCherry tag. Therefore, we concluded that although the editing and insertion efficiency was high at the sg2[−] position of the Arc 5' UTR, the frameshift mutations prevented proper fusion of the fluorescent protein with the Arc protein.
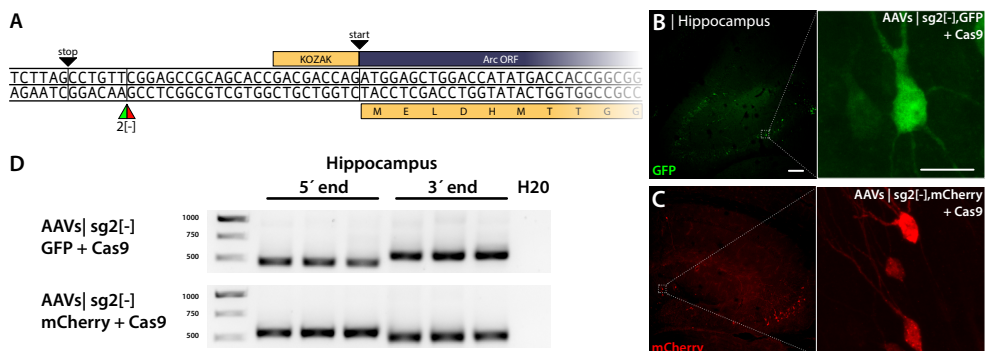
Figure 8 | HITI-mediated gene editing when targeting the Arc 5´ UTR [–] strand. [A] 5´ Arc sequence. TAG stop codon in frame with the ATG start codon of the Arc gene. 2[–] is the target site of the gRNA designed to insert the fluorescent tag. **[B-D]** IHC hippocampal brain sections from animals injected with the HITI system targeting the 2[–] site. **[B, C]** GFP and mCherry knock-in, showing green and red fluorescent cells, respectively. In **[B]**, the left scale bar is 50 µm, and in the right, it is 20 µm. **[D]** PCR amplicons on bulk DNA extracted from the hippocampus, amplifying the 5´ and 3´ regions of the knocked-in DT.

Targeting Arc at the ORF 5' region results in a functional mCherry-Arc fused protein

Following our initial findings, we investigated the potential benefits of targeting the [+] strand instead of the [-] strand using the HITI technique. Our rationale was based on the assumption that a shorter microhomology sequence at the 3' edit site would improve knock-in accuracy. To evaluate this hypothesis, we designed AAVs-HITI constructs to target the coding strand of the Arc 5' UTR sg1[+] and a specific region within the Arc ORF 9[+] (Figure 9A).

Both experimental approaches yielded a sparse number of fluorescent cells (Figures 9B, C). PCR amplification targeting the 5' and 3' regions of the insert generated the expected bands (Figure 9D). Interestingly, the sg1[+] approach unexpectedly resulted in a high frequency of frameshift mutations at the 3' edit site, as confirmed by both Sanger sequencing and NGS analyses. On the other hand, the sg9[+] insertion exhibited a high frequency of accurate edits in both the 5' and 3' regions, leading to the expected in-frame insertion, prompting us to focus our subsequent investigations on this specific combination of AAVs.
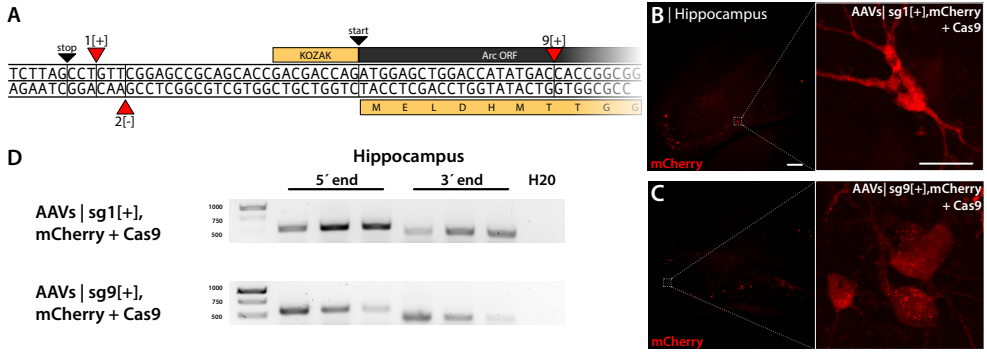
Figure 9 | HITI-mediated gene editing when targeting the Arc ORF [+] strand. [A] 5′ Arc sequence. 1[+] and 9[+] are the insertion sites of the gRNA designed for mCherry. **[B, C]** IHC hippocampal brain sections from animals injected with the HITI system targeting the 1[+] and 9[+] sites. **[B, C]** mCherry knock-in showing in red fluorescent cells. **[D]** Control group. In **[B]**, the left scale bar is 50 µm, and in the right, it is 20 µm. **[E]** PCR amplicons on bulk DNA extracted from the hippocampus, amplifying the 5′ and 3′ regions of the knocked-in mCherry.

LTP induces mCherry-Arc expression in the DG

In our investigation of mCherry-Arc fusion protein expression in transduced neurons following LTP induction, we conducted unilateral electrical stimulation of the perforant path while recording field excitatory postsynaptic potentials (fEPSPs) in the DG hilar region. All mice received bilateral injections of AAV|sg9[+] carrying mCherry in the hippocampus. The experimental group underwent high-frequency stimulation (HFS) to induce LTP, along with low-frequency stimulation (LFS) test pulses, while the control group received LFS only (Patil et al., 2023).

Upon HFS stimulation, we observed a robust induction of mCherry fluorescence, coinciding with highly specific Arc induction in the DG (Figures 10A–C). Additionally, the IEG c-Fos was equally induced in the ipsilateral DG (Figures 10 D–F"). On the stimulated side, the HFS resulted in significantly more Arc+/mCherry+ double-positive granule cells than the contralateral side (one-way ANOVA followed by Tukey HSD, $p < 0.01$). Furthermore, we noted an increased number of Arc+/mCherry+ neurons in the DG after LFS and in the contralateral DG of HFS-treated animals compared to the contralateral DG of LFS-treated animals, albeit at lower levels (one-way ANOVA followed by Tukey HSD, $p < 0.05$) (Figure 10G).

To evaluate the disparity in induction between the two stimulation paradigms, we quantified the number of c-Fos+ cells, revealing a non-significant trend towards higher c-Fos+ cell density in the HFS group (Figure 10H). Notably, the number of mCherry+ cells exhibited a significant correlation with both Arc+ cells (Figure 10I) (Pearson R 0.92 and 0.91, respectively, $p < 0.001$).
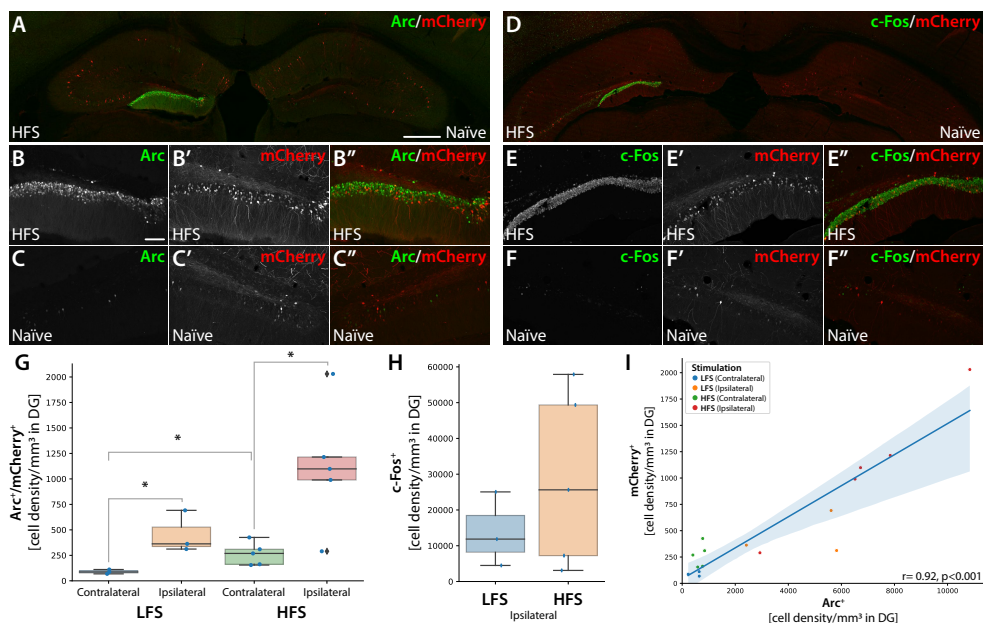
Figure 10 | Knocked-in mCherry as an activity reporter gene in the dentate gyrus following HFS-induced LTP. [A-F˝]. Immunohistochemistry (IHC) images depicting Arc and c-Fos expression in bilaterally injected mice with AAV|sg9[+], mCherry, and Cas9 in the HFS (left) and Naïve (right) hippocampus. The scale bar in **[D]** represents 500 μm, while in **[E]**, it corresponds to 100 μm. **[J]** Box plot showing cell density of double-positive cells for Arc and mCherry in the DG. *Statistically different (one-way ANOVA, p ≤ 0.05, followed by Tukey's HSD) (LFS n = 3, HFS n = 5). **[K]** Box plot illustrating c-Fos immunoreactive cell density in the DG for LFS and HFS. LFS n = 3, HFS n = 5. **[L]** Correlation plot depicting the relationship between mCherry+ and Arc+ cells in the dentate gyrus. Each animal sample is denoted by hemisphere (contralateral or ipsilateral) and group (LFS or HFS).

Proximity ligation assay shows the chimeric mCherry-Arc protein interaction with pre- and post-synaptic modules

Initially, we employed the PLA using mCherry and Arc antibodies as molecular tools to validate the correct expression of the fused mCherry and Arc proteins. Subsequently, we sought to investigate whether the insertion of mCherry was affecting the biological function of Arc. Previous research has indicated that Arc interacts with other post-synaptic proteins such as Stargazin. A functional chimeric mCherry-Arc protein would therefore form an RCA (Rolling Circle Amplification) product from PLA when in proximity with Stargazin.

Upon quantifying the mCherry/Stargazin PLA in the hippocampus injected with sg9[+], we observed a significantly higher number of mCherry-Arc RCA puncta on mCherry+ neurons compared to the frameshift control group. This effect was also evident when quantifying the RCA puncta in the neuropil (Figure 11A´). Notably, this difference was not attributable to an increased number of mCherry+ cells detected in the sg9[+] group compared to the frameshift control (Figure 11A´´).
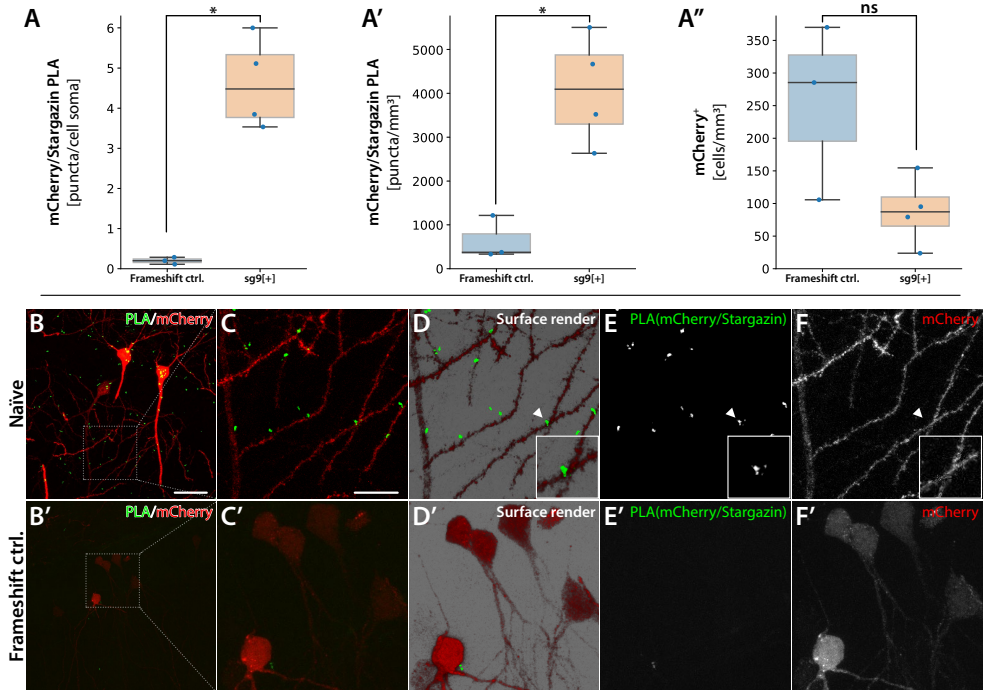
Figure 11 | PLA for mCherry-Arc/Stargazin. Panel **[A]** presents the quantification of RCA puncta per mCherry+ neuron in animals injected with sg2[−], causing a frameshift, and sg9[+], being in frame. Panel **[A´]** shows the number of RCA puncta over the neuropil. In panel **[A´´]**, the number of mCherry+ cells detected per mm3 is indicated. Statistical analysis (*statistically different, ns = not significant) was conducted using one-way ANOVA, with $p \leq 0.05$, followed by Tukey's HSD test (n = 3). The naïve tissue was not stimulated with HFS. Panel **[B]** displays pyramidal neurons from the hippocampal region CA1 of sg9[+] and frameshift control-injected naïve tissue **[B´]**. Red mCherry-labeled neurons show green RCA puncta, indicating the presence of mCherry interacting with stargazin. Panels **[C–C´]** magnify the inset in the surface render panel **[D–D´]**, revealing mCherry-stargazin on a dendritic spine (arrowhead). In panels **[E–E´]**, the RCA puncta signal represents the protein-protein interaction of the mCherry-stargazin proteins. In panel **[F–F´]**, the signal comes from mCherry-labeled cells. The scale bar in **[B]** is 50 μm, and **[B´]** is 20 μm.

Furthermore, the mCherry/Stargazin PLA revealed RCA puncta predominantly on dendritic spines (Figures 11B–F). Importantly, we did not observe any RCA puncta on the dendrites in the frameshift control (Figures 11B′–F′), nor when the Stargazin primary antibody was omitted. These results suggest that the mCherry-Arc fusion protein retains its functional interaction with Stargazin, highlighting the potential for advanced cell imaging techniques in neuroscience research. The stable and observable interaction between mCherry-Arc and Stargazin opens new avenues for investigating synaptic dynamics, protein-protein interactions, and activity-dependent plasticity in real-time, providing valuable insights into the molecular mechanisms underlying neural communication and memory formation.

Direct evidence of Arc transfer within the intact brain has been lacking to date. Considering that Arc is primarily localized in the postsynaptic neuronal compartment, we investigated the possibility of Arc transfer from postsynaptic neurons to presynaptic terminals. If mCherry-Arc is transferred from spines to boutons, it should be detectable through PLA with bassoon, an abundant presynaptic scaffolding protein.

Performing PLA in the hippocampus of animals injected with sg9[+], we utilized primary antibodies against mCherry and bassoon, which revealed the formation of several RCA puncta near mCherry+ neurons, often in the vicinity of dendritic spines, indicative of the transfer of the chimeric protein from its originating cell (Figure 12). Quantitative analysis demonstrated a significantly higher percentage of cells with RCA puncta in mCherry+/Arc+ cells (one-way ANOVA followed by Tukey HSD, $p<0.05$, Figure 12A). The mCherry/bassoon RCA puncta were predominantly found adjacent to, but not on, dendrites (Figure 12B-F), appearing sparsely around mCherry+ cells (Figures 12A′–F′).

Our findings suggest that the sg9[+] HITI approach successfully produced a functional chimeric mCherry-Arc protein with pre- and postsynaptic activity. Moreover, our in vivo data provide evidence supporting the inter-neuronal transfer of Arc.
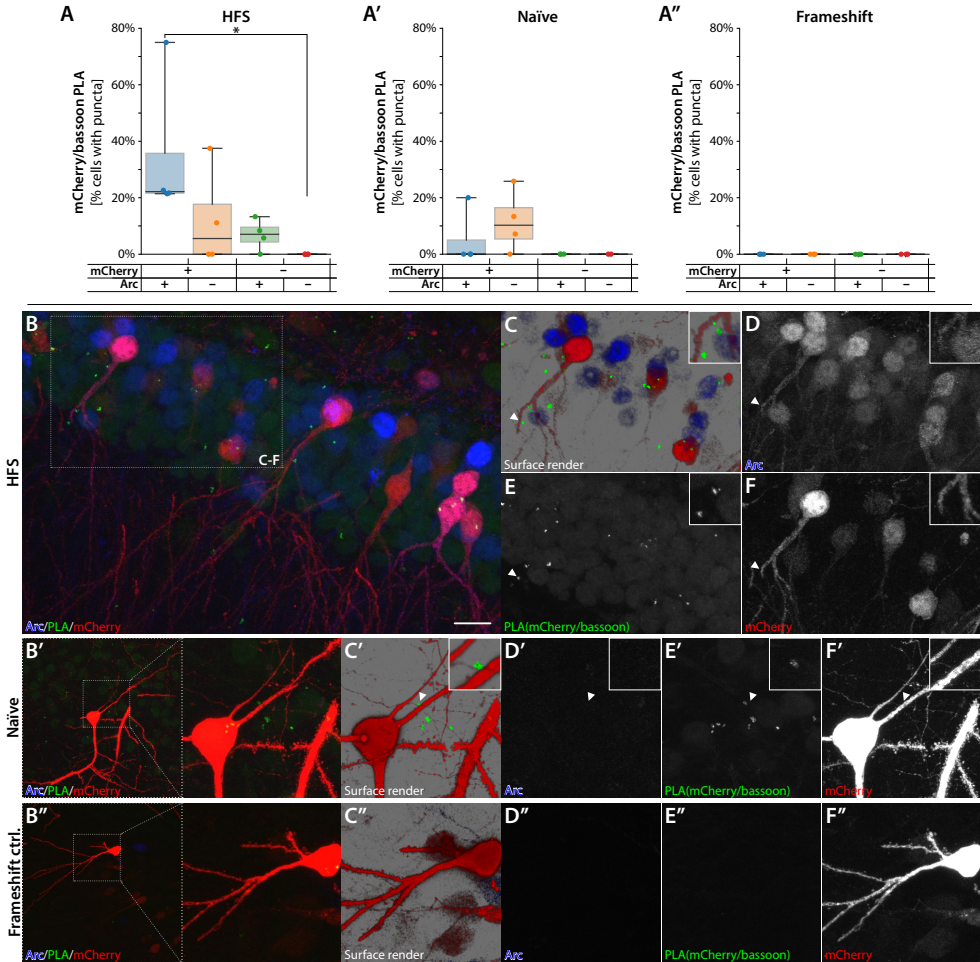
Figure 12 | PLA for mCherry-Arc/Bassoon. In panels **[A, A']**, the quantification of RCA puncta is presented for animals injected with sg9[+] in HFS and Naïve tissue, respectively. In panel **[A"]**, the quantification of RCA puncta is shown for animals injected with sg2[−], causing the frameshift. Statistical analysis (*statistically different, one-way ANOVA, $p \leq 0.05$, followed by Tukey's HSD). Panels **[B–F"]** display images acquired from the DG, with fluorescent signals coming from granule cells. Red indicates mCherry-labeled neurons, green represents RCAs for mCherry interacting with bassoon, and blue indicates Arc-positive cells. In panels **[C–C"]**, surface render images with magnified insets show mCherry-bassoon PLA adjacent to a granule cell dendrite. In panels **[D–D"]**, the signal is derived from Arc-positive cells. In panels **[E–E"]**, the RCA puncta result from the protein-protein interaction of the mCherry-bassoon proteins. In panels **[F–F"]**, the signal is from mCherry-labeled cells. The scale bar in panel **[B]** is 20 µm.

Paper II

Animal models have been instrumental in replicating PD by inducing overexpression of αSyn in DA neurons through AAV injection into the SN. Nevertheless, this approach presents certain challenges in differentiating the specific effects of αSyn from those induced by injection damage and the cellular response to AAV transduction or protein overexpression. This study shows a comprehensive report of all the experimental efforts to address and overcome these obstacles. Importantly, we compared three different single nuclei RNA sequencing techniques to answer the molecular changes induced by αSyn overexpression. The results reported in **Paper II** set a straightforward strategy, key to **Paper III**'s success.

Overexpression of tagBFP in the SN of WT rats did not lead to behavioral impairments

We begin by investigating the potential toxicity of different genes expressed under the ubiquitous CBA promoter. We packaged the constructs in AAV5 and directly injected them into the SN of WT animals (Figure 13A). After eight weeks, we conducted corridor, amphetamine-induced rotations, and cylinder tests to assess the animals' behavioral performance.

In the corridor test, the group injected with the AAV vector expressing αSyn showed a significantly lower percentage of left retrievals than the tagBFP group (Figure 13B). Based on these findings, we concluded that tagBFP serves as a suitable control protein for comparison against αSyn toxicity in the AAV-αSyn injection paradigm in the SN.
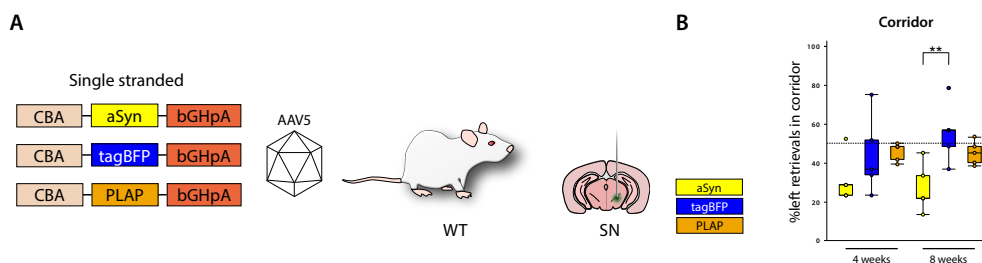
Figure 13 | Lack of Behavioral Impairment with tagBFP overexpression via AAV direct infusion into the SN. [A] Schematic representation of AAV constructs for αSyn, tagBFP, and PLAP overexpression encapsulated in the AAV5 capsid. **[B]** Stereotaxic coordinate rendering for the administration of viral vectors as depicted in **[A** and **C]** in wild-type rats. **[C]** Box plots presenting the performance results of animals injected with respective viruses at 4 and 8 weeks in the corridor, amphetamine-induced rotations, and cylinder tests. The horizontal dashed lines represent the expected outcome for unimpaired animals. N=4. ** P<0.01.

MNM008 successfully targeted SN DA cells

Our next experimental design focused on testing three different promoters (ALD-H1A1, SYN1, and TH) to express the αSyn protein. We packaged the constructs into our newly developed capsid MNM008 which efficiently facilitates retrograde viral transport (Figure 14A). The advantage of using this capsid allowed us to perform injections in two new routes, the medial forebrain bundle (MFB) and the striatum, while leaving the SN area unaffected by the surgery procedure (Figure 14B). Notably, all our approaches demonstrated successful αSyn expression along the SN-MFB-Striatum axis. Notably, the SYN1-promoter AAV exhibited robust αSyn expression in the targeted regions, as depicted in Figure 14C, C'.

Since the approach using TH CRE rats and CRE-inducible AAVs demonstrated superior on-target DAergic transduction and lower off-target effects compared to the model with WT rats and DAergic neuron promoters, we continued our investigations with the former model injecting in the striatum.
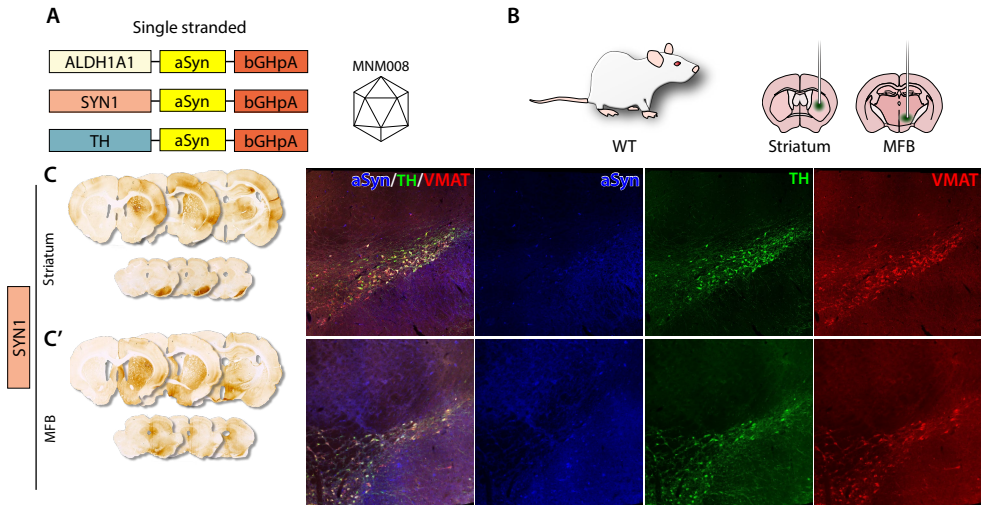
Figure 14 | Transduction of SN DA cells by injecting rat striatum and MFB with MNM008 AAVs expressing αSyn under specific Promoters. [A] Illustration of AAV-MNM008 constructs encoding αSyn under the control of DA-specific promoters. **[B]** Stereotaxic coordinate rendering for the precise delivery of the viral vectors in WT rats depicted in **[A]**. **[C-C']** Representative images of αSyn DAB staining and triple IF for αSyn, TH, and VMAT in animals injected with ALDH1A1-αSyn-bGHpA AAVs into the Striatum and MFB.

Cre-inducible vectors are successfully expressed in DA cell

To specifically target DA cells, we employed rats expressing Cre-recombinase exclusively in TH-positive cells for our experiment. The AAV constructs carried the SYN1 promoter, followed by a loxP-flanked CTE element, encoding either αSyn or tagBFP as a control (Figure 15A). These viral vectors, packaged in the MNM008 capsid, were

injected into the SN, MFB, and Striatum (Figure 15B). Immunostaining against αSyn and tagBFP confirmed uniform transduction of SN DA cells in all injected regions (Figure 15C, C'). Remarkably, this combination resulted in significantly higher on-target DA cell transduction when compared to wild-type rats injected with the SYN1-αSyn-bGHpA vector.

In summary, we successfully established a novel PD model by injecting MNM008 AAVs expressing αSyn into DA neurons using the loxP-flanked CTE-CRE system. This paradigm allowed for αSyn expression in SN DA neurons without the need for AVV injection into the SN, presenting a valuable and efficient approach to our study.
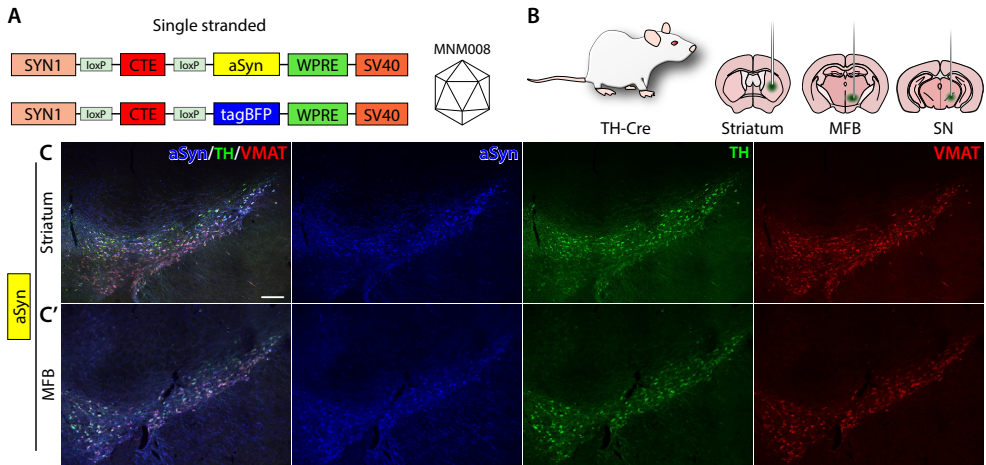
Figure 15 | Targeting DA Cells in TH CRE Rats. [A] Illustration of AAV-MNM008 constructs containing the Synapsin1 promoter (SYN1), loxP flanked CTE element, and αSyn or tagBFP genes. **[B]** Stereotaxic coordinates rendering for precise delivery of the viral vectors in TH CRE rats. **[C-C']** Representative images of triple IF for αSyn, TH, and VMAT in TH CRE rats injected with the SYN1-loxP-CTE-loxP-αSyn-WPRE-SV40 AAV in the Striatum and MFB.

A three-MNM008 AAV injections in the Striatum cover entirely SNpc projections

As a subsequent step in our investigation, we hypothesized that the strategic administration of our novel paradigm into three distinct locations within the Striatum would comprehensively target all DAergic projections originating from the SN. To verify this, we conducted IF analysis which corroborated our hypothesis, as the spatial distribution of each gene in the Striatum precisely corresponded to the expected DAergic population originating from the SN (Figure 16A-C). Building upon these findings, we further enhanced our PD model by developing self-complementary barcoded AAVs.
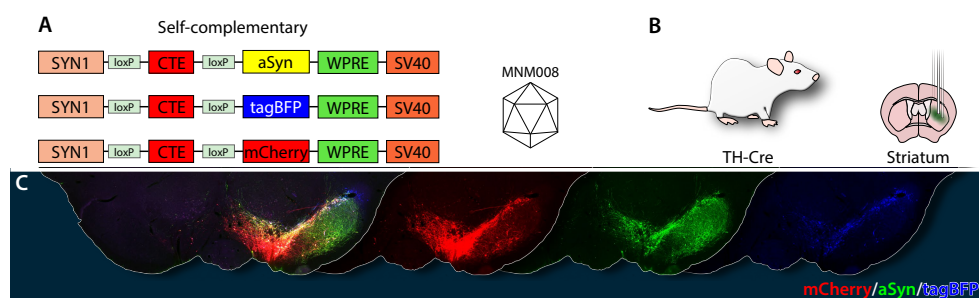
Figure 16 | Transduction of SN DA Cells along Rostrocaudal Axis by MNM008 Vectors Injected in the Striatum. [A] Illustration of self-complementary AAV-MNM008 constructs containing the Synapsin1 promoter (SYN1), loxP flanked CTE element, and αSyn, tagBFP, or mCherry. **[B]** Stereotaxic coordinates rendering for precise delivery of the viral vectors in TH CRE rats. **[C´]** Triple IF images showing the expression of the viruses retrogradely transported to the SN along the rostrocaudal axis.

Cre-inducible H2B-GFP strategy allows DA cells enrichment

To probe molecular changes occurring in the DA cells, we incorporated a 24-nucleotide long barcode downstream of the transgene in our viruses. This innovative approach enabled us to precisely quantify viral particles and transgene payload within individual DA cells. Additionally, based on the Cre-inducible H2B-GFP virus included during the AAVs injection, we set a strategy to selectively sort DA nuclei using the FACS machine (Figure 17A). This enabled us to enrich our POI around 50-fold, downsizing the cost of single-cell RNA techniques.
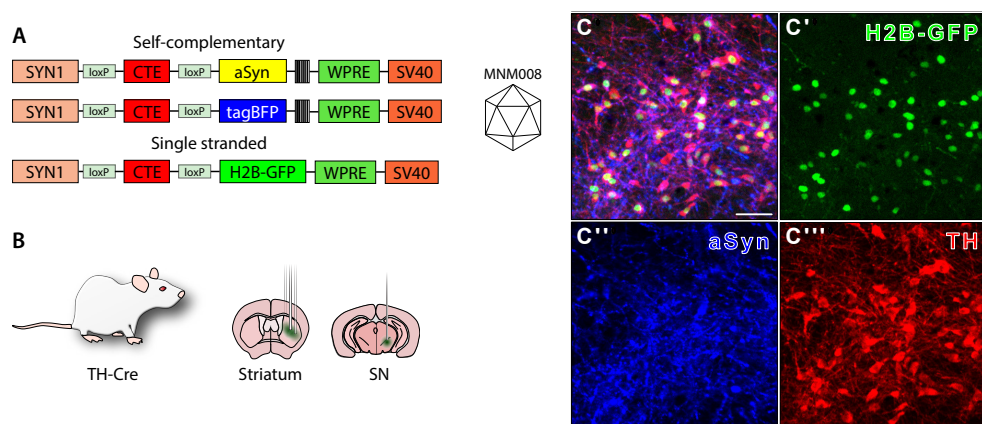
Figure 17 | DA Cell-Targeting in TH CRE Rats using Single-Cell Barcoded AAVs and H2B-GFP Tagging. **[A]** Schematic representation of AAV-MNM008 constructs containing the SYN1, loxP flanked CTE element, and either αSyn or tagBFP genes, followed by a molecular barcode. Below, the single-stranded AAV construct encodes a CRE-dependent H2B-GFP. **[B]** Stereotaxic coordinates rendering for precise delivery of the viral vectors in TH CRE rats. **[C-C´´´]** Representative IF images of the SN showing staining against H2B-GFP, αSyn, and TH in a TH CRE rat injected into the Striatum. The scale bar in **[C]** represents 200 μm.

Bioinformatic analysis of snRNA-seq samples together with published datasets

We aimed to comprehensively evaluate and compare the performance of the three sequencing techniques used, namely 10X Genomics, Parse-Bio, and Sci-Fi Seq, by integrating the snRNA-seq data from these approaches with two published datasets. Using the Machine Learning based tool scVI for dimensionality reduction and batch correction enabled us to bring all samples into the same analytical space. The Parse sample retained a comprehensive cell type composition but had a few DA neurons population. The 10X samples with intranigral injections contained the most significant fraction of DA neurons. On the contrary, SciFi samples only clustered and shared no similarity with other cells, therefore excluded from all further analyses (Figure 18A, B).
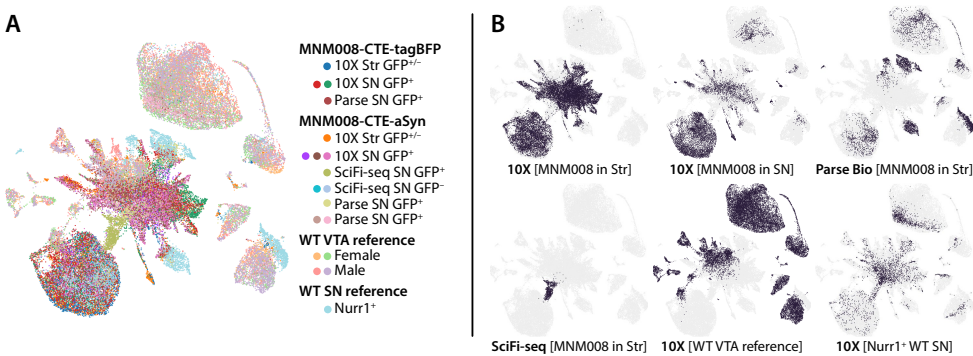
Figure 18 | Integrated Assessment of 10X snRNA-seq Samples with Two Reference Data Sets. **[A]** Uniform Manifold Approximation and Projection (UMAP) dimensionality reduction after scVI integration of seven 10X samples, three SciFi-seq samples, and three Parse Bioscience samples, alongside four published samples from WT VTA and one from Nurr1+ nuclei from SNpc. **[B]** Distribution of each sample group within the 31 Leiden clusters.

Paper III

Experimental setup

The work conducted in **Paper II** laid the foundation for the investigation presented in **Paper III**. In this study, we chose to concentrate on the mouse brain due to the wealth of available single-cell sequencing data and comprehensive bioinformatic tools from previously published studies, which bolstered our investigation and understanding. In this study, we focused our research on the mouse brain, leveraging the vast knowledge obtained from previously published studies to enhance our understanding. To leave the SN unperturbed from the surgical procedure while targeting all DA SN axonal projections, we employed a two-injection approach delivering the MNM008 virus directly into the Striatum. Certain animals were injected with a viral preparation that included PFF to investigate the molecular changes caused by αSyn seeding (Figure 19).
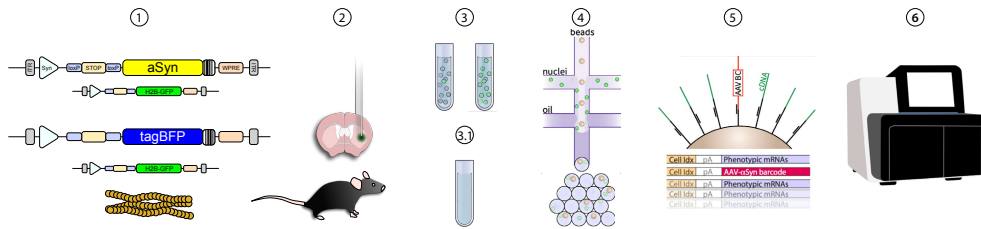
Figure 19 | Study Design Schematics: [1] AAV constructs containing barcoded αSyn (yellow) and barcoded tagBFP (blue) along with a smaller-sized H2B-GFP construct (green). All transgenes are preceded by a STOP sequence CTE flanked by two loxP sites. A representation of preformed fibrils is shown below in ochre. **[2]** Injection sites in the striatum of Dat-Cre mice. **[3]** Nuclear extraction preparation and GFP enrichment using FANS. **[3.1]** Supernatant from the nuclear preparation is stored for further analysis. **[4]** Utilization of the 10X microfluidics system **[5]** for cDNA synthesis with the bead barcode. **[6]** Indexing and sequencing of libraries using NextSeq 2000.

The transgenic DAT-Cre mice were divided into three groups. The first group received αSyn virus along with PFF, the second group received only the αSyn virus and PBS, and the third group received the tagBFP virus and PBS. The tagBFP group allowed us to investigate any molecular changes resulting from the expression of an exogenous protein. PBS was used as a control to ensure the volume injected remained consistent when fibrils were not used. To assess these viral vectors' specificity and off-target effects, we evaluated their function in WT mice receiving the tagBFP virus and fibrils. After tissue dissection, the nuclei sorted were further processed for scRNAseq analysis using the classic 10X Chromium protocol.

KEY RESULTS

These experimental strategies enabled us to delve deeper into the underlying mechanisms related to αSyn and its impact on the DA system. By adopting this approach, we aimed to gain valuable insights that would significantly contribute to our understanding of Parkinson's disease pathogenesis.

Immunofluorescence validation of αSyn aggregates and viral transduction in SNpc DAergic neurons

Immunohistological assessments were conducted in processed brain tissue to verify the transgene expression, specificity, and effective retrograde transport of the viral vectors together with αSyn seeding. IF staining targeting αSyn, GFP, and TH phosphorylated 129 Serine (pSer129) was performed on animals injected with αSyn and PFF. Images acquired from the ipsilateral SNpc revealed efficient transduction of all viruses (Figure 20A). As expected, αSyn expressions were predominantly localized in the DAergic neurons of the SN (Figure 20A'). The H2B-GFP protein exhibited selective expression within the nuclei of DAergic neurons, especially in cases where αSyn was expressed (Figure 20A'). Moreover, IF for pSer129 demonstrated the presence of an aggregated form of αSyn protein in TH-positive cells (Figure 20B").

Dat Cre | aSyn + Fib
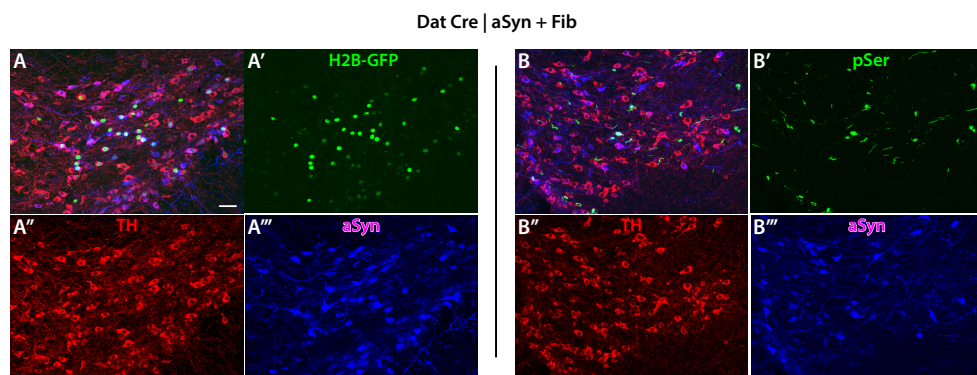
Figure 20 | IF validation for virus expression and PFF aggregation in the SN. Representative DAT-Cre mouse injected ipsilaterally in the striatum with αSyn and fibrils is depicted in the figure above. TH-positive cells are marked in red. The blue color indicates αSyn positive. The Magenta color highlights double positive TH and αSyn cells. In **[A']**, Nuclei expressing H2B-GFP are labeled in green, while in panel **[B']**, the green signal comes from aggregated form of αSyn protein. The scale bar in **[A]** is 50 μm.

DA nuclei were enriched through FANS gating using the Nurr1 antibody

Using the previously validated gating strategy established in **Paper II**, we successfully enriched DA nuclei expressing H2B-GFP through the cell sorter FACS Aria III. However, due to the absence of the CRE enzyme in the wild-type mouse, this approach was unsuitable for the WT group that received the tagBFP virus in conjunction with fibrils, as it required CRE-inducible gene expression. To isolate the DA cell population from the SN in this group, we adopted a recently published approach by Kamath et al. In their study, they selectively enriched DA nuclei using the Nurr1 marker, which is known to be expressed in ventral midbrain DAergic neurons (Figure 21A-A").

We successfully obtained 53,478 GFP-positive nuclei from the Dat-Cre animal groups and collected 28,970 GFP-negative nuclei. As for the WT animal group, a total of 35 575 Nurr1-positive nuclei and 15 000 Nurr1-negative nuclei were sorted.
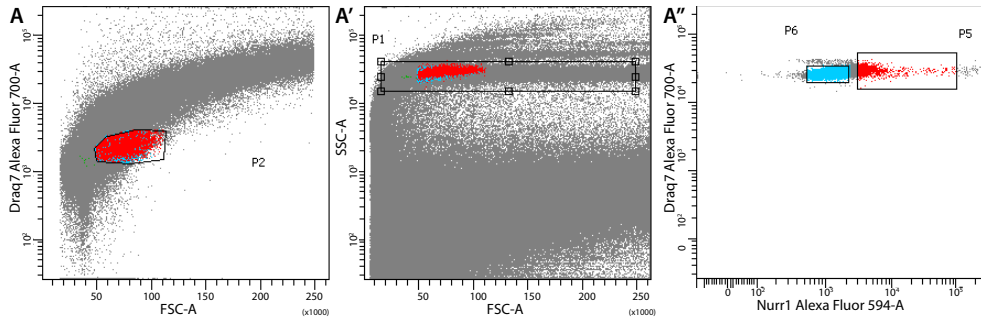
Figure 21 | FACS Gating Strategy. From **[A]** to **[A"]** , we outline the FACS gating strategy for Nurr1-stained nuclei extracted from WT-injected animals. **[B]** The side-scattered area (SSC-A) vs forward-scattered area (FSC-A) gate is shown. **[A']** A gate is applied for the nuclei section using DRAQ7 vs FSC-A. In quadrant **[A"]** , gates are established for Nurr1+ nuclei (in red) and Nurr1- nuclei (in light blue).

Leiden representation of the 10X samples

In the two MNM008-αSyn groups, the distribution of cell types remained highly similar, regardless of the addition of pre-formed fibrils (Figure 22B). However, with the MNM008-tagBFP group, we observed a higher abundance of Glutamatergic and GABAergic neurons and fewer DA neurons.

For the WT animals, which were DAT-Cre⁻ animals receiving the MNM008-tagBFP vectors along with pre-formed fibrils, nuclei were FANS sorted based on Nurr1 immunofluorescence. The Nurr1+ fraction exhibited a significant enrichment of DA neurons, aligning the cell type distribution more closely to that of the H2B-GFP sorted groups (Figure 22B).
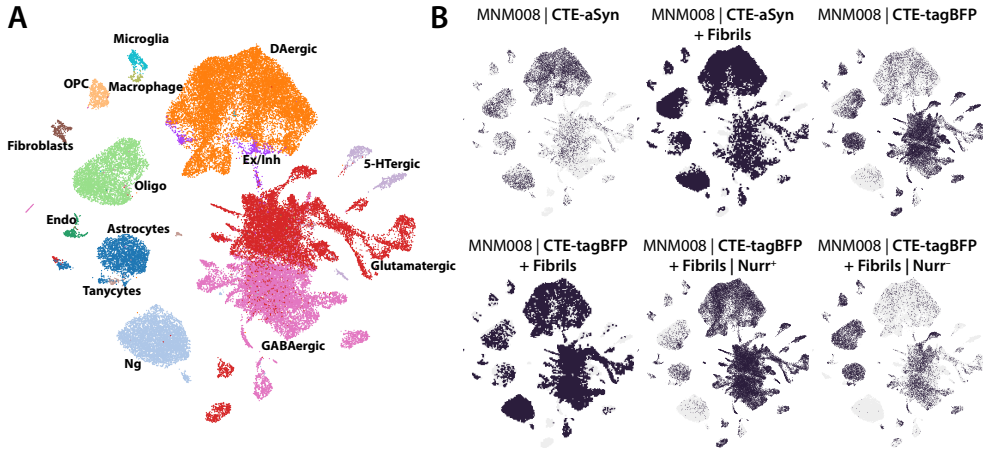
Figure 22 | Recovered Cell Types. [A] UMAP dimensionality reduction of the twelve 10X samples with integrated scVI transferred cell type labels. The top-level annotation is displayed. **[B]** Distribution of cells from the different treatment groups projected onto the UMAP.

Linear regression analysis of transcriptomic changes using barcoded viruses

Implementing a highly diverse barcoded AAV library enables precise quantification of individual viral particles that have infected each DA neuron. To investigate the impact of αSyn load on each gene, we conducted a linear regression analysis on all 10 000 highly variable genes within the DA neurons. Following Bonferroni correction for multiple comparisons, we selected genes that exhibited a significant linear correlation ($p < 0.05$) and depicted the linear correlation slope between the tagBFP and αSyn groups (Figure 23A). This analysis yielded 1 894 genes, most of which strongly correlated with the viral load, regardless of the transgene.

However, of particular interest were the genes that displayed a significant difference in slope direction between the αSyn and tagBFP treatments (depicted as blue dots in Figure 23A). From this group, we extracted the genes with the largest Δ-slope ratio and then selected the top 40 genes with the greatest disparity in expression (Figure 23B).

Our findings revealed several genes that were either positively or negatively correlated with αSyn expression. Among the upregulated genes, we observed increased expression of ITGA6, a protein found to be upregulated in the midbrain of mice injected with αSyn fibrils (Ma et al., 2021). Additionally, single nucleotide polymorphisms (SNPs) in AFAP1L1 were associated with Parkinson's disease in a study utilizing machine learning to predict neurological disease biomarkers (Lam et al., 2022). Similarly, a study using AAV-mediated αSyn overexpression in the rat substantia nigra reported upregulation of RSPO2 in the ventral midbrain (Qin et al., 2016). Furthermore, our
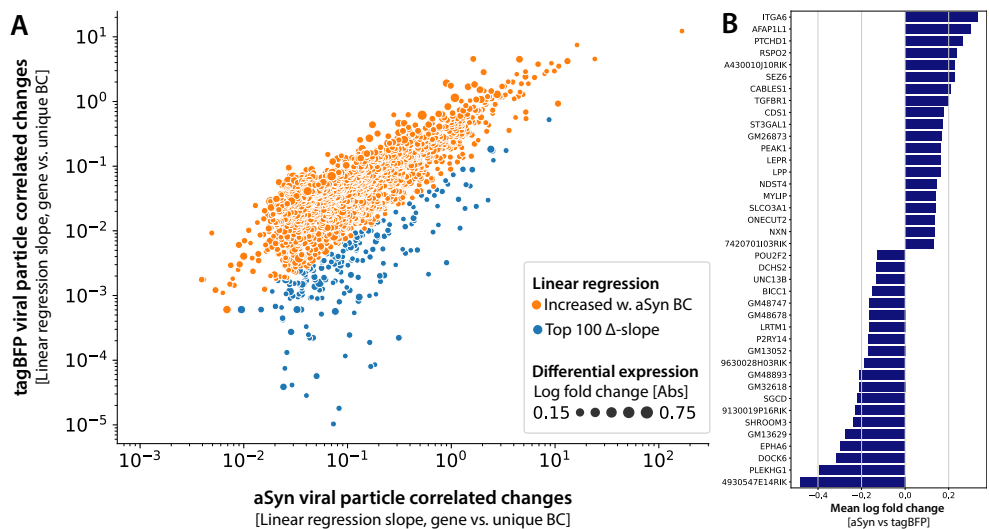
Figure 23 | Linear regression with viral BCs. [A] Modeling the correlation between unique viral particles per cell and gene expression using linear regression correlation analysis. **[B]** Top 40 genes with the highest Δ-slope ratio in linear regression, ranked by log-fold change.

results also demonstrated upregulation of TGFBR1 in DAergic neurons overexpressing αSyn, consistent with previous findings in microglia from a different study (Choi et al., 2020).

Conversely, we identified genes that showed a negative correlation with αSyn expression. Notably, the small GTPase DOCK6 (Arrazola Sastre et al., 2020) and the GTPase regulatory protein PLEKHG1 (Nakano et al., 2022) were among the genes found to be reversely associated with αSyn. However, the specific interactions of these genes with αSyn or their roles in Parkinson's disease have not been fully elucidated, warranting further investigation to unravel their potential implications in PD pathology. Our comprehensive analysis of positively and negatively correlated genes provides valuable insights into the intricate molecular network involved in αSyn-associated changes within DAergic neurons. These findings contribute to understanding PD pathogenesis and offer promising avenues for future research and therapeutic interventions.

Modeling a pseudotime based on AAV-derived unique barcodes

We investigated the impact of αSyn-carrying viral vectors on DAergic cells through pseudotime analysis using CellRank. The RealTimeKernel assessed the dataset's pseudotime structure based on the number of unique viral barcodes and 10X UMIs per cell, serving as a pseudotime marker. This allowed us to infer a Markov chain and transition matrix for the dataset, depicted in Figure (24C, F). Notably, the comparison

between the number of barcodes per cell and the pseudotime analysis revealed a similar pattern, indicating the preservation of the biological signal (Figure 24A, D). We identified a subset of cells likely representing a terminal state within the population and assigned probabilities of belonging to this state to all cells in the dataset (Figure 24B, E). Genes associated with the terminal states further supported the presence of many AAV vectors, indicated by WPRE presence and increasing human αSyn expression. Notably, genes linked to Parkinson's disease (Tenm4) (Hor et al., 2015) and neuroinflammation (Asic2) (Ortega-Ramírez et al., 2017) were also found in the αSyn group, suggesting a potential pathological signature related to αSyn-carrying AAVs. In contrast, tagBFP-carrying AAV vectors did not exhibit a similar pattern of increased pathology-associated gene expression.
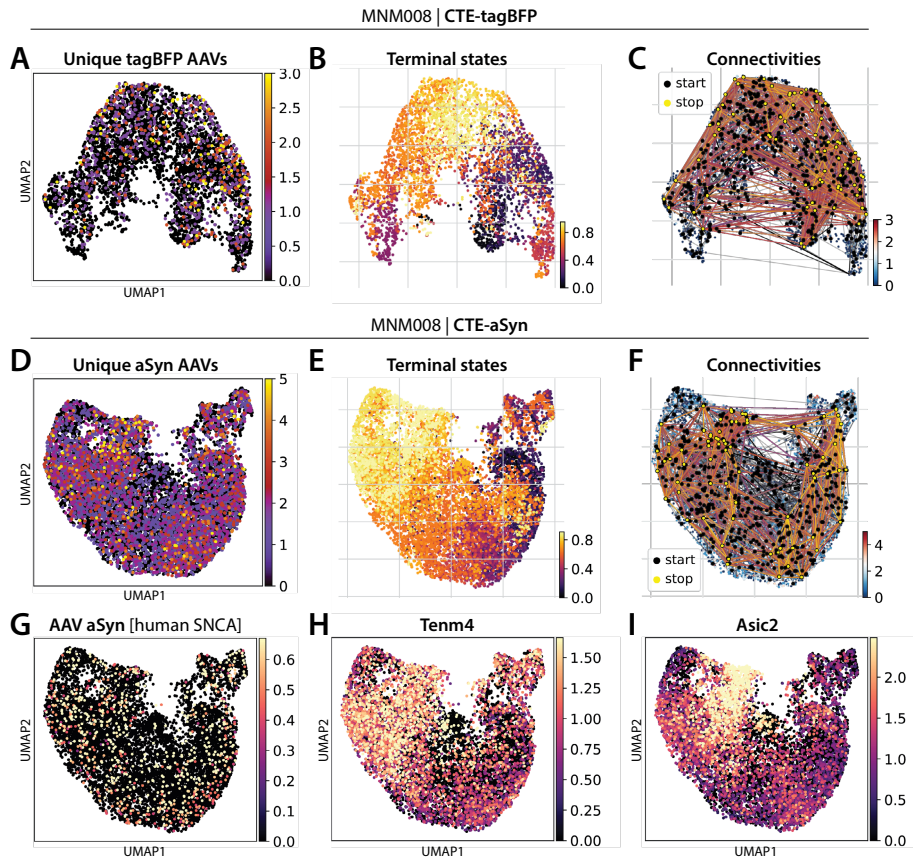
Figure 24 | Modelling of a disease progression pseudotime using viral BCs. [A-C] Dopaminergic neurons from tagBFP groups. **[A]** Number of unique viral barcodes per cell. **[B]** Probability of cells to belong to the terminal state. **[C]** Simulated random walks based on the dataset's inferred Markov chain. **[D-I]** Dopaminergic neurons from αSyn groups. **[D]** Number of unique viral barcodes per cell. [B] Probability of cells to belong to the terminal state. **[C]** Simulated random walks based on the dataset's inferred Markov chain. **[G-I]** Normalized gene expression of selected lineage driver genes.

Paper IV

In **Papers II** and **III**, our investigation into the molecular changes underlying the development of PD in animal models involved the comprehensive utilization of various single-cell technologies. These cutting-edge techniques provided invaluable information at the individual cell level, enabling us to decipher the intricate alterations occurring within DAergic neurons and surrounding cells during disease progression. However, it is essential to acknowledge that while single-cell technologies offer unprecedented resolution, they inherently lack the spatial context of the cellular environment in PD pathology.

We recognize the importance of incorporating spatial transcriptomics into our research to address this limitation and better understand the disease process. Spatial transcriptomics represents a powerful approach that can bridge the gap between the single-cell resolution and the spatial distribution of cells within the brain. By capturing the spatial organization of gene expression patterns, we can elucidate the specific regions within the brain that undergo significant molecular changes during PD development.

One aspect that we find particularly compelling in this context is the potential involvement of immune activation in PD pathology. Immune dysregulation and inflammation have emerged as critical players in neurodegenerative disorders, including PD. By integrating spatial transcriptomic data with the immune cell profiling performed in **Papers II** and **III**, we can uncover spatially localized immune activation patterns within the midbrain and other brain regions affected by PD. This information could provide crucial insights into the interplay between the immune system and DAergic neurons, shedding light on potential therapeutic targets to mitigate inflammation-induced neurodegeneration.

Moreover, spatial transcriptomics can further our understanding of the crosstalk between DAergic neurons, glial cells, and other neuronal populations within the substantia nigra and other brain regions relevant to PD. The spatial distribution of specific gene expression changes may reveal intricate cellular interactions and molecular networks driving disease progression.

Therefore, in this study, we present a comprehensive *in situ* transcriptome analysis of transplanted human embryonic-derived stem cell (hESC) derived DA neurons in a rat model of PD to showcase the potential advantages of spatial transcriptomics technology.

Experimental setup

We conducted a transplantation procedure using DAergic progenitors derived from hESCs and differentiated to display a ventral mesencephalic (VM) phenotype. These differentiated cells were then grafted into the lesioned striatum of an immunocompromised rat model of PD, induced by 6-OHDA injection into the right MFB.

The animals were euthanized after 6-15 months post-grafting to allow for the functional maturation of the transplanted cells. Coronal sections from brain tissue were mounted on amine-binding slides with ST oligo-dT array-printed spots (100 mm in diameter) for analysis (Figure 25A). Subsequently, the tissue was fixed and subjected to H&E staining, enabling the visualization of the grafted areas in the injected striatal region (Figures 25B-B").

Comparison of batch correction approaches for spatial transcriptomics

In the initial analysis, we observed considerable variation when comparing data between different animals and sections, indicating the presence of nested batch effects (Figure 25C). To address this issue, we implemented various batch-correction approaches to rectify these errors (Figure 25C-F").

All three algorithms displayed noticeable differences in how clusters based on the corrected gene expression were separated. They effectively distinguished striatal, cortical, and septal regions, white matter tracts, and transplanted areas (Figure 25C-F") with varying degrees of modularity. DESC and Seurat separated tissues based on morphological areas, whereas Scanorama showed separation based on the host animal (Figure 25D, D'). Interestingly, grafts appeared to be consistently united across all animals, indicating higher similarity than other anatomical structures.

Considering the performance of the algorithms, Seurat demonstrated superior batch correction both at the level of animals and sections without compromising the division within the tissues or creating outlier clusters (Figure 25F, F'), as seen with DESC. The UMAP representation of the corrected dataset did not indicate any bias at the slide, animal, or tissue section level. Moreover, the UMAP revealed a distinct separation of layers and functional regions within the cortex, aligning with the known anatomy of the rat brain. Based on these results, we found the Seurat batch-correction approach to be the most suitable and continued our analysis.

ST versus scRNA-seq composition analysis

A previous study extensively characterized The DAergic transplanted cells using single-cell RNA sequencing (scRNA-seq). Upon reanalysis, the scRNA-seq data revealed three major clusters based on their transcriptomic profiles (Figure 26A). Among these clusters, the smallest one exhibited neuronal characteristics, while the two larger
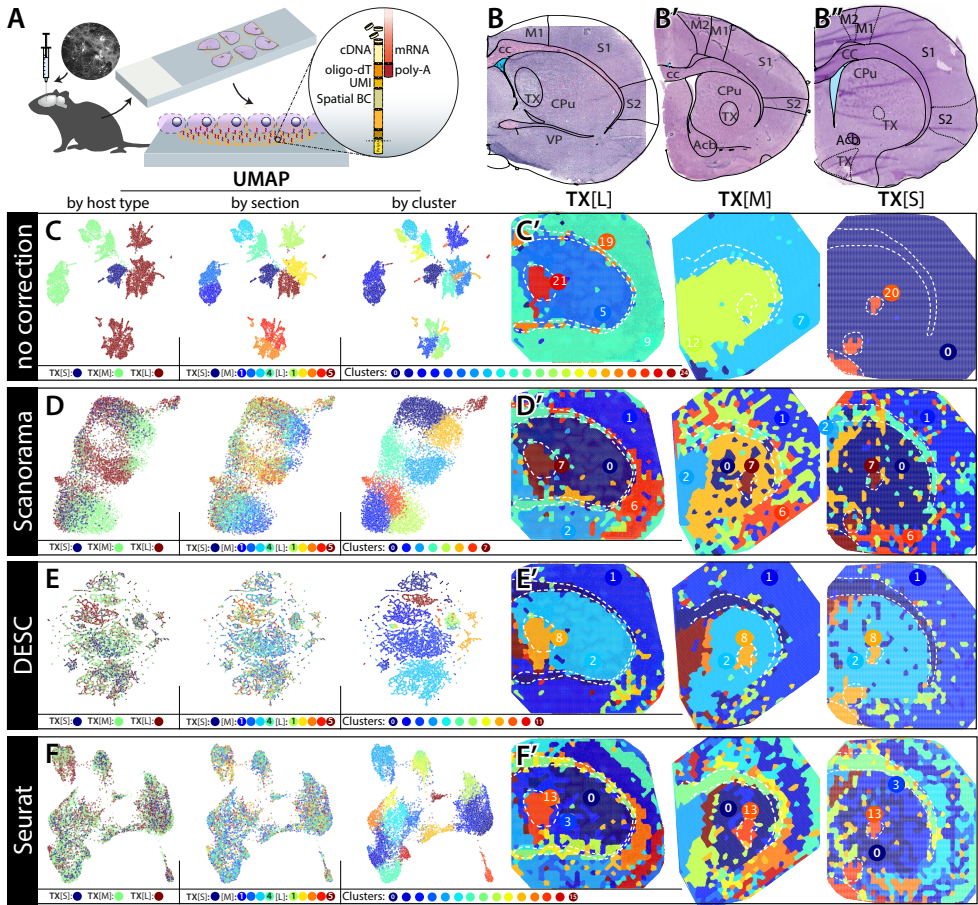
Figure 25 | Experimental setup and batch correction comparison. In panel **[A]**, the schematic of ST slides and the immobilized mRNA capturing probes on the features. H&E staining of sections shows large **[B]**, medium **[B´]**, and small **[B´´´]** transplants in the forebrain tissue, with annotations for various brain regions (CPu, M1/M2, S1/S2, cc, Acb, VP). The ST dataset of all transplanted sections is shown in C, with a UMAP representation labeled by the host, section, or cluster. The distribution of clusters throughout the tissue sections is visualized in **C´**. Batch effects correction approaches used: Scanorama **[D]**, DESC **[E]**, and Seurat **[F´]** to the dataset. The UMAP representations of the batch-corrected datasets and the distribution of clusters in tissues are presented in **[D-F´]**.

clusters expressed markers associated with glial and vascular leptomeningeal cells (VLMCs). However, despite the limited neuronal cell recovery, this population was well-differentiated from the larger population of captured glial cells. Interestingly, the expression of marker genes for DAergic neurons, astrocytes, and VLMCs was evident in both the scRNA-seq data and the ST analysis of both the grafted tissue sections and the non-lesioned SN regions (Figures 26B and 26C).

TH and DAT expression were more concentrated towards the edges of the large transplant in the ST analysis while covering a substantial portion of the transplants' features. Notably, the species-specific analysis of the expressed DAergic marker genes in the grafted sections indicated their nearly universal human origin. In contrast, in the scRNA-seq data, only a minority of cells in the neuronal cluster exhibited expression of TH or DAT. Additionally, glial cell markers (AQP4 and SOX9 for astrocytes and COL1A1 for VLMCs) were predominantly expressed at the center of the graft in situ (Figure 26 B).
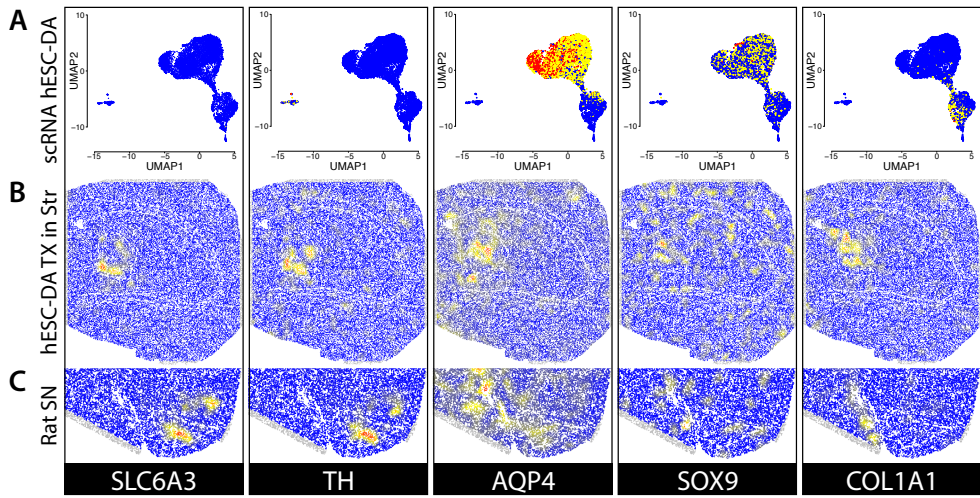
Figure 26 | Comparison of gene expression in a scRNA-seq and Spatial Transcriptomics analysis of hESC-derived DA neurons. Expression of genes associated with dopaminergic neurons (SLC6A3, TH), astrocytes (AQP4, SOX9), and VLMCs (COL1A1) in **[A]** scRNA-seq of previously analyzed transplant, **[B]** ST analysis of grafted tissue (transplant area is delineated in the medial striatum), and **[C]** ST analysis of intact substantia nigra.

The use of scRNA-seq data for Spatial Transcriptomics deconvolution analysis

We employed transcriptome deconvolution algorithms to investigate the cell type composition of the tissues analyzed using ST. Upon deconvolution of the grafted striatal sections, known cell populations were found in their expected regions within the host tissues, and the transplant areas were distinguishable from their surroundings (Figure 27F). Comparing the distribution of cell types in the transplant area and the surrounding striatal tissues, we observed a significant enrichment of DA neurons, astrocytes, and neuronal progenitor cells (Figures 27C, D). Additionally, a portion of the transplant population was assigned to an inhibitory neuronal population closely related to septal and ventral midbrain neurons (Figure 27F).

Figure 27 | Deconvolution of Spatial Transcriptomics to Determine Transplant Composition In Situ. [A] A representation of the distribution of the most abundant cell types from the SingleR assignment of the scRNA-seq dataset shown on a UMAP plot. **[B]** Deconvolution of a tissue containing the substantia nigra and the distribution of host cell types. **[C]** Distribution of cell types in the grafted striatal sections, with a detailed focus on the transplant area **[D]**. **[E]** Proportion of cell types in the transplant area compared to the striatum as determined by deconvolution of the ST slides and their comparison to the proportion of the same cell types in the scRNA-seq dataset (the dashed red line signifies their percentage). **[F]** Distribution of control populations of host cell types throughout the same tissue. Key: Str - Striatum; TX - Transplant; Ctx - Cortex; CC - Corpus Callosum; Hipp - Hippocampus; AC - Anterior Commissure.

Comparing the ST deconvolution results with the transplants' scRNA-seq analysis; we found substantial differences in the proportion of cell types (Figure 27E). The ST deconvolution estimated a large fraction of transplanted cells as DAergic neurons. Remarkably, the same DAergic neuron population constituted less than 1% of cells in the scRNA-seq dataset. VLMCs were also enriched in the transplant area in both datasets, but their numbers were much smaller in the ST analysis compared to the scRNA-seq. This difference was even more pronounced for the radial glia-like cell population. The neuronal progenitors were the only cell population in similar proportions in both scRNA-seq and ST datasets.

Discussion and future perspectives

Paper I introduces a groundbreaking in vivo method for investigating the dynamics of the Arc protein, essential for synaptic plasticity and memory formation. Recent discoveries revealed that the Arc gene has ancient retroviral origins, retaining structural GAG retrotransposon remnants, resulting in the production of capsid-like structures enclosing Arc mRNA (Ashley et al., 2018; Pastuzyn et al., 2018). This suggests a potential novel inter-cellular mRNA transmission mechanism in living organisms, as observed in laboratory settings where Arc capsids are released from neurons. Studying Arc in vivo presented challenges due to its widespread expression in various neuronal types and rapid regulation at dendritic spines. To address this, we devised an innovative technique using CRISPR/Cas9 and AAV-based target integration called HITI for in vivo knock-in into the Arc open reading frame (Suzuki et al., 2016).

Extensive research has been conducted on the optimization process with precise tools for in-frame insertion. The validity of this approach was demonstrated through in vivo electrophysiological induction of long-term potentiation and post-mortem proximity ligation. The results showed that labeled Arc retains its natural induction patterns after synaptic plasticity and interacts with verified synaptic proteins. This research using CRISPR/Cas9-based methodology has numerous applications beyond Arc research, as it allows for the investigation of various genes. A major breakthrough was achieved by identifying labeled Arc in pre-synaptic terminals of unlabeled neurons, which then connected to labeled neurons in the hippocampus. This finding enhances our comprehension of how Arc is transported between neurons in the mammalian brain. Furthermore, future experiments utilizing expansion microscopy and spatial sequencing will reveal the genetic message exchanged between neurons.

Our analysis in **Papers II** and **III** focuses on changes in gene expression in individual DA cells in response to a measurable genetic load of αSyn in the rat and mouse brain, respectively. To distinguish between viral load and any local injury related to the injection, we utilized the MNM008 AAV capsid and a molecular barcode downstream of the transgenes. In **Paper II**, we developed, optimized, and refined an accurate approach to studying gene perturbations in an in vivo PD animal model. Our findings revealed that targeting the SN DA cells with tailored AAVs in TH Cre rats provided the most precise results. Interestingly, when comparing control proteins, we observed suboptimal performance with PLAP, leading us to select BFP as the control gene for subsequent sequencing studies.

DISCUSSION

To enhance the recovery of DA nuclei during FANS, a small amount of Cre-dependent H2B-GFP AAV was added to the injection cocktail. This method was found to be robust and reproducible across both **Paper II** and **III**. Unlike **Paper II**, which only used transgenic (TH-Cre) animals, **Paper III** utilized both Dat Cre and WT mice. Interestingly, the Nurr1 antibody was discovered to be effective in enriching DA neurons in WT animals. This discovery emphasizes the importance of using the Nurr1 immunofluorescence-based approach to accurately identify and isolate DAergic (DA) neurons in wild-type tissue. This technique has been consistently proven to be effective in aligning with current literature findings, as seen in a study published by Macosko's laboratory (Kamath et al., 2022). It expands our methods for studying DA neurons and provides a reliable alternative.

Out of the three single-cell RNA sequencing technologies, namely 10X genomics, Parse Bioscience, and the Scifi-Seq protocol, 10X genomics emerged as the method of choice. It delivered high-quality nuclear transcriptomes and was compatible with the FANS approach. Therefore, this approach was used for the study discussed in **Paper III**. The initial bioinformatic analysis revealed how the striatal system we developed is tailored to precisely investigate molecular perturbations generated by viral transgenes observed particles. Our analysis of bioinformatics has given us important information about the effectiveness of the striatal injected-AAV method and the H2B-GFP FANS enrichment strategy. These techniques have been successful in retrieving A9 nuclei from the SNpc DA population. In addition, our linear regression analysis has provided a comprehensive list of genes that respond to AAV dose, regardless of the gene being studied.

In **Papers II** and **III**, we have identified two distinct groups of genes, consisting of 30 and 40 candidates, respectively, that show a significant specific correlation with αSyn dose compared to tagBFP dose. These genes display either a positive or negative slope and require further investigation to determine their roles and implications in our research. By understanding the functions of these genes, we can gain valuable insights into the mechanisms that cause αSyn pathology and its potential implications in neurodegenerative diseases. Furthermore, exploring the effects of AAV-mediated gene delivery in various neuronal populations could provide further insights into cell-type-specific responses and potential therapeutic targets.

A recent study employing DAT CRE-RC-LSL-Sun1/GFP mice conducted single nuclei RNA sequencing of the SNpc DAergic neurons. This approach was enabled by the specific labeling of DAergic nuclei through a cross that results in the expression of a nuclear membrane protein fused to GFP under the control of the DAT promoter. This labeling strategy facilitated the isolation of DAergic nuclei through fluorescence-activated cell sorting. The study identified and characterized three distinct genetic subtypes, marked by the expression of Slc17a6 (Vglut2), Calb1, and Anxa1, each

exhibiting distinct responses to rewards, aversive stimuli, and changes in movement dynamics. This discovery underscores the intricate relationship between genetic subtypes and functional diversity in DAergic neurons, contributing to our understanding of their roles in various physiological contexts (Azcorra et al., 2023).

As we have explored the utilization of cutting-edge single-cell technologies, spatial transcriptomics, and viral vectors to dissect the molecular intricacies of DAergic neurons in the context of PD, we follow a similar thread to the aforementioned study. Just as they illuminated the interplay between genetic subtypes and functional responses within DA neurons, we aspire to illuminate the complexities of PD pathology by mapping αSyn overexpression onto distinct molecular and functional subsets of these neurons. Through the application of pseudotime analysis, the trajectory of DAergic neurons spanning from a basal state characterized by minimal αSyn expression to a pathological condition marked by elevated αSyn levels can be effectively unraveled. This innovative method leverages the quantification of AAV barcodes as surrogate indicators of αSyn content within the cells, thereby enabling us to dissect the gene expression dynamics within DAergic neurons across the continuum of Parkinson's disease progression.

Our study focused on analyzing the single cells of rats that were given injections in both the SN and the striatum. This resulted in a significant number of DAergic neurons that exhibited various conditions. Therefore, we can use this diverse dataset to construct a comprehensive analysis of the mice study. Although there were fewer neurons in the mouse model, it provided a clean environment for αSyn overexpression, without any disturbances from SN tissue. With this innovative approach, we can capitalize on these varied datasets to gain a more complete understanding of the dynamics of αSyn-mediated pathogenesis in PD.

Our research in **Paper IV** extensively investigated the transcriptome of DA neurons transplanted from hESCs into a rat model of PD. Stem cell transplantation holds great potential as a treatment for PD, with current clinical trials using hESCs and iPSCs. Although these transplants generate DA neurons and other cell types, it is vital to comprehend the fate, spatial distribution, and relative proportions of these cells.

We used advanced techniques such as spatial transcriptomics, batch correction, and deconvolution to gather precise and quantitative data on the maturation of transplants and the types of cells formed. Our analysis of single-cell RNAseq data from hESC-derived transplants revealed an interesting finding. While scRNAseq data accurately profiled transcriptomes at the single-cell level, it was misleading in assessing relative quantities, especially in the representation of DA neurons. In contrast, the deconvoluted spatial transcriptomics provided a cell-type distribution within the grafts that aligned closely with immunohistochemical analysis. As hESC-based transplantation

gains importance in clinical settings, standardized and robust analytical methods are crucial for the post-mortem evaluation of graft survival and maturation using patient samples.

Our combination of spatial transcriptomics, batch correction, and deconvolution provides a valuable tool to accurately assess graft survival and maturation. This tool holds great potential for future clinical applications, helping us understand the complex transcriptomic landscape of transplanted DA neurons and surrounding cell types. By combining spatial transcriptomics with advanced analysis techniques, our study provides invaluable insights for advancing PD therapy.

Summary of key methods

In this section, I will outline the key methods utilized in this study, which have been crucial for the successful execution of the research presented in this thesis. Additionally, I will provide valuable guidance and insights regarding effectively implementing various techniques. For comprehensive and in-depth information, please refer to each corresponding paper's specific material and methods (M&M) sections.

Evaluation of CRISPR/Cas9 target sequences

In **Paper I**, we focused on the 5' region of the C57bl/6 Arc locus. We utilized gRNAs targeting the specific DNA sequence to modify by the Cas9 to modify this region precisely. These gRNAs were carefully designed to be compatible with the spCas9 system. This approach allowed us to accurately and efficiently edit the 5' region of the C57bl/6 Arc locus for our experimental purposes.

Implementing web-based tools, we identified and evaluated 11 possible insertion sites (Figure 28A). Two of these sites were unsuitable for the HITI system since repair with the DT would introduce an in-frame stop codon between the inserted sequence and the Arc gene.
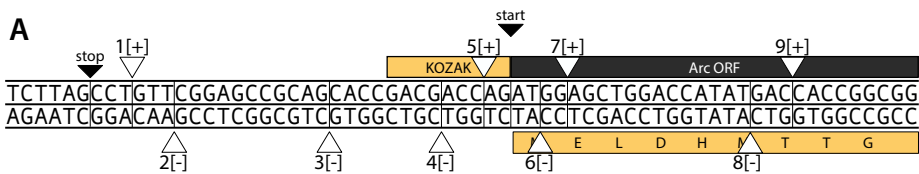
Figure 28 | Schematic of the Arc 5'region. [A] 5' Arc sequence showing all possible insertion sites in the coding strand [+] and the template strand [-] based on the PAM sequence for spCas9. TAG stop codon in frame with the ATG start codon of the Arc gene.

Luckily, we identified four potential guides that could be used. We used the CCTop—CRISPR/Cas9 target online predictor as our primary screening tool to select the most suitable candidates (Stemmer et al., 2015). Additionally, we cross-referenced these guides using two other websites for further insights: the IDT CRISPR-Cas9

guide RNA design checker and "CHOP-CHOP" (Montague et al., 2014; Labun et al., 2016; Labun et al., 2019; IDT, 2022). Based on the combined information from these sources, and experimental tests, we selected guide RNA accordingly (sg2[-] and sg4[-], sg1[+] and sg9[+]).

AAV viral production

AAV production was a key component for **Paper I, II,** and **III** as it was used for gene delivery for *in vivo* experiments. The chloroform extraction and precipitation protocol used is written in detail in the M&M sections of the papers attached. Purified AAVs were titrated using ddPCR with primers specific for the ITRs (Table 1) (Lock et al., 2014).

Animal research

Female and male C57bl/6 J mice from Charles River (Germany), weighing 20 g and aged 8-9 weeks, were utilized in **Paper I**. WT Sprague-Dawley rats (225-250g, Charles River, Germany) and in-house breeding of transgenic TH-Cre Sprague-Dawley rats were used in **Paper II** for the *in vivo* experiments. In **Paper III**, Dat-Cre transgenic mice were bred in-house. For **Paper IV**, Adult athymic nude female rats were purchased from Envigo (Hsd:RH-Foxn1rnu). The animals were housed in a facility with unrestricted access to food and water, and they were subjected to a 12-hour light/dark cycle.

The *in vivo* part from **Paper II**, **III**, **IV** was conducted at Lund University in Sweden, following the regulations set forth by the Swedish Animal Welfare Agency. The study also received approval from the local ethical committee responsible for overseeing the use of laboratory animals (Ethical permit no. M 66-16 and 4111/2021-m).

From **Paper II**, intrahippocampal AAV injections and *in vivo* electrophysiological experiments on LTP, were conducted at the University of Bergen. These experiments were ethically approved by the Norwegian National Research Ethics Committee and adhered to the guidelines outlined in EU Directive 2010/63/EU and the ARRIVE recommendations.

The researchers are responsible for the experiments were fully trained and certified in accordance with the rigorous standards of the Federation of Laboratory and Animal Science Associations (FELASA) C course requirements.

Behavioral tests

In **Paper III** when conducting behavioral tests on mice, the corridor and the cylinder test followed the same settings as previously described (Grealish et al., 2010). We used ANYmaze software to record whole-body activity in an open-filed arena (Plexiglas boxes of 50x50cm). The Animal's head, body, and tail travel distance were measured for 45 min. Spontaneous rotations were monitored based on body axes movements were classified as clockwise or anticlockwise full turns.

Stereotactic surgeries

In **Paper I** and **III**, during surgical procedures, mice were kept under anesthesia with a 1.2 % isoflurane/O2+NO2 mixture, while in **Paper II**, rats were deeply anesthetized with a dose of Fentanyl and Dormitol, which was intraperitoneally injected. Plus/ minus and left/right 2.0 mm from the Bregma was ensuring to have the skull in a flat position. The coordinates for all injection sites were identified relative to bregma.

A small hole was drilled in the skull and each volume was infused in the targeted site using a 5 uL Hamilton syringe fitted with a pulled capillary glass. Surgeries on rats were carried on with 25 uL Hamilton connected to an automatic pump. The infusions were carried at 0.2 ul/min following 5 min with the needle left in place to let the volume diffuse. Once the animals were sutured, they were kept in quarantine under daily observation. Antisedan and Tamgesic were administered after surgery to all rats. The anatomical brain region and the respective coordinates used are reported in the table below.

Study	Structure	AP	ML	DV
Paper I (Mouse)	Str	0.3	1.9	-3.5/-3.2
	Hipp	-2	-1.5 /1.5	-2/-1.5
Paper II (Rat)	Str	1.0	2.3	-5.5/-4.5
	Str	0.0	3.4	-5.5/-4.5
	Str	-1.0	4.5	-5.6
	MFB	-3.8	-1.2	-7.8
	SN	-5.3	1.7	-7.2
Paper III (Mouse)	Str	0.8	1.7	-3.6
	Str	-0.2	2.6	-3.6

Table 1 | Coordinates were taken from Bregma. Numbers are expressed in mm. Striatum (Str), Medial forebrain bundle (MFB), Substantia nigra (SN). (AP) Anteroposterior, (ML) Mediolateral, (DV) Dorsoventral

In **Paper II**, we used bigger apparatus when investigating the behavior of rats. The cylinder used during the cylinder test was wider and taller compared to the mice settings (21cm diameter, 34cm tall). The corridor was 240 cm long x 7 cm wide x 23 cm deep. The whole-body movement was monitored in a 1.2 m x 1.2 m arena surrounded by black plastic walls 50 cm high. Once the rat was placed in it was allowed to explore it for 15 min. Rats were also tested for drug-induced rotation using an automated rotometer system (AccuScan instrument, Columbus, OH, USA). Intraperitoneal injection of amphetamine (5 mg/kg) dissolved in 0.9% of saline was administrated 5 min before the recording of rotations began. Asymmetric rotations were counted over 40 min of testing.

Electrical stimulation in LTP-induced experiment

The LTP-induced experiments for **Paper I** initially began at the two-photon microscopy core facility in Lund. To induce Arc expression, we applied HFS trains in *ex vivo* mouse brain slices and used time-lapse imagining acquisition to track Arc protein activity through the fluorescent fused tag mCherry.

However, we encountered difficulties as we could not record the fEPSP response. This lack of response indicated stressed and dying neurons, likely not solely due to the experimental procedure but rather from using too aged mice for the experiment.

We sought guidance on HFS experiments by reaching out to experts in the field. We contacted Bramham's laboratory at Bergen University, and together we began planning how to execute this experiment successfully. They facilitated the order of 12-week-old mice, which were then bilaterally injected into the hippocampus with the HITI construct (Figure A').

After three weeks from the viral injection, we performed LTP induction through HFS in the dentate gyrus (DG) following the protocol established by Panja and collaborators (Panja et al., 2014) (Figure 29A). To have internal control, one hemisphere was kept unstimulated. The animals were then immediately sacrificed, and the brain was prepared for IHC, as described below. For more comprehensive details of the protocol, please refer to the attached paper (**Paper I**).

Immunofluorescence

For each IHC protocol, the tissue sections were initially rinsed three times in phosphate-buffered saline (PBS) at pH 7.4. Subsequently, the sections were subjected to a blocking step for 1 hour using a solution composed of 2.5% bovine serum albumin (BSA), 2.5% serum derived from the species in which the secondary antibody was raised, and 0.25% Triton X-100, all diluted in PBS. Following the blocking step, the
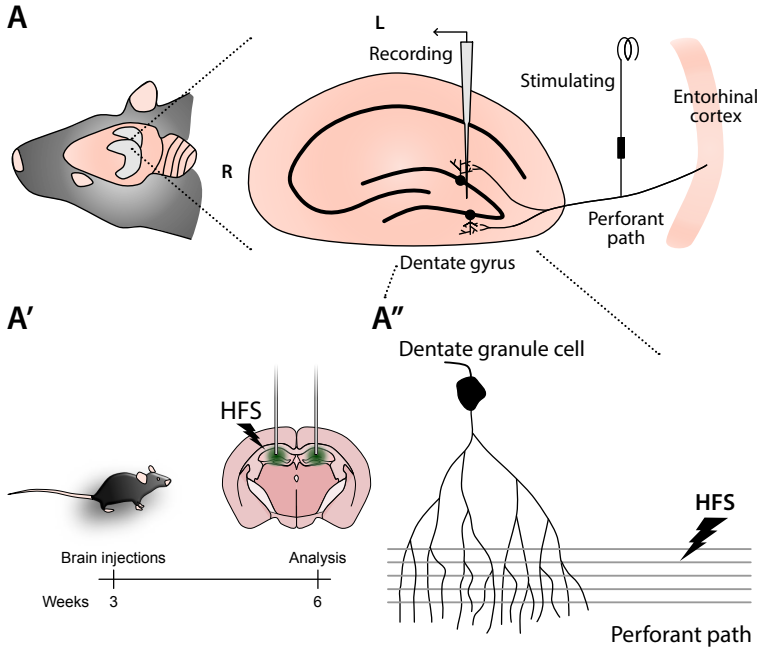
Figure 29 | Schematic representation of the LTP-induced experiment. [A] Mouse anatomical part (R) rostral, (L) lateral, entorhinal cortex with the perforant path projecting to granule cells in the hilus of the dentate gyrus (DG). **[A']** experimental design with the timeline.

brain slices were incubated overnight with the primary antibody at room temperature (rt). The next day, the primary antibody was washed away with PBS (three washes), followed by a 1-hour incubation in the blocking solution. Depending on the instructions provided by the manufacturer, the secondary antibody was diluted in a 2.5% blocking solution, added to the sections, and incubated for 2 hours at room temperature. For detailed information regarding the antibodies used and their respective dilutions, please refer to Table 3.

Proximity Ligation Assay

NaveniFlex PLA kit was a fundamental method used in **Paper I** to investigate protein-protein interactions of Arc. A common IHC was always conducted to localize the edited neurons parallel to PLA experiments. To minimize the consumption of reagents from the PLA kit, the manufacturer's protocol is designed to be conducted on tissue slices attached to the glass slide.

During PLAs on multiple brain slices, the total volume used proved sufficient for slices to float freely in tilted glass bottles. We found that adopting these settings for all PLA experiments considerably reduced background noise and provided cleaner, more accurate, and precise RCA signals. Therefore, these settings were consistently applied throughout all our PLA experiments. Importantly, this method is extremely sensitive, and accurate dilution tests must be performed for each antibody to determine the optimal concentration (table 3). For a detailed protocol of the NaveniFlex kits used, I am forwarding you the methods section of **Paper I.**

Antibody	Host	Company	Cat. Nr.	Dilution
GFP	Chicken	Abcam	AB13970	1:10000
mCherry	Goat	LSBio	LS-C204207	1:500
mCherry	Chicken	Abcam	Ab205402	1:1000
Arc	Rabbit	SynSys	156003	1:1000
TH	Rabbit	Millipore	AB152	1:2000
TH	Chicken	Abcam	AB76442	1:2000
αSyn	Mouse	Santacruz	SC12767	1:2000
tagBFP	Mouse	Invitrogen	MA5-15257	1:1000
Cy3 anti-chicken	Goat	Thermofisher	A21236	1:400
Alexa 488 anti-chicken	Goat	Thermofisher	a11039	1:500
Alexa 555 anti-rabbit	Goat	Thermofisher	A-11011	1:500
Alexa 555 anti-mouse	Goat	Thermofisher	AB96880	1:500
Alexa 647 anti-goat	Goat	Thermofisher	a21447	1:500
Alexa 647 anti-mouse	Goat	Thermofisher	a21236	1:500
Alexa 647 anti-rabbit	Goat	Thermofisher	A21245	1:400
(for PLAs)	*Host*	*Company*	*Cat. Nr.*	*Dilution*
mCherry	Chicken	Abcam	AB13970	1:5000
mCherry	Rabbit	LSBio	LS-C204207	1:2500
Arc	Mouse	Santa Cruz	sc-17839	1:500
Stargazin	Mouse	Abcam	Ab167445	1:500
Bassoon	Mouse	Thermofisher	a21447	1:500

Table 2 | Antibody information

Confocal scanning microscopy

The IHC analyses were carried out utilizing a Leica SP8 microscope. Image acquisition was performed with a HyD detector, and to prevent serial excitation, the lasers were activated in sequential mode. Solid-state lasers with wavelengths of 405 nm, 448 nm, 552 nm, and 650 nm were used for exciting the corresponding fluorophores. Throughout the image acquisition process, a pinhole of 1AU was maintained. Leica objectives including 5X/0.15, 20X/0.75, and 63X/1.40 were employed.

The BaSiC ImageJ plugin was utilized for multi-field imaging normalization, while image stitching was conducted using the MIST plugin (Chalfoun et al., 2017; Peng et al., 2017). In addition, 3D surface render images were generated using a 3D module in the SP8 Leica software. These images were created from z-stack images obtained with a 63X objective at a resolution of 1024×1024 pixels.

Aiforia

In **Paper I**, fluorescent cells and PLA signals were quantified using an automated convolutional neural networks (CNN) algorithm implemented in Aiforia Create, a cloud-based platform developed by Aiforia Technologies Oyj in Finland. This computer-assisted cell counting method utilizes supervised learning, as previously described (Penttinen et al., 2018).

Each digitized image was first converted in a single Leica Image File (lif) file and subsequently uploaded to Aiforia Hub. The CNN algorithm was trained to identify either the cell bodies or the PLA puncta from the digital images within the regions of interest.

The CNN algorithm consisted of two layers. The first layer performed semantic segmentation to segment the brain tissue, while the second layer used object detection in Aiforia Create to count the cells or PLA puncta. The brain tissue semantic segmentation was trained with a complexity setting of 'complex'. On the other hand, object detection was trained with a complexity setting of "very complex".

To train the CNN algorithm, specific regions of the brain tissue were identified and annotated by marking the cells or PLA puncta objects in digital images. The algorithm was then tested using a separate set of regions. For fluorescent cells, the intensity of each channel was measured for every detected object and compared to the background to obtain the overall signal of the cells stained for different proteins.

Midbrain tissue dissection and nuclei extraction

This method played a crucial role in the success of **Paper II** and **Paper III**, with comprehensive and in-depth descriptions found in their respective M&M sections. Here, I want to emphasize the optimization process and essential steps to enhance the viability and RNA quality of the cell population of interest (POI).

When using the 1.5 mm biopsy punches to dissect the midbrain region, we observed that strictly confining the dissection to the SN increased the risk of missing the region of interest (ROI). Therefore, a helpful suggestion is to be slightly generous with the boundaries while dissecting the designated area. Coating all tubes and tips with 2 % BSA at least 1 hour before usage is beneficial. All reagents, instruments, and sample preparation should not exceed 4 °C. We found that adopting these strategies significantly increased the number of our POI during enrichment at the FACS machine.

The nuclei extraction process releases numerous RNAse enzymes into the solution, which can lead to unwanted RNA degradation. To protect the transcriptomes, RNAse inhibitors should be added freshly at the desired concentration to all preparations on the same day of the experiment. This practice reflected the high-quality libraries sequenced in **Paper III**.

Fluorescent-activated nuclei sorting (FANS)

To sort for GFP-positive single nuclei events, we employed the FACS Aria III machine with the Diva software, utilizing the gating strategies reported in the M&M of **Paper II** and **III**.

In **Paper II**, as part of the preparation for the SciFi and Parse Bioscience protocols, the sorted GFP⁺ and GFP⁻ nuclei were collected in Eppendorf tubes containing 100 µL of 2 % BSA. After sorting, the samples were snap-frozen with liquid nitrogen and stored at -80 °C until further analysis. **Paper III** only employs 10X Genomics. Throughout the sorting process, samples were handled on ice and briefly at room temperature. The sorted GFP+ and GFP- nuclei were collected in empty pre-coated 2% BSA Eppendorf 1.5 mL tubes. Each sorting procedure aimed to collect approximately 11 000 to 12 000 nuclei per tube which were transferred to the 10X Chromium droplet generator immediately after.

Single Cell Technologies

Scifi-seq

In this section, I will focus on describing the optimization process and implementations we adopted to address our research question, building upon the scifi-seq protocol. We acknowledge that the original scifi-seq protocol, developed by Datlinger and colleagues, was specifically designed for cells or nuclei from established human or mouse cell lines, which are stronger and mechanically resistant due to their application (Datlinger et al., 2021). However, our research objective centered around studying the transcriptomes of DA nuclei extracted from the SN of rat and mouse PD animal models, which are, on the contrary, notoriously fragile. Moreover, our POI accounts for less than 1% of the total nuclei suspension. To overcome this challenge, we implemented an enriching strategy based on FANS described in **Paper II** and **III.**

Our investigation examined whether fixation before or after FANS could enhance nuclei viability without compromising RNA quality. We also tested several RNAse inhibitors from different manufacturers and assessed the efficacy of various reverse transcription enzymes operating at different temperatures. Throughout these experiments, we developed the ultimate adapted scifi protocol, which is detailed in the M&M section of **Paper II**.

Parse Bioscience

The Parse Bioscience manufacturer's protocol did not include a FANS enrichment step. To explore this aspect, we conducted a test using the WT mini on 10 previously fixed and FANS-enriched nuclei suspensions. After thawing samples stored at -80 °C in a water bath at 37°C, we made the decision to follow the protocol from the beginning and performed a second round of fixation on the nuclei using their reagents, which were appropriately diluted based on our samples' volume.

We strictly adhered to the manufacturer's protocol available on their website (Evercode WT mini v1) and subsequently sequenced the prepared libraries using an Illumina NextSeq 500. The results were highly satisfactory and encouraged us to utilize the WT kit on 50 samples. However, we encountered an issue when a larger fraction of BSA was carried over from previously FANS-enriched samples throughout the protocol. This led to the precipitation of the manufacturer's reagents, rendering the sample preparations irrecoverable.

10X Genomics experiments

Samples were handled on ice and briefly at room temperature when enriching our POI through the sorting process. Nuclei were collected in empty pre-coated 2 % BSA Eppendorf 1.5 mL tubes. Each sorting procedure aimed to collect approximately 11 000 to 12 000 nuclei per tube. Subsequently, the samples were transferred to the 10X Chromium droplet generator.

To perform single-nuclei RNA sequencing using 10X Genomics technology, the single-nuclei suspensions were loaded onto 10X Genomics Single Cell 3′ Chips in combination with the master mix following the guidelines provided in the manufacturer's protocol (Chromium Single Cell 3′v3). This protocol pertains to the Chromium Single Cell 3′ Library, which utilizes the version 3 chemistry to generate single cell gel beads in emulsion (10X Genomics).

After library preparation, the resulting libraries were subjected to sequencing on a Illumina NovaSeq 6000 instrument using 100-cycle reagents. The sequencing run included 28 cycles for Read 1, 90 cycles for Read 2, and 10 cycles for each index.

References

Abbott, A. (2010). Levodopa: the story so far. Nature 466(7310), S6-7. doi: 10.1038/466S6a.

Adachi, K., Enoki, T., Kawano, Y., Veraz, M., and Nakai, H. (2014). Drawing a high-resolution functional map of adeno-associated virus capsid by massively parallel sequencing. Nat Commun 5, 3075. doi: 10.1038/ncomms4075.

Akache, B., Grimm, D., Pandey, K., Yant, S.R., Xu, H., and Kay, M.A. (2006). The 37/67-kilodalton laminin receptor is a receptor for adeno-associated virus serotypes 8, 2, 3, and 9. J Virol 80(19), 9831-9836. doi: 10.1128/jvi.00878-06.

Albin, R.L., Young, A.B., and Penney, J.B. (1989). The functional anatomy of basal ganglia disorders. Trends Neurosci 12(10), 366-375. doi: 10.1016/0166-2236(89)90074-x.

Allen, F., Crepaldi, L., Alsinet, C., Strong, A.J., Kleshchevnikov, V., De Angeli, P., et al. (2018). Predicting the mutations generated by repair of Cas9-induced double-strand breaks. Nat Biotechnol. doi: 10.1038/nbt.4317.

Appel-Cresswell, S., Vilarino-Guell, C., Encarnacion, M., Sherman, H., Yu, I, Shah, B., et al. (2013). Alpha-synuclein p.H50Q, a novel pathogenic mutation for Parkinson's disease. Mov Disord 28(6), 811-813. doi: 10.1002/mds.25421.

Arendt, D. (2021). Elementary nervous systems. Philosophical Transactions of the Royal Society B: Biological Sciences 376(1821), 20200347. doi: doi:10.1098/rstb.2020.0347.

Arendt, D., Benito-Gutierrez, E., Brunet, T., and Marlow, H. (2015). Gastric pouches and the mucociliary sole: setting the stage for nervous system evolution. Philosophical Transactions of the Royal Society B: Biological Sciences 370(1684), 20150286. doi: doi:10.1098/rstb.2015.0286.

Arrazola Sastre, A., Luque Montoro, M., Gálvez-Martín, P., Lacerda, H.M., Lucia, A.M., Llavero, F., et al. (2020). Small GTPases of the Ras and Rho Families Switch on/off Signaling Pathways in Neurodegenerative Diseases. Int J Mol Sci 21(17). doi: 10.3390/ijms21176312.

Ashley, J., Cordy, B., Lucia, D., Fradkin, L.G., Budnik, V., and Thomson, T. (2018). Retrovirus-like Gag Protein Arc1 Binds RNA and Traffics across Synaptic Boutons. Cell 172(1-2), 262-274.e211. doi: 10.1016/j.cell.2017.12.022.

Asuri, P., Bartel, M.A., Vazin, T., Jang, J.H., Wong, T.B., and Schaffer, D.V. (2012). Directed evolution of adeno-associated virus for enhanced gene delivery and gene targeting in human pluripotent stem cells. Mol Ther 20(2), 329-338. doi: 10.1038/mt.2011.255.

REFERENCES

Atchison, R.W., Casto, B.C., and Hammon, W.M. (1965). ADENOVIRUS-ASSOCIATED DEFECTIVE VIRUS PARTICLES. Science 149(3685), 754-756. doi: 10.1126/science.149.3685.754.

Avallone, M., Pardo, J., Mergiya, T.F., Rájová, J., Räsänen, A., Davidsson, M., et al. (2023). Visualizing Arc protein dynamics and localization in the mammalian brain using AAV-mediated in situ gene labeling. Front Mol Neurosci 16, 1140785. doi: 10.3389/fnmol.2023.1140785.

Azcorra, M., Gaertner, Z., Davidson, C., He, Q., Kim, H., Nagappan, S., et al. (2023). Unique functional responses differentially map onto genetic subtypes of dopamine neurons. Nat Neurosci. doi: 10.1038/s41593-023-01401-9.

Balavoine, G., and Adoutte, A. (2003). The Segmented Urbilateria: A Testable Scenario1. Integrative and Comparative Biology 43(1), 137-147. doi: 10.1093/icb/43.1.137.

Banér, J., Nilsson, M., Mendel-Hartvig, M., and Landegren, U. (1998). Signal amplification of padlock probes by rolling circle replication. Nucleic Acids Res 26(22), 5073-5078. doi: 10.1093/nar/26.22.5073.

Bankiewicz, K.S., Eberling, J.L., Kohutnicka, M., Jagust, W., Pivirotto, P., Bringas, J., et al. (2000). Convection-enhanced delivery of AAV vector in parkinsonian monkeys; in vivo detection of gene expression and restoration of dopaminergic function using pro-drug approach. Exp Neurol 164(1), 2-14. doi: 10.1006/exnr.2000.7408.

Barker, R.A., Barrett, J., Mason, S.L., and Björklund, A. (2013). Fetal dopaminergic transplantation trials and the future of neural grafting in Parkinson's disease. Lancet Neurol 12(1), 84-91. doi: 10.1016/s1474-4422(12)70295-8.

Bartus, R.T., Weinberg, M.S., and Samulski, R.J. (2014). Parkinson's disease gene therapy: success by design meets failure by efficacy. Mol Ther 22(3), 487-497. doi: 10.1038/mt.2013.281.

Bendor, J.T., Logan, T.P., and Edwards, R.H. (2013). The function of α-synuclein. Neuron 79(6), 1044-1066. doi: 10.1016/j.neuron.2013.09.004.

Bertoncini, C.W., Jung, Y.S., Fernandez, C.O., Hoyer, W., Griesinger, C., Jovin, T.M., et al. (2005). Release of long-range tertiary interactions potentiates aggregation of natively unstructured alpha-synuclein. Proc Natl Acad Sci U S A 102(5), 1430-1435. doi: 10.1073/pnas.0407146102.

Bioscience, P. Parse Bioscience - WT Manufacturer protocol Parse Biosciece.

Björklund, T., and Davidsson, M. (2021). Next-Generation Gene Therapy for Parkinson's Disease Using Engineered Viral Vectors. J Parkinsons Dis 11(s2), S209-s217. doi: 10.3233/jpd-212674.

Bolam, J.P., Hanley, J.J., Booth, P.A., and Bevan, M.D. (2000). Synaptic organisation of the basal ganglia. J Anat 196 (Pt 4)(Pt 4), 527-542. doi: 10.1046/j.1469-7580.2000.19640527.x.

Bourdenx, M., Dovero, S., Engeln, M., Bido, S., Bastide, M.F., Dutheil, N., et al. (2015). Lack of additive role of ageing in nigrostriatal neurodegeneration triggered by α-synuclein overexpression. Acta Neuropathol Commun 3, 46. doi: 10.1186/s40478-015-0222-2.

Braak, H., Del Tredici, K., Rüb, U., de Vos, R.A., Jansen Steur, E.N., and Braak, E. (2003). Staging of brain pathology related to sporadic Parkinson's disease. Neurobiol Aging 24(2), 197-211. doi: 10.1016/s0197-4580(02)00065-9.

Bramham, C.R., Alme, M.N., Bittins, M., Kuipers, S.D., Nair, R.R., Pai, B., et al. (2010). The Arc of synaptic memory. Exp Brain Res 200(2), 125-140. doi: 10.1007/s00221-009-1959-2.

Brundin, P., Pogarell, O., Hagell, P., Piccini, P., Widner, H., Schrag, A., et al. (2000). Bilateral caudate and putamen grafts of embryonic mesencephalic tissue treated with lazaroids in Parkinson's disease. Brain 123 (Pt 7), 1380-1390. doi: 10.1093/brain/123.7.1380.

Burkhardt, P., and Sprecher, S.G. (2017). Evolutionary origin of synapses and neurons – Bridging the gap. BioEssays 39(10), 1700024. doi: https://doi.org/10.1002/bies.201700024.

Burré, J. (2015). The Synaptic Function of α-Synuclein. J Parkinsons Dis 5(4), 699-713. doi: 10.3233/jpd-150642.

Cenci, M.A., and Björklund, A. (2020). Animal models for preclinical Parkinson's research: An update and critical appraisal. Prog Brain Res 252, 27-59. doi: 10.1016/bs.pbr.2020.02.003.

Chalfoun, J., Majurski, M., Blattner, T., Bhadriraju, K., Keyrouz, W., Bajcsy, P., et al. (2017). MIST: Accurate and Scalable Microscopy Image Stitching Tool with Stage Modeling and Error Minimization. Sci Rep 7(1), 4988. doi: 10.1038/s41598-017-04567-y.

Chartier-Harlin, M.C., Kachergus, J., Roumier, C., Mouroux, V., Douay, X., Lincoln, S., et al. (2004). Alpha-synuclein locus duplication as a cause of familial Parkinson's disease. Lancet 364(9440), 1167-1169. doi: 10.1016/s0140-6736(04)17103-1.

Chen, W., McKenna, A., Schreiber, J., Haeussler, M., Yin, Y., Agarwal, V., et al. (2019). Massively parallel profiling and predictive modeling of the outcomes of CRISPR/Cas9-mediated double-strand break repair. Nucleic Acids Research 47(15), 7989-8003. doi: 10.1093/nar/gkz487.

Chirmule, N., Propert, K., Magosin, S., Qian, Y., Qian, R., and Wilson, J. (1999). Immune responses to adenovirus and adeno-associated virus in humans. Gene Ther 6(9), 1574-1583. doi: 10.1038/sj.gt.3300994.

Choi, I., Zhang, Y., Seegobin, S.P., Pruvost, M., Wang, Q., Purtell, K., et al. (2020). Microglia clear neuron-released α-synuclein via selective autophagy and prevent neurodegeneration. Nat Commun 11(1), 1386. doi: 10.1038/s41467-020-15119-w.

REFERENCES

Chowdhury, S., Shepherd, J.D., Okuno, H., Lyford, G., Petralia, R.S., Plath, N., et al. (2006). Arc/Arg3.1 interacts with the endocytic machinery to regulate AMPA receptor trafficking. Neuron 52(3), 445-459. doi: 10.1016/j.neuron.2006.08.033.

Christian, M., Cermak, T., Doyle, E.L., Schmidt, C., Zhang, F., Hummel, A., et al. (2010). Targeting DNA double-strand breaks with TAL effector nucleases. Genetics 186(2), 757-761. doi: 10.1534/genetics.110.120717.

Ciurleo, R., Corallo, F., Bonanno, L., Lo Buono, V., Di Lorenzo, G., Versaci, R., et al. (2018). Assessment of Duodopa(®) effects on quality of life of patients with advanced Parkinson's disease and their caregivers. J Neurol 265(9), 2005-2014. doi: 10.1007/s00415-018-8951-3.

Contin, M., and Martinelli, P. (2010). Pharmacokinetics of levodopa. J Neurol 257(Suppl 2), S253-261. doi: 10.1007/s00415-010-5728-8.

Conway, K.A., Lee, S.J., Rochet, J.C., Ding, T.T., Williamson, R.E., and Lansbury, P.T., Jr. (2000). Acceleration of oligomerization, not fibrillization, is a shared property of both alpha-synuclein mutations linked to early-onset Parkinson's disease: implications for pathogenesis and therapy. Proc Natl Acad Sci U S A 97(2), 571-576. doi: 10.1073/pnas.97.2.571.

Crick, F. (1989). The recent excitement about neural networks. Nature 337(6203), 129-132. doi: 10.1038/337129a0.

Crittenden, J.R., and Graybiel, A.M. (2011). Basal Ganglia disorders associated with imbalances in the striatal striosome and matrix compartments. Front Neuroanat 5, 59. doi: 10.3389/fnana.2011.00059.

Crosby, N., Deane, K.H., and Clarke, C.E. (2003). Amantadine in Parkinson's disease. Cochrane Database Syst Rev 2003(1), Cd003468. doi: 10.1002/14651858.Cd003468.

Dashkoff, J., Lerner, E.P., Truong, N., Klickstein, J.A., Fan, Z., Mu, D., et al. (2016). Tailored transgene expression to specific cell types in the central nervous system after peripheral injection with AAV9. Mol Ther Methods Clin Dev 3, 16081. doi: 10.1038/mtm.2016.81.

DaSilva, L.L., Wall, M.J., L, P.d.A., Wauters, S.C., Januário, Y.C., Müller, J., et al. (2016). Activity-Regulated Cytoskeleton-Associated Protein Controls AMPAR Endocytosis through a Direct Interaction with Clathrin-Adaptor Protein 2. eNeuro 3(3). doi: 10.1523/eneuro.0144-15.2016.

Datlinger, P., Rendeiro, A.F., Boenke, T., Senekowitsch, M., Krausgruber, T., Barreca, D., et al. (2021). Ultra-high-throughput single-cell RNA sequencing and perturbation screening with combinatorial fluidic indexing. Nat Methods 18(6), 635-642. doi: 10.1038/s41592-021-01153-z.

Davidsson, M., Wang, G., Aldrin-Kirk, P., Cardoso, T., Nolbrant, S., Hartnor, M., et al. (2019). A systematic capsid evolution approach performed in vivo for the design of AAV vectors with tailored properties and tropism. Proceedings of the National Academy of Sciences 116(52), 27053-27062. doi: doi:10.1073/pnas.1910061116.

Decressac, M., Kadkhodaei, B., Mattsson, B., Laguna, A., Perlmann, T., and Björklund, A. (2012a). α-Synuclein-induced down-regulation of Nurr1 disrupts GDNF signaling in nigral dopamine neurons. Sci Transl Med 4(163), 163ra156. doi: 10.1126/scitranslmed.3004676.

Decressac, M., Mattsson, B., Lundblad, M., Weikop, P., and Björklund, A. (2012b). Progressive neurodegenerative and behavioural changes induced by AAV-mediated overexpression of α-synuclein in midbrain dopamine neurons. Neurobiol Dis 45(3), 939-953. doi: 10.1016/j.nbd.2011.12.013.

Del Ser, T., McKeith, I., Anand, R., Cicin-Sain, A., Ferrara, R., and Spiegel, R. (2000). Dementia with lewy bodies: findings from an international multicentre study. Int J Geriatr Psychiatry 15(11), 1034-1045. doi: 10.1002/1099-1166(200011)15:11<1034::aid-gps231>3.0.co;2-5.

Delley, C.L., and Abate, A.R. (2021). Modular barcode beads for microfluidic single cell genomics. Scientific Reports 11(1), 10857. doi: 10.1038/s41598-021-90255-x.

DeLong, M.R. (1990). Primate models of movement disorders of basal ganglia origin. Trends Neurosci 13(7), 281-285. doi: 10.1016/0166-2236(90)90110-v.

Dickson, D.W. (1999). Tau and synuclein and their role in neuropathology. Brain Pathol 9(4), 657-661. doi: 10.1111/j.1750-3639.1999.tb00548.x.

Dickson, D.W., Crystal, H., Mattiace, L.A., Kress, Y., Schwagerl, A., Ksiezak-Reding, H., et al. (1989). Diffuse Lewy body disease: light and electron microscopic immunocytochemistry of senile plaques. Acta Neuropathol 78(6), 572-584. doi: 10.1007/bf00691284.

Doudna, J.A., and Charpentier, E. (2014). Genome editing. The new frontier of genome engineering with CRISPR-Cas9. Science 346(6213), 1258096. doi: 10.1126/science.1258096.

Dougherty, D.D. (2018). Deep Brain Stimulation: Clinical Applications. Psychiatr Clin North Am 41(3), 385-394. doi: 10.1016/j.psc.2018.04.004.

Dunbar, C.E., High, K.A., Joung, J.K., Kohn, D.B., Ozawa, K., and Sadelain, M. (2018). Gene therapy comes of age. Science 359(6372). doi: 10.1126/science.aan4672.

Ehringer, H., and Hornykiewicz, O. (1960). [Distribution of noradrenaline and dopamine (3-hydroxytyramine) in the human brain and their behavior in diseases of the extrapyramidal system]. Klin Wochenschr 38, 1236-1239. doi: 10.1007/bf01485901.

REFERENCES

Emborg, M.E., Carbon, M., Holden, J.E., During, M.J., Ma, Y., Tang, C., et al. (2007). Subthalamic glutamic acid decarboxylase gene therapy: changes in motor function and cortical metabolism. J Cereb Blood Flow Metab 27(3), 501-509. doi: 10.1038/sj.jcbfm.9600364.

Eriksen, M.S., and Bramham, C.R. (2022). Molecular physiology of Arc/Arg3.1: The oligomeric state hypothesis of synaptic plasticity. Acta Physiol (Oxf) 236(3), e13886. doi: 10.1111/apha.13886.

Eriksen, M.S., Nikolaienko, O., Hallin, E.I., Grødem, S., Bustad, H.J., Flydal, M.I., et al. (2021). Arc self-association and formation of virus-like capsids are mediated by an N-terminal helical coil motif. Febs j 288(9), 2930-2955. doi: 10.1111/febs.15618.

Fanciulli, A., and Wenning, G.K. (2015). Multiple-system atrophy. N Engl J Med 372(3), 249-263. doi: 10.1056/NEJMra1311488.

Fearnley, J.M., and Lees, A.J. (1991). Ageing and Parkinson's disease: substantia nigra regional selectivity. Brain 114 (Pt 5), 2283-2301. doi: 10.1093/brain/114.5.2283.

Fredriksson, S., Gullberg, M., Jarvius, J., Olsson, C., Pietras, K., Gústafsdóttir, S.M., et al. (2002). Protein detection using proximity-dependent DNA ligation assays. Nature Biotechnology 20(5), 473-477. doi: 10.1038/nbt0502-473.

Freeman, T.B., Olanow, C.W., Hauser, R.A., Nauert, G.M., Smith, D.A., Borlongan, C.V., et al. (1995). Bilateral fetal nigral transplantation into the postcommissural putamen in Parkinson's disease. Ann Neurol 38(3), 379-388. doi: 10.1002/ana.410380307.

Gao, G., Alvira, M.R., Somanathan, S., Lu, Y., Vandenberghe, L.H., Rux, J.J., et al. (2003). Adeno-associated viruses undergo substantial evolution in primates during natural infections. Proc Natl Acad Sci U S A 100(10), 6081-6086. doi: 10.1073/pnas.0937739100.

Gao, Y., Hisey, E., Bradshaw, T.W.A., Erata, E., Brown, W.E., Courtland, J.L., et al. (2019). Plug-and-Play Protein Modification Using Homology-Independent Universal Genome Engineering. Neuron 103(4), 583-597.e588. doi: https://doi.org/10.1016/j.neuron.2019.05.047.

Genomics, X. Chromium Single Cell 3 v3 Reagent, Workflow & Software Updates [Online]. Available: https://www.10xgenomics.com/support/single-cell-gene-expression/documentation/steps/library-prep/chromium-single-cell-3-v-3-reagent-workflow-and-software-updates [Accessed].

George, J., Li, Y., Kadamberi, I.P., Parashar, D., Tsaih, S.-W., Gupta, P., et al. (2021). RNA-binding protein FXR1 drives cMYC translation by recruiting eIF4F complex to the translation start site. Cell Reports 37(5). doi: 10.1016/j.celrep.2021.109934.

George, J.M. (2002). The synucleins. Genome Biol 3(1), Reviews3002. doi: 10.1186/gb-2001-3-1-reviews3002.

Gerfen, C.R., Engber, T.M., Mahan, L.C., Susel, Z., Chase, T.N., Monsma, F.J., Jr., et al. (1990). D1 and D2 dopamine receptor-regulated gene expression of striatonigral and striatopallidal neurons. Science 250(4986), 1429-1432. doi: 10.1126/science.2147780.

Ghanipour, L., Darmanis, S., Landegren, U., Glimelius, B., Påhlman, L., and Birgisson, H. (2016). Detection of Biomarkers with Solid-Phase Proximity Ligation Assay in Patients with Colorectal Cancer. Translational Oncology 9(3), 251-255. doi: https://doi.org/10.1016/j.tranon.2016.04.001.

Ghorbani, S., Jelinek, E., Jain, R., Buehner, B., Li, C., Lozinski, B.M., et al. (2022). Versican promotes T helper 17 cytotoxic inflammation and impedes oligodendrocyte precursor cell remyelination. Nature Communications 13(1), 2445. doi: 10.1038/s41467-022-30032-0.

Giasson, B.I., Uryu, K., Trojanowski, J.Q., and Lee, V.M. (1999). Mutant and wild type human alpha-synucleins assemble into elongated filaments with distinct morphologies in vitro. J Biol Chem 274(12), 7619-7622. doi: 10.1074/jbc.274.12.7619.

Graham, J.G., and Oppenheimer, D.R. (1969). Orthostatic hypotension and nicotine sensitivity in a case of multiple system atrophy. J Neurol Neurosurg Psychiatry 32(1), 28-34. doi: 10.1136/jnnp.32.1.28.

Grealish, S., Mattsson, B., Draxler, P., and Björklund, A. (2010). Characterisation of behavioural and neurodegenerative changes induced by intranigral 6-hydroxydopamine lesions in a mouse model of Parkinson's disease. Eur J Neurosci 31(12), 2266-2278. doi: 10.1111/j.1460-9568.2010.07265.x.

Greffard, S., Verny, M., Bonnet, A.M., Beinis, J.Y., Gallinari, C., Meaume, S., et al. (2006). Motor score of the Unified Parkinson Disease Rating Scale as a good predictor of Lewy body-associated neuronal loss in the substantia nigra. Arch Neurol 63(4), 584-588. doi: 10.1001/archneur.63.4.584.

Groiss, S.J., Wojtecki, L., Südmeyer, M., and Schnitzler, A. (2009). Deep brain stimulation in Parkinson's disease. Ther Adv Neurol Disord 2(6), 20-28. doi: 10.1177/1756285609339382.

Guo, M. (2010). What have we learned from Drosophila models of Parkinson's disease? Prog Brain Res 184, 3-16. doi: 10.1016/s0079-6123(10)84001-4.

Haery, L., Deverman, B.E., Matho, K.S., Cetin, A., Woodard, K., Cepko, C., et al. (2019). Adeno-Associated Virus Technologies and Methods for Targeted Neuronal Manipulation. Frontiers in Neuroanatomy 13. doi: 10.3389/fnana.2019.00093.

Hallin, E.I., Eriksen, M.S., Baryshnikov, S., Nikolaienko, O., Grødem, S., Hosokawa, T., et al. (2018). Structure of monomeric full-length ARC sheds light on molecular flexibility, protein interactions, and functional modalities. J Neurochem 147(3), 323-343. doi: 10.1111/jnc.14556.

REFERENCES

Hantak, M.P., Einstein, J., Kearns, R.B., and Shepherd, J.D. (2021). Intercellular Communication in the Nervous System Goes Viral. Trends Neurosci 44(4), 248-259. doi: 10.1016/j.tins.2020.12.003.

Harari, Y.N.a. (2015). Sapiens : a brief history of humankind. First U.S. edition. New York : Harper, [2015].

Hermonat, P.L., and Muzyczka, N. (1984). Use of adeno-associated virus as a mammalian DNA cloning vector: transduction of neomycin resistance into mammalian tissue culture cells. Proc Natl Acad Sci U S A 81(20), 6466-6470. doi: 10.1073/pnas.81.20.6466.

Hernandez, Y.J., Wang, J., Kearns, W.G., Loiler, S., Poirier, A., and Flotte, T.R. (1999). Latent Adeno-Associated Virus Infection Elicits Humoral but Not Cell-Mediated Immune Responses in a Nonhuman Primate Model. Journal of Virology 73(10), 8549-8558. doi: doi:10.1128/jvi.73.10.8549-8558.1999.

Heyer, W.-D., Ehmsen, K.T., and Liu, J. (2010). Regulation of Homologous Recombination in Eukaryotes. Annual Review of Genetics 44(1), 113-139. doi: 10.1146/annurev-genet-051710-150955.

Hoban, D.B., Shrigley, S., Mattsson, B., Breger, L.S., Jarl, U., Cardoso, T., et al. (2020). Impact of α-synuclein pathology on transplanted hESC-derived dopaminergic neurons in a humanized α-synuclein rat model of PD. Proc Natl Acad Sci U S A 117(26), 15209-15220. doi: 10.1073/pnas.2001305117.

Hogan, D.B., Fiest, K.M., Roberts, J.I., Maxwell, C.J., Dykeman, J., Pringsheim, T., et al. (2016). The Prevalence and Incidence of Dementia with Lewy Bodies: a Systematic Review. Can J Neurol Sci 43 Suppl 1, S83-95. doi: 10.1017/cjn.2016.2.

Hor, H., Francescatto, L., Bartesaghi, L., Ortega-Cubero, S., Kousi, M., Lorenzo-Betancor, O., et al. (2015). Missense mutations in TENM4, a regulator of axon guidance and central myelination, cause essential tremor. Human Molecular Genetics 24(20), 5677-5686. doi: 10.1093/hmg/ddv281.

Hsu, P.D., Lander, E.S., and Zhang, F. (2014). Development and applications of CRISPR-Cas9 for genome engineering. Cell 157(6), 1262-1278. doi: 10.1016/j.cell.2014.05.010.

IDT (2022). CRISPR-Cas9 guide RNA design checker [Online]. Available: https://eu.idtdna.com/site/order/designtool/index/CRISPR_SEQUENCE [Accessed].

Islam, S., Kjällquist, U., Moliner, A., Zajac, P., Fan, J.B., Lönnerberg, P., et al. (2011). Characterization of the single-cell transcriptional landscape by highly multiplex RNA-seq. Genome Res 21(7), 1160-1167. doi: 10.1101/gr.110882.110.

Islam, S., Zeisel, A., Joost, S., La Manno, G., Zajac, P., Kasper, M., et al. (2014). Quantitative single-cell RNA-seq with unique molecular identifiers. Nature Methods 11(2), 163-166. doi: 10.1038/nmeth.2772.

Jékely, G. (2011). Origin and early evolution of neural circuits for the control of ciliary locomotion. Proc Biol Sci 278(1707), 914-922. doi: 10.1098/rspb.2010.2027.

Jinek, M., Chylinski, K., Fonfara, I., Hauer, M., Doudna, J.A., and Charpentier, E. (2012). A programmable dual-RNA-guided DNA endonuclease in adaptive bacterial immunity. Science 337(6096), 816-821. doi: 10.1126/science.1225829.

Kalargyrou, A.A., Basche, M., Hare, A., West, E.L., Smith, A.J., Ali, R.R., et al. (2021). Nanotube-like processes facilitate material transfer between photoreceptors. EMBO Rep 22(11), e53732. doi: 10.15252/embr.202153732.

Kaludov, N., Brown, K.E., Walters, R.W., Zabner, J., and Chiorini, J.A. (2001). Adeno-associated virus serotype 4 (AAV4) and AAV5 both require sialic acid binding for hemagglutination and efficient transduction but differ in sialic acid linkage specificity. J Virol 75(15), 6884-6893. doi: 10.1128/jvi.75.15.6884-6893.2001.

Kamath, T., Abdulraouf, A., Burris, S.J., Langlieb, J., Gazestani, V., Nadaf, N.M., et al. (2022). Single-cell genomic profiling of human dopamine neurons identifies a population that selectively degenerates in Parkinson's disease. Nat Neurosci 25(5), 588-595. doi: 10.1038/s41593-022-01061-1.

Kanaan, N.M., Sellnow, R.C., Boye, S.L., Coberly, B., Bennett, A., Agbandje-McKenna, M., et al. (2017). Rationally Engineered AAV Capsids Improve Transduction and Volumetric Spread in the CNS. Mol Ther Nucleic Acids 8, 184-197. doi: 10.1016/j.omtn.2017.06.011.

Katzenschlager, R., Sampaio, C., Costa, J., and Lees, A. (2003). Anticholinergics for symptomatic management of Parkinson's disease. Cochrane Database Syst Rev 2002(2), Cd003735. doi: 10.1002/14651858.Cd003735.

Kawashima, T., Okuno, H., Nonaka, M., Adachi-Morishima, A., Kyo, N., Okamura, M., et al. (2009). Synaptic activity-responsive element in the <i>Arc</i>/<i>Arg3.1</i> promoter essential for synapse-to-nucleus signaling in activated neurons. Proceedings of the National Academy of Sciences 106(1), 316-321. doi: doi:10.1073/pnas.0806518106.

Kebschull, J.M., Garcia da Silva, P., Reid, A.P., Peikon, I.D., Albeanu, D.F., and Zador, A.M. (2016). High-Throughput Mapping of Single-Neuron Projections by Sequencing of Barcoded RNA. Neuron 91(5), 975-987. doi: 10.1016/j.neuron.2016.07.036.

Kefalopoulou, Z., Politis, M., Piccini, P., Mencacci, N., Bhatia, K., Jahanshahi, M., et al. (2014). Long-term clinical outcome of fetal cell transplantation for Parkinson disease: two case reports. JAMA Neurol 71(1), 83-87. doi: 10.1001/jamaneurol.2013.4749.

Khattar, K.E., Safi, J., Rodriguez, A.-M., and Vignais, M.-L. (2022). Intercellular Communication in the Brain through Tunneling Nanotubes. Cancers 14(5), 1207.

Khoo, T.K., Yarnall, A.J., Duncan, G.W., Coleman, S., O'Brien, J.T., Brooks, D.J., et al. (2013). The spectrum of nonmotor symptoms in early Parkinson disease. Neurology 80(3), 276-281. doi: 10.1212/WNL.0b013e31827deb74.

REFERENCES

Kirik, D., Rosenblad, C., Burger, C., Lundberg, C., Johansen, T.E., Muzyczka, N., et al. (2002). Parkinson-like neurodegeneration induced by targeted overexpression of alpha-synuclein in the nigrostriatal system. J Neurosci 22(7), 2780-2791. doi: 10.1523/jneurosci.22-07-02780.2002.

Kirkeby, A., Nolbrant, S., Tiklova, K., Heuer, A., Kee, N., Cardoso, T., et al. (2017). Predictive Markers Guide Differentiation to Improve Graft Outcome in Clinical Translation of hESC-Based Therapy for Parkinson's Disease. Cell Stem Cell 20(1), 135-148. doi: 10.1016/j.stem.2016.09.004.

Klaesson, A., Grannas, K., Ebai, T., Heldin, J., Koos, B., Leino, M., et al. (2018). Improved efficiency of in situ protein analysis by proximity ligation using UnFold probes. Scientific Reports 8(1), 5400. doi: 10.1038/s41598-018-23582-1.

Klein, A.M., Mazutis, L., Akartuna, I., Tallapragada, N., Veres, A., Li, V., et al. (2015). Droplet barcoding for single-cell transcriptomics applied to embryonic stem cells. Cell 161(5), 1187-1201. doi: 10.1016/j.cell.2015.04.044.

Kobayashi, H., Yamamoto, S., Maruo, T., and Murakami, F. (2005). Identification of a cis-acting element required for dendritic targeting of activity-regulated cytoskeleton-associated protein mRNA. Eur J Neurosci 22(12), 2977-2984. doi: 10.1111/j.1460-9568.2005.04508.x.

Komor, A.C., Badran, A.H., and Liu, D.R. (2017). CRISPR-Based Technologies for the Manipulation of Eukaryotic Genomes. Cell 168(1-2), 20-36. doi: 10.1016/j.cell.2016.10.044.

Konno, T., Ross, O.A., Puschmann, A., Dickson, D.W., and Wszolek, Z.K. (2016). Autosomal dominant Parkinson's disease caused by SNCA duplications. Parkinsonism Relat Disord 22 Suppl 1(Suppl 1), S1-6. doi: 10.1016/j.parkreldis.2015.09.007.

Kosaka, K., Yoshimura, M., Ikeda, K., and Budka, H. (1984). Diffuse type of Lewy body disease: progressive dementia with abundant cortical Lewy bodies and senile changes of varying degree--a new disease? Clin Neuropathol 3(5), 185-192.

Kotin, R.M., Siniscalco, M., Samulski, R.J., Zhu, X.D., Hunter, L., Laughlin, C.A., et al. (1990). Site-specific integration by adeno-associated virus. Proc Natl Acad Sci U S A 87(6), 2211-2215. doi: 10.1073/pnas.87.6.2211.

Krüger, R., Kuhn, W., Müller, T., Woitalla, D., Graeber, M., Kösel, S., et al. (1998). Ala30Pro mutation in the gene encoding alpha-synuclein in Parkinson's disease. Nat Genet 18(2), 106-108. doi: 10.1038/ng0298-106.

Kügler, S., Kilic, E., and Bähr, M. (2003). Human synapsin 1 gene promoter confers highly neuron-specific long-term transgene expression from an adenoviral vector in the adult rat brain depending on the transduced area. Gene Ther 10(4), 337-347. doi: 10.1038/sj.gt.3301905.

Labun, K., Montague, T.G., Gagnon, J.A., Thyme, S.B., and Valen, E. (2016). CHOPCHOP v2: a web tool for the next generation of CRISPR genome engineering. Nucleic Acids Res 44(W1), W272-276. doi: 10.1093/nar/gkw398.

Labun, K., Montague, T.G., Krause, M., Torres Cleuren, Y.N., Tjeldnes, H., and Valen, E. (2019). CHOPCHOP v3: expanding the CRISPR web toolbox beyond genome editing. Nucleic Acids Res 47(W1), W171-W174. doi: 10.1093/nar/gkz365.

Lake, B.B., Ai, R., Kaeser, G.E., Salathia, N.S., Yung, Y.C., Liu, R., et al. (2016). Neuronal subtypes and diversity revealed by single-nucleus RNA sequencing of the human brain. Science 352(6293), 1586-1590. doi: 10.1126/science.aaf1204.

Lake, B.B., Codeluppi, S., Yung, Y.C., Gao, D., Chun, J., Kharchenko, P.V., et al. (2017). A comparative strategy for single-nucleus and single-cell transcriptomes confirms accuracy in predicted cell-type expression from nuclear RNA. Scientific Reports 7(1), 6031. doi: 10.1038/s41598-017-04426-w.

Lam, S., Arif, M., Song, X., Uhlén, M., and Mardinoglu, A. (2022). Machine Learning Analysis Reveals Biomarkers for the Detection of Neurological Diseases. Front Mol Neurosci 15, 889728. doi: 10.3389/fnmol.2022.889728.

Lashuel, H.A., Hartley, D., Petre, B.M., Walz, T., and Lansbury, P.T., Jr. (2002). Neurodegenerative disease: amyloid pores from pathogenic mutations. Nature 418(6895), 291. doi: 10.1038/418291a.

Lashuel, H.A., Overk, C.R., Oueslati, A., and Masliah, E. (2013). The many faces of α-synuclein: from structure and toxicity to therapeutic target. Nat Rev Neurosci 14(1), 38-48. doi: 10.1038/nrn3406.

Lawlor, P.A., Bland, R.J., Mouravlev, A., Young, D., and During, M.J. (2009). Efficient gene delivery and selective transduction of glial cells in the mammalian brain by AAV serotypes isolated from nonhuman primates. Mol Ther 17(10), 1692-1702. doi: 10.1038/mt.2009.170.

Lee, H.J., Ricarte, D., Ortiz, D., and Lee, S.J. (2019). Models of multiple system atrophy. Exp Mol Med 51(11), 1-10. doi: 10.1038/s12276-019-0346-8.

Lesage, S., Anheim, M., Letournel, F., Bousset, L., Honoré, A., Rozas, N., et al. (2013). G51D α-synuclein mutation causes a novel parkinsonian-pyramidal syndrome. Ann Neurol 73(4), 459-471. doi: 10.1002/ana.23894.

Li, C., and Samulski, R.J. (2020). Engineering adeno-associated virus vectors for gene therapy. Nature Reviews Genetics 21(4), 255-272. doi: 10.1038/s41576-019-0205-4.

Li, W., Englund, E., Widner, H., Mattsson, B., van Westen, D., Lätt, J., et al. (2016). Extensive graft-derived dopaminergic innervation is maintained 24 years after transplantation in the degenerating parkinsonian brain. Proc Natl Acad Sci U S A 113(23), 6544-6549. doi: 10.1073/pnas.1605245113.

REFERENCES

Lindvall, O., Brundin, P., Widner, H., Rehncrona, S., Gustavii, B., Frackowiak, R., et al. (1990). Grafts of fetal dopamine neurons survive and improve motor function in Parkinson's disease. Science 247(4942), 574-577. doi: 10.1126/science.2105529.

Lindvall, O., Rehncrona, S., Brundin, P., Gustavii, B., Astedt, B., Widner, H., et al. (1989). Human fetal dopamine neurons grafted into the striatum in two patients with severe Parkinson's disease. A detailed account of methodology and a 6-month follow-up. Arch Neurol 46(6), 615-631. doi: 10.1001/archneur.1989.00520420033021.

Lindvall, O., Sawle, G., Widner, H., Rothwell, J.C., Björklund, A., Brooks, D., et al. (1994). Evidence for long-term survival and function of dopaminergic grafts in progressive Parkinson's disease. Ann Neurol 35(2), 172-180. doi: 10.1002/ana.410350208.

Litvan, I., MacIntyre, A., Goetz, C.G., Wenning, G.K., Jellinger, K., Verny, M., et al. (1998). Accuracy of the clinical diagnoses of Lewy body disease, Parkinson disease, and dementia with Lewy bodies: a clinicopathologic study. Arch Neurol 55(7), 969-978. doi: 10.1001/archneur.55.7.969.

Lock, M., Alvira, M.R., Chen, S.J., and Wilson, J.M. (2014). Absolute determination of single-stranded and self-complementary adeno-associated viral vector genome titers by droplet digital PCR. Hum Gene Ther Methods 25(2), 115-125. doi: 10.1089/hgtb.2013.131.

Luk, K.C., Covell, D.J., Kehm, V.M., Zhang, B., Song, I.Y., Byrne, M.D., et al. (2016). Molecular and Biological Compatibility with Host Alpha-Synuclein Influences Fibril Pathogenicity. Cell Reports 16(12), 3373-3387. doi: https://doi.org/10.1016/j.celrep.2016.08.053.

Lundblad, M., Decressac, M., Mattsson, B., and Björklund, A. (2012a). Impaired neurotransmission caused by overexpression of α-synuclein in nigral dopamine neurons. Proceedings of the National Academy of Sciences 109(9), 3213-3219. doi: doi:10.1073/pnas.1200575109.

Lundblad, M., Decressac, M., Mattsson, B., and Björklund, A. (2012b). Impaired neurotransmission caused by overexpression of α-synuclein in nigral dopamine neurons. Proc Natl Acad Sci U S A 109(9), 3213-3219. doi: 10.1073/pnas.1200575109.

Luo, J., Kaplitt, M.G., Fitzsimons, H.L., Zuzga, D.S., Liu, Y., Oshinsky, M.L., et al. (2002). Subthalamic GAD gene therapy in a Parkinson's disease rat model. Science 298(5592), 425-429. doi: 10.1126/science.1074549.

Lyford, G.L., Yamagata, K., Kaufmann, W.E., Barnes, C.A., Sanders, L.K., Copeland, N.G., et al. (1995). Arc, a growth factor and activity-regulated gene, encodes a novel cytoskeleton-associated protein that is enriched in neuronal dendrites. Neuron 14(2), 433-445. doi: 10.1016/0896-6273(95)90299-6.

Ma, S.X., Seo, B.A., Kim, D., Xiong, Y., Kwon, S.H., Brahmachari, S., et al. (2021). Complement and Coagulation Cascades are Potentially Involved in Dopaminergic Neurodegeneration in α-Synuclein-Based Mouse Models of Parkinson's Disease. J Proteome Res 20(7), 3428-3443. doi: 10.1021/acs.jproteome.0c01002.

Macosko, E.Z., Basu, A., Satija, R., Nemesh, J., Shekhar, K., Goldman, M., et al. (2015). Highly Parallel Genome-wide Expression Profiling of Individual Cells Using Nanoliter Droplets. Cell 161(5), 1202-1214. doi: 10.1016/j.cell.2015.05.002.

Maheshri, N., Koerber, J.T., Kaspar, B.K., and Schaffer, D.V. (2006). Directed evolution of adeno-associated virus yields enhanced gene delivery vectors. Nat Biotechnol 24(2), 198-204. doi: 10.1038/nbt1182.

Mao, Z., Bozzella, M., Seluanov, A., and Gorbunova, V. (2008). DNA repair by nonhomologous end joining and homologous recombination during cell cycle in human cells. Cell cycle 7(18), 2902-2906.

Maroteaux, L., Campanelli, J.T., and Scheller, R.H. (1988). Synuclein: a neuron-specific protein localized to the nucleus and presynaptic nerve terminal. J Neurosci 8(8), 2804-2815. doi: 10.1523/jneurosci.08-08-02804.1988.

Marui, W., Iseki, E., Nakai, T., Miura, S., Kato, M., Uéda, K., et al. (2002). Progression and staging of Lewy pathology in brains from patients with dementia with Lewy bodies. J Neurol Sci 195(2), 153-159. doi: 10.1016/s0022-510x(02)00006-0.

Matsui, H., and Takahashi, R. (2018). Parkinson's disease pathogenesis from the viewpoint of small fish models. J Neural Transm (Vienna) 125(1), 25-33. doi: 10.1007/s00702-017-1772-1.

Maulik, M., Mitra, S., Bult-Ito, A., Taylor, B.E., and Vayndorf, E.M. (2017). Behavioral Phenotyping and Pathological Indicators of Parkinson's Disease in C. elegans Models. Front Genet 8, 77. doi: 10.3389/fgene.2017.00077.

McCarty, D.M., Monahan, P.E., and Samulski, R.J. (2001). Self-complementary recombinant adeno-associated virus (scAAV) vectors promote efficient transduction independently of DNA synthesis. Gene Ther 8(16), 1248-1254. doi: 10.1038/sj.gt.3301514.

McCurry, C.L., Shepherd, J.D., Tropea, D., Wang, K.H., Bear, M.F., and Sur, M. (2010). Loss of Arc renders the visual cortex impervious to the effects of sensory experience or deprivation. Nature Neuroscience 13(4), 450-457. doi: 10.1038/nn.2508.

McKeith, I.G., Boeve, B.F., Dickson, D.W., Halliday, G., Taylor, J.P., Weintraub, D., et al. (2017). Diagnosis and management of dementia with Lewy bodies: Fourth consensus report of the DLB Consortium. Neurology 89(1), 88-100. doi: 10.1212/wnl.0000000000004058.

McVey, M., and Lee, S.E. (2008). MMEJ repair of double-strand breaks (director's cut): deleted sequences and alternative endings. Trends Genet 24(11), 529-538. doi: 10.1016/j.tig.2008.08.007.

REFERENCES

Men, Y., Yelick, J., Jin, S., Tian, Y., Chiang, M.S.R., Higashimori, H., et al. (2019). Exosome reporter mice reveal the involvement of exosomes in mediating neuron to astroglia communication in the CNS. Nat Commun 10(1), 4136. doi: 10.1038/s41467-019-11534-w.

Messaoudi, E., Kanhema, T., Soulé, J., Tiron, A., Dagyte, G., da Silva, B., et al. (2007). Sustained Arc/Arg3.1 synthesis controls long-term potentiation consolidation through regulation of local actin polymerization in the dentate gyrus in vivo. J Neurosci 27(39), 10445-10455. doi: 10.1523/jneurosci.2883-07.2007.

Montague, T.G., Cruz, J.M., Gagnon, J.A., Church, G.M., and Valen, E. (2014). CHOP-CHOP: a CRISPR/Cas9 and TALEN web tool for genome editing. Nucleic Acids Res 42(Web Server issue), W401-407. doi: 10.1093/nar/gku410.

Nair, R.R., Patil, S., Tiron, A., Kanhema, T., Panja, D., Schiro, L., et al. (2017). Dynamic Arc SUMOylation and Selective Interaction with F-Actin-Binding Protein Drebrin A in LTP Consolidation In Vivo. Frontiers in Synaptic Neuroscience 9. doi: 10.3389/fnsyn.2017.00008.

Nakano, S., Nishikawa, M., Kobayashi, T., Harlin, E.W., Ito, T., Sato, K., et al. (2022). The Rho guanine nucleotide exchange factor PLEKHG1 is activated by interaction with and phosphorylation by Src family kinase member FYN. J Biol Chem 298(2), 101579. doi: 10.1016/j.jbc.2022.101579.

Naldini, L. (2015). Gene therapy returns to centre stage. Nature 526(7573), 351-360. doi: 10.1038/nature15818.

Negrini, M., Tomasello, G., Davidsson, M., Fenyi, A., Adant, C., Hauser, S., et al. (2022). Sequential or Simultaneous Injection of Preformed Fibrils and AAV Overexpression of Alpha-Synuclein Are Equipotent in Producing Relevant Pathology and Behavioral Deficits. J Parkinsons Dis 12(4), 1133-1153. doi: 10.3233/jpd-212555.

Nemani, V.M., Lu, W., Berge, V., Nakamura, K., Onoa, B., Lee, M.K., et al. (2010). Increased expression of alpha-synuclein reduces neurotransmitter release by inhibiting synaptic vesicle reclustering after endocytosis. Neuron 65(1), 66-79. doi: 10.1016/j.neuron.2009.12.023.

Nicholls, J.G., Martin, A.R., Fuchs, P.A., Brown, D.A., Diamond, M.E., and Weisblat, D.A. (2012). From Neuron to Brain. Sinauer.

Nishiyama, J., Mikuni, T., and Yasuda, R. (2017). Virus-Mediated Genome Editing via Homology-Directed Repair in Mitotic and Postmitotic Cells in Mammalian Brain. Neuron 96(4), 755-768.e755. doi: 10.1016/j.neuron.2017.10.004.

Nishizono, H., Yasuda, R., and Laviv, T. (2020). Methodologies and Challenges for CRISPR/Cas9 Mediated Genome Editing of the Mammalian Brain. Front Genome Ed 2, 602970. doi: 10.3389/fgeed.2020.602970.

Niyonambaza, S.D., Kumar, P., Xing, P., Mathault, J., De Koninck, P., Boisselier, E., et al. (2019). A Review of Neurotransmitters Sensing Methods for Neuro-Engineering Research. Applied Sciences 9(21), 4719.

Nolbrant, S., Giacomoni, J., Hoban, D.B., Bruzelius, A., Birtele, M., Chandler-Militello, D., et al. (2020). Direct Reprogramming of Human Fetal- and Stem Cell-Derived Glial Progenitor Cells into Midbrain Dopaminergic Neurons. Stem Cell Reports 15(4), 869-882. doi: 10.1016/j.stemcr.2020.08.013.

Nolbrant, S., Heuer, A., Parmar, M., and Kirkeby, A. (2017). Generation of high-purity human ventral midbrain dopaminergic progenitors for in vitro maturation and intracerebral transplantation. Nat Protoc 12(9), 1962-1979. doi: 10.1038/nprot.2017.078.

Nutt, J.G., Woodward, W.R., Beckner, R.M., Stone, C.K., Berggren, K., Carter, J.H., et al. (1994). Effect of peripheral catechol-O-methyltransferase inhibition on the pharmacokinetics and pharmacodynamics of levodopa in parkinsonian patients. Neurology 44(5), 913-919. doi: 10.1212/wnl.44.5.913.

Nyholm, D., Klangemo, K., and Johansson, A. (2012). Levodopa/carbidopa intestinal gel infusion long-term therapy in advanced Parkinson's disease. Eur J Neurol 19(8), 1079-1085. doi: 10.1111/j.1468-1331.2012.03679.x.

Oliveira, L.M., Falomir-Lockhart, L.J., Botelho, M.G., Lin, K.H., Wales, P., Koch, J.C., et al. (2015). Elevated α-synuclein caused by SNCA gene triplication impairs neuronal differentiation and maturation in Parkinson's patient-derived induced pluripotent stem cells. Cell Death Dis 6(11), e1994. doi: 10.1038/cddis.2015.318.

Ortega-Ramírez, A., Vega, R., and Soto, E. (2017). Acid-Sensing Ion Channels as Potential Therapeutic Targets in Neurodegeneration and Neuroinflammation. Mediators Inflamm 2017, 3728096. doi: 10.1155/2017/3728096.

Orthwein, A., Noordermeer, S.M., Wilson, M.D., Landry, S., Enchev, R.I., Sherker, A., et al. (2015). A mechanism for the suppression of homologous recombination in G1 cells. Nature 528(7582), 422-426. doi: 10.1038/nature16142.

Panja, D., Kenney, J.W., D'Andrea, L., Zalfa, F., Vedeler, A., Wibrand, K., et al. (2014). Two-stage translational control of dentate gyrus LTP consolidation is mediated by sustained BDNF-TrkB signaling to MNK. Cell Rep 9(4), 1430-1445. doi: 10.1016/j.celrep.2014.10.016.

Parkinson, J. (2002). An essay on the shaking palsy. 1817. J Neuropsychiatry Clin Neurosci 14(2), 223-236; discussion 222. doi: 10.1176/jnp.14.2.223.

Pasanen, P., Myllykangas, L., Siitonen, M., Raunio, A., Kaakkola, S., Lyytinen, J., et al. (2014). Novel α-synuclein mutation A53E associated with atypical multiple system atrophy and Parkinson's disease-type pathology. Neurobiol Aging 35(9), 2180.e2181-2185. doi: 10.1016/j.neurobiolaging.2014.03.024.

REFERENCES

Pascual, M., Ibáñez, F., and Guerri, C. (2020). Exosomes as mediators of neuron-glia communication in neuroinflammation. Neural Regen Res 15(5), 796-801. doi: 10.4103/1673-5374.268893.

Pastuzyn, E.D., Day, C.E., Kearns, R.B., Kyrke-Smith, M., Taibi, A.V., McCormick, J., et al. (2018). The Neuronal Gene Arc Encodes a Repurposed Retrotransposon Gag Protein that Mediates Intercellular RNA Transfer. Cell 172(1-2), 275-288.e218. doi: 10.1016/j.cell.2017.12.024.

Peelaerts, W., Bousset, L., Van der Perren, A., Moskalyuk, A., Pulizzi, R., Giugliano, M., et al. (2015). α-Synuclein strains cause distinct synucleinopathies after local and systemic administration. Nature 522(7556), 340-344. doi: 10.1038/nature14547.

Peng, T., Thorn, K., Schroeder, T., Wang, L., Theis, F.J., Marr, C., et al. (2017). A BaSiC tool for background and shading correction of optical microscopy images. Nat Commun 8, 14836. doi: 10.1038/ncomms14836.

Penttinen, A.M., Parkkinen, I., Blom, S., Kopra, J., Andressoo, J.O., Pitkanen, K., et al. (2018). Implementation of deep neural networks to count dopamine neurons in substantia nigra. Eur J Neurosci 48(6), 2354-2361. doi: 10.1111/ejn.14129.

Perez, R.G., Waymire, J.C., Lin, E., Liu, J.J., Guo, F., and Zigmond, M.J. (2002). A role for alpha-synuclein in the regulation of dopamine biosynthesis. J Neurosci 22(8), 3090-3099. doi: 10.1523/jneurosci.22-08-03090.2002.

Periquet, M., Fulga, T., Myllykangas, L., Schlossmacher, M.G., and Feany, M.B. (2007). Aggregated alpha-synuclein mediates dopaminergic neurotoxicity in vivo. J Neurosci 27(12), 3338-3346. doi: 10.1523/jneurosci.0285-07.2007.

Perry, E.K., Curtis, M., Dick, D.J., Candy, J.M., Atack, J.R., Bloxham, C.A., et al. (1985). Cholinergic correlates of cognitive impairment in Parkinson's disease: comparisons with Alzheimer's disease. J Neurol Neurosurg Psychiatry 48(5), 413-421. doi: 10.1136/jnnp.48.5.413.

Picelli, S., Faridani, O.R., Björklund, Å.K., Winberg, G., Sagasser, S., and Sandberg, R. (2014). Full-length RNA-seq from single cells using Smart-seq2. Nature Protocols 9(1), 171-181. doi: 10.1038/nprot.2014.006.

Pintchovski, S.A., Peebles, C.L., Kim, H.J., Verdin, E., and Finkbeiner, S. (2009). The Serum Response Factor and a Putative Novel Transcription Factor Regulate Expression of the Immediate-Early Gene Arc/Arg3.1 in Neurons. The Journal of Neuroscience 29(5), 1525-1537. doi: 10.1523/jneurosci.5575-08.2009.

Polymeropoulos, M.H., Lavedan, C., Leroy, E., Ide, S.E., Dehejia, A., Dutra, A., et al. (1997). Mutation in the alpha-synuclein gene identified in families with Parkinson's disease. Science 276(5321), 2045-2047. doi: 10.1126/science.276.5321.2045.

Powell, S.K., Rivera-Soto, R., and Gray, S.J. (2015). Viral expression cassette elements to enhance transgene target specificity and expression in gene therapy. Discov Med 19(102), 49-57.

Qi, J., Sun, H., Zhang, Y., Wang, Z., Xun, Z., Li, Z., et al. (2022). Single-cell and spatial analysis reveal interaction of FAP+ fibroblasts and SPP1+ macrophages in colorectal cancer. Nature Communications 13(1), 1742. doi: 10.1038/s41467-022-29366-6.

Qin, H., Buckley, J.A., Li, X., Liu, Y., Fox, T.H., 3rd, Meares, G.P., et al. (2016). Inhibition of the JAK/STAT Pathway Protects Against α-Synuclein-Induced Neuroinflammation and Dopaminergic Neurodegeneration. J Neurosci 36(18), 5144-5159. doi: 10.1523/jneurosci.4658-15.2016.

Qing, K., Mah, C., Hansen, J., Zhou, S., Dwarki, V., and Srivastava, A. (1999). Human fibroblast growth factor receptor 1 is a co-receptor for infection by adeno-associated virus 2. Nat Med 5(1), 71-77. doi: 10.1038/4758.

Rabey, J.M., Sagi, I., Huberman, M., Melamed, E., Korczyn, A., Giladi, N., et al. (2000). Rasagiline mesylate, a new MAO-B inhibitor for the treatment of Parkinson's disease: a double-blind study as adjunctive therapy to levodopa. Clin Neuropharmacol 23(6), 324-330. doi: 10.1097/00002826-200011000-00005.

Rajpurkar, P., Chen, E., Banerjee, O., and Topol, E.J. (2022). AI in health and medicine. Nature Medicine 28(1), 31-38. doi: 10.1038/s41591-021-01614-0.

Ramsköld, D., Luo, S., Wang, Y.C., Li, R., Deng, Q., Faridani, O.R., et al. (2012). Full-length mRNA-Seq from single-cell levels of RNA and individual circulating tumor cells. Nat Biotechnol 30(8), 777-782. doi: 10.1038/nbt.2282.

Rascol, O., Brooks, D.J., Melamed, E., Oertel, W., Poewe, W., Stocchi, F., et al. (2005). Rasagiline as an adjunct to levodopa in patients with Parkinson's disease and motor fluctuations (LARGO, Lasting effect in Adjunct therapy with Rasagiline Given Once daily, study): a randomised, double-blind, parallel-group trial. Lancet 365(9463), 947-954. doi: 10.1016/s0140-6736(05)71083-7.

Reuter, J.A., Spacek, D.V., and Snyder, M.P. (2015). High-throughput sequencing technologies. Mol Cell 58(4), 586-597. doi: 10.1016/j.molcel.2015.05.004.

Rochet, J.C., Outeiro, T.F., Conway, K.A., Ding, T.T., Volles, M.J., Lashuel, H.A., et al. (2004). Interactions among alpha-synuclein, dopamine, and biomembranes: some clues for understanding neurodegeneration in Parkinson's disease. J Mol Neurosci 23(1-2), 23-34. doi: 10.1385/jmn:23:1-2:023.

Rodriques, S.G., Stickels, R.R., Goeva, A., Martin, C.A., Murray, E., Vanderburg, C.R., et al. (2019). Slide-seq: A scalable technology for measuring genome-wide expression at high spatial resolution. Science 363(6434), 1463-1467. doi: doi:10.1126/science.aaw1219.

REFERENCES

Rosenberg, A.B., Roco, C.M., Muscat, R.A., Kuchina, A., Sample, P., Yao, Z., et al. (2018). Single-cell profiling of the developing mouse brain and spinal cord with split-pool barcoding. Science 360(6385), 176-182. doi: 10.1126/science.aam8999.

Rosenblad, C., Kirik, D., Devaux, B., Moffat, B., Phillips, H.S., and Björklund, A. (1999). Protection and regeneration of nigral dopaminergic neurons by neurturin or GDNF in a partial lesion model of Parkinson's disease after administration into the striatum or the lateral ventricle. Eur J Neurosci 11(5), 1554-1566. doi: 10.1046/j.1460-9568.1999.00566.x.

Sander, J.D., and Joung, J.K. (2014). CRISPR-Cas systems for editing, regulating and targeting genomes. Nat Biotechnol 32(4), 347-355. doi: 10.1038/nbt.2842.

Sarnat, H.B., and Netsky, M.G. (2002). When does a ganglion become a brain? Evolutionary origin of the central nervous system. Semin Pediatr Neurol 9(4), 240-253. doi: 10.1053/spen.2002.32502.

Schrag, A., Wenning, G.K., Quinn, N., and Ben-Shlomo, Y. (2008). Survival in multiple system atrophy. Mov Disord 23(2), 294-296. doi: 10.1002/mds.21839.

Scott, D., and Roy, S. (2012). α-Synuclein inhibits intersynaptic vesicle mobility and maintains recycling-pool homeostasis. J Neurosci 32(30), 10129-10135. doi: 10.1523/jneurosci.0535-12.2012.

Scott, D.A., Tabarean, I., Tang, Y., Cartier, A., Masliah, E., and Roy, S. (2010). A pathologic cascade leading to synaptic dysfunction in alpha-synuclein-induced neurodegeneration. J Neurosci 30(24), 8083-8095. doi: 10.1523/jneurosci.1091-10.2010.

Shapiro, E., Biezuner, T., and Linnarsson, S. (2013). Single-cell sequencing-based technologies will revolutionize whole-organism science. Nature Reviews Genetics 14(9), 618-630. doi: 10.1038/nrg3542.

Shen, S., Bryant, K.D., Brown, S.M., Randell, S.H., and Asokan, A. (2011). Terminal N-linked galactose is the primary receptor for adeno-associated virus 9. J Biol Chem 286(15), 13532-13540. doi: 10.1074/jbc.M110.210922.

Shepherd, J.D., Rumbaugh, G., Wu, J., Chowdhury, S., Plath, N., Kuhl, D., et al. (2006). Arc/Arg3.1 mediates homeostatic synaptic scaling of AMPA receptors. Neuron 52(3), 475-484. doi: 10.1016/j.neuron.2006.08.034.

Singleton, A.B., Farrer, M., Johnson, J., Singleton, A., Hague, S., Kachergus, J., et al. (2003). alpha-Synuclein locus triplication causes Parkinson's disease. Science 302(5646), 841. doi: 10.1126/science.1090278.

Söderberg, O., Gullberg, M., Jarvius, M., Ridderstråle, K., Leuchowius, K.-J., Jarvius, J., et al. (2006). Direct observation of individual endogenous protein complexes in situ by proximity ligation. Nature Methods 3(12), 995-1000. doi: 10.1038/nmeth947.

Soper, J.H., Roy, S., Stieber, A., Lee, E., Wilson, R.B., Trojanowski, J.Q., et al. (2008). Alpha-synuclein-induced aggregation of cytoplasmic vesicles in Saccharomyces cerevisiae. Mol Biol Cell 19(3), 1093-1103. doi: 10.1091/mbc.e07-08-0827.

Spillantini, M.G. (1999). Parkinson's disease, dementia with Lewy bodies and multiple system atrophy are α-synucleinopathies. Parkinsonism & Related Disorders 5(4), 157-162. doi: https://doi.org/10.1016/S1353-8020(99)00031-0.

Spillantini, M.G., Schmidt, M.L., Lee, V.M.Y., Trojanowski, J.Q., Jakes, R., and Goedert, M. (1997). α-Synuclein in Lewy bodies. Nature 388(6645), 839-840. doi: 10.1038/42166.

Ståhl, P.L., Salmén, F., Vickovic, S., Lundmark, A., Navarro, J.F., Magnusson, J., et al. (2016). Visualization and analysis of gene expression in tissue sections by spatial transcriptomics. Science 353(6294), 78-82. doi: 10.1126/science.aaf2403.

Stemmer, M., Thumberger, T., Del Sol Keyer, M., Wittbrodt, J., and Mateo, J.L. (2015). CCTop: An Intuitive, Flexible and Reliable CRISPR/Cas9 Target Prediction Tool. PLoS One 10(4), e0124633. doi: 10.1371/journal.pone.0124633.

Sullivan, A.M. (2017). Neuronal Signaling: an introduction. Neuronal Signal 1(1), Ns20160025. doi: 10.1042/ns20160025.

Summerford, C., Bartlett, J.S., and Samulski, R.J. (1999). AlphaVbeta5 integrin: a co-receptor for adeno-associated virus type 2 infection. Nat Med 5(1), 78-82. doi: 10.1038/4768.

Summerford, C., and Samulski, R.J. (1998). Membrane-associated heparan sulfate proteoglycan is a receptor for adeno-associated virus type 2 virions. J Virol 72(2), 1438-1445. doi: 10.1128/jvi.72.2.1438-1445.1998.

Suzuki, K., Tsunekawa, Y., Hernandez-Benitez, R., Wu, J., Zhu, J., Kim, E.J., et al. (2016). In vivo genome editing via CRISPR/Cas9 mediated homology-independent targeted integration. Nature 540(7631), 144-149. doi: 10.1038/nature20565.

Tang, F., Barbacioru, C., Wang, Y., Nordman, E., Lee, C., Xu, N., et al. (2009). mRNA-Seq whole-transcriptome analysis of a single cell. Nature Methods 6(5), 377-382. doi: 10.1038/nmeth.1315.

Tardivel, M., Bégard, S., Bousset, L., Dujardin, S., Coens, A., Melki, R., et al. (2016). Tunneling nanotube (TNT)-mediated neuron-to neuron transfer of pathological Tau protein assemblies. Acta Neuropathol Commun 4(1), 117. doi: 10.1186/s40478-016-0386-4.

Teleanu, R.I., Niculescu, A.G., Roza, E., Vladâcenco, O., Grumezescu, A.M., and Teleanu, D.M. (2022). Neurotransmitters-Key Factors in Neurological and Neurodegenerative Disorders of the Central Nervous System. Int J Mol Sci 23(11). doi: 10.3390/ijms23115954.

Thakur, P., Breger, L.S., Lundblad, M., Wan, O.W., Mattsson, B., Luk, K.C., et al. (2017). Modeling Parkinson's disease pathology by combination of fibril seeds and α-synuclein overexpression in the rat brain. Proc Natl Acad Sci U S A 114(39), E8284-e8293. doi: 10.1073/pnas.1710442114.

REFERENCES

Triarhou., L.C. (2013). Dopamine and Parkinson's Disease.

Tu, P.H., Galvin, J.E., Baba, M., Giasson, B., Tomita, T., Leight, S., et al. (1998). Glial cytoplasmic inclusions in white matter oligodendrocytes of multiple system atrophy brains contain insoluble alpha-synuclein. Ann Neurol 44(3), 415-422. doi: 10.1002/ana.410440324.

Ungerstedt, U. (1968). 6-Hydroxy-dopamine induced degeneration of central monoamine neurons. Eur J Pharmacol 5(1), 107-110. doi: 10.1016/0014-2999(68)90164-7.

Urnov, F.D., Rebar, E.J., Holmes, M.C., Zhang, H.S., and Gregory, P.D. (2010). Genome editing with engineered zinc finger nucleases. Nature Reviews Genetics 11(9), 636-646. doi: 10.1038/nrg2842.

Van der Perren, A., Gelders, G., Fenyi, A., Bousset, L., Brito, F., Peelaerts, W., et al. (2020). The structural differences between patient-derived α-synuclein strains dictate characteristics of Parkinson's disease, multiple system atrophy and dementia with Lewy bodies. Acta Neuropathol 139(6), 977-1000. doi: 10.1007/s00401-020-02157-3.

Van der Perren, A., Toelen, J., Casteels, C., Macchi, F., Van Rompuy, A.S., Sarre, S., et al. (2015a). Longitudinal follow-up and characterization of a robust rat model for Parkinson's disease based on overexpression of alpha-synuclein with adeno-associated viral vectors. Neurobiol Aging 36(3), 1543-1558. doi: 10.1016/j.neurobiolaging.2014.11.015.

Van der Perren, A., Van den Haute, C., and Baekelandt, V. (2015b). Viral vector-based models of Parkinson's disease. Curr Top Behav Neurosci 22, 271-301. doi: 10.1007/7854_2014_310.

van der Putten, H., Wiederhold, K.H., Probst, A., Barbieri, S., Mistl, C., Danner, S., et al. (2000). Neuropathology in mice expressing human alpha-synuclein. J Neurosci 20(16), 6021-6029. doi: 10.1523/jneurosci.20-16-06021.2000.

Vilcaes, A.A., Chanaday, N.L., and Kavalali, E.T. (2021). Interneuronal exchange and functional integration of synaptobrevin via extracellular vesicles. Neuron 109(6), 971-983. e975. doi: 10.1016/j.neuron.2021.01.007.

Volpicelli-Daley, L.A., Kirik, D., Stoyka, L.E., Standaert, D.G., and Harms, A.S. (2016). How can rAAV-α-synuclein and the fibril α-synuclein models advance our understanding of Parkinson's disease? Journal of Neurochemistry 139(S1), 131-155. doi: https://doi.org/10.1111/jnc.13627.

Walters, R.W., Yi, S.M., Keshavjee, S., Brown, K.E., Welsh, M.J., Chiorini, J.A., et al. (2001). Binding of adeno-associated virus type 5 to 2,3-linked sialic acid is required for gene transfer. J Biol Chem 276(23), 20610-20616. doi: 10.1074/jbc.M101559200.

Wang, X., Allen, W.E., Wright, M.A., Sylwestrak, E.L., Samusik, N., Vesuna, S., et al. (2018). Three-dimensional intact-tissue sequencing of single-cell transcriptional states. Science 361(6400). doi: 10.1126/science.aat5691.

Wenning, G.K., Ben Shlomo, Y., Magalhães, M., Daniel, S.E., and Quinn, N.P. (1994). Clinical features and natural history of multiple system atrophy. An analysis of 100 cases. Brain 117 (Pt 4), 835-845. doi: 10.1093/brain/117.4.835.

Westra, E.R., Dowling, A.J., Broniewski, J.M., and Houte, S.v. (2016). Evolution and Ecology of CRISPR. Annual Review of Ecology, Evolution, and Systematics 47(1), 307-331. doi: 10.1146/annurev-ecolsys-121415-032428.

WHO (2022). Launch of WHO's Parkinson disease technical brief [Online]. Available: https://www.who.int/news/item/14-06-2022-launch-of-who-s-parkinson-disease-technical-brief [Accessed].

Willems, J., de Jong, A.P.H., Scheefhals, N., Mertens, E., Catsburg, L.A.E., Poorthuis, R.B., et al. (2020). ORANGE: A CRISPR/Cas9-based genome editing toolbox for epitope tagging of endogenous proteins in neurons. PLoS Biol 18(4), e3000665. doi: 10.1371/journal.pbio.3000665.

Wood, S.J., Wypych, J., Steavenson, S., Louis, J.C., Citron, M., and Biere, A.L. (1999). alpha-synuclein fibrillogenesis is nucleation-dependent. Implications for the pathogenesis of Parkinson's disease. J Biol Chem 274(28), 19509-19512. doi: 10.1074/jbc.274.28.19509.

Wright, A.V., Nuñez, J.K., and Doudna, J.A. (2016). Biology and Applications of CRISPR Systems: Harnessing Nature's Toolbox for Genome Engineering. Cell 164(1-2), 29-44. doi: 10.1016/j.cell.2015.12.035.

Xia, X., Wang, Y., Qin, Y., Zhao, S., and Zheng, J.C. (2022). Exosome: A novel neurotransmission modulator or non-canonical neurotransmitter? Ageing Res Rev 74, 101558. doi: 10.1016/j.arr.2021.101558.

Xie, Q., Bu, W., Bhatia, S., Hare, J., Somasundaram, T., Azzi, A., et al. (2002). The atomic structure of adeno-associated virus (AAV-2), a vector for human gene therapy. Proc Natl Acad Sci U S A 99(16), 10405-10410. doi: 10.1073/pnas.162250899.

Xue, C., and Greene, E.C. (2021). DNA Repair Pathway Choices in CRISPR-Cas9-Mediated Genome Editing. Trends Genet 37(7), 639-656. doi: 10.1016/j.tig.2021.02.008.

Yartsev, M.M. (2017). The emperor's new wardrobe: Rebalancing diversity of animal models in neuroscience research. Science 358(6362), 466-469. doi: 10.1126/science.aan8865.

Zarranz, J.J., Alegre, J., Gómez-Esteban, J.C., Lezcano, E., Ros, R., Ampuero, I., et al. (2004). The new mutation, E46K, of alpha-synuclein causes Parkinson and Lewy body dementia. Ann Neurol 55(2), 164-173. doi: 10.1002/ana.10795.

Zeisel, A., Muñoz-Manchado, A.B., Codeluppi, S., Lönnerberg, P., La Manno, G., Juréus, A., et al. (2015). Brain structure. Cell types in the mouse cortex and hippocampus revealed by single-cell RNA-seq. Science 347(6226), 1138-1142. doi: 10.1126/science.aaa1934.

Zhang, W., Wu, J., Ward, M.D., Yang, S., Chuang, Y.A., Xiao, M., et al. (2015). Structural basis of arc binding to synaptic proteins: implications for cognitive disease. Neuron 86(2), 490-500. doi: 10.1016/j.neuron.2015.03.030.

Acknowledgments

Undoubtedly, by far the most difficult section for me to write with the limited time I had left. I feel personally restricted, and I find it limiting to use some "body text" to express all the sparse emotions, memories, and images I have shared with you throughout these years. It's emotionally difficult to dig into what you all meant for me. To help me out, I thought I could use food, something, as you know, that I take seriously, to symbolize the impact you have each had on me during this adventure - to get a better flavor, if you will, of the person you were to me. Not sure how you will take it. But here we go.

I am deeply grateful, **Tomas**, for the valuable knowledge and professional growth I have gained as a scientist during these years under your guidance. I feel lucky, and I thank you for allowing me to "play" with fancy and expensive technologies that other PhDs could only dream about.

I am grateful for the challenging research line conducted inside MNM. Here we shape the future. For being professional and for your scientific rigor. I hope there will be chances to collaborate with you in the future, as I know MNM will continue to push the limits of knowledge. (coffee).

I want to express my gratitude to my two co-supervisors, **Malin** and **Luis**, for their technical expertise and unwavering support throughout my projects. You two inspired me daily to balance work and personal life. Thanks, **Luis,** for all the BBJ sessions, which have helped ease my frustration when experiments didn't go as planned. (tugg). **Malin**, your dedication and focus at the gym would make even Dwayne Johnson - The Rock envious. (carrot). **Marcus** - Boss. I appreciate your support during these years. (snus)

I would like to immensely thank the people who worked hands on with the projects contained in this thesis. With your technical expertise, experience, and knowledge, I felt blessed to have you by my side, pushing through all the experiments. You did not have to, you didn't need these publications, but yet, you were there. Big shoutout to **Anna H.**, **Jenny J**, and **Ulla J.**, the Michelangelo of IHC stainings.

Tomas D. and **Olga G.** - The Batman and James Gordon of BMC. The EMV department is so lucky to have you.

a leggere questi "acklogmentz" con la giusta intonazione. Spiegaglielo va. **Paul** - Aubergine. Quando smetti di vincere grants t'insegno a giocare a pallone. (liquore alla carota). **Michael** - Magic Mike. Amico stretto, socio, mentore. A noi due, che vediamo il mondo "with a different lens and angle" e cerchiamo di comunicarlo agli altri. Ho la certezza di poter contare sempre sul tuo aiuto. Unconditional love. (domino's pizza)

I would like to thank all the people who were there at the beginning of this journey back when it started in the best corridor room in Lund. Möllevången. **Alex** - El tio. **Stefano** - Focaccioso. **Dorotee** - Sweet, like a pie. **Fabio D** - Caralho. **Niels** - Banana bread. **Seb** - Bristol boy. **Bobby** -The shark of Dutch cannals. **Beppe** - Beppo. il tuo essere genuino ti ha circodato di persone fantastiche, grazie per averle condivise con me. Te ne sono grato. (focaccia barese). **Monica**, la tua determinazione ti ha portato a raggiungere qualsiasi ti fossi prefissata. T'ammiro. Prenditi cura di Beppo.

Tiago - Tiá. Penso piú che un amico tu qui sia stato un fratello con cui sono potuto crescere durante st'avventura. Per tutto quello che abbiamo passato insieme, per tutto quello che passeremo, ti ringrazio per esserci sempre. Per me la nostra amicizia é importante e so che perdurerá nonostante le distanze. Ti auguro il meglio con **Eva.** (minestrone)

"Montagna" e **"Carne de Chiesa"**. **Gianluca** - Kikko. A te che hai visto con i tuoi occhi quello che i miei racconti cercano di descrivere ogni volta che ritorno in patria. A **Francesco G. -** Er granchio. Fin'ora non ho ancora trovato un'altra persona con cui condivido un piatto come lo faccio con te. Fratm' te vojo bene assai. **Simone C.** - Bri. Te ringranzio per essere stato sempre presente quando tornavo a casa. Per i pensieri rivoluzionari che nascevano dale nostre lunghe riflessioni. Ti auguro di il meglio. (pizza rossa dell'olmo)

Matilde - Ne ho troppi. Se ripenso a tutti gli ostacoli che hai superato, mi vengono I brividi. Ho difficoltá a tracciare un limite alla tua forza e coraggio. Ti ringrazio per essermi stata vicina, per aver portato pazienza, e per avermi aiutato durante questo percorso. Senza di te non ne sarei uscito. Io ci sono. (besciamella).

Bro - Puó. Ho il privilegio di andare in giro e vantarmi di avere il fratello piú dotto, piú bello e piú grosso del mondo. Se oggi sono quello che sono é perché sono cresciuto al riparo protetto dalla tua ombra. **Madre** - Mommy. Tu pensi di aver svolto il semplice dovere di mamma. Per me non é stato scontato. Ogni mio traguardo, é anche tuo. Ti voglio bene. **Papá**. La luce che le persone vedono in me é il dono piú prezioso che mi hai lasciato. (toast con gli spinaci).

I am the result of all the contaminations I had from all your encounters. Thank you.

Martino